Modulating angiogenic balance to establish novel treatment strategies and a disease model for preeclampsia

Inaugural-Dissertation

zur

Erlangung des Doktorgrades der Mathematisch-Naturwissenschaftlichen Fakultät

der Universität zu Köln

vorgelegt von

Mahsa Matin

aus dem Iran

Köln 2022

Berichterstatter: Prof. Dr. Thomas Benzing

(Gutachter) Prof. Dr. Marcus Krüger

Tag der mündlichen Prüfung: 07.06.2022

Table of Contents

Tables Directory

Figures Directory

Abbreviations and Acronyms

µg	Microgram
µl	Microliter
µM	Micromolar
ACR	Albumin to creatinine ratio
BSA	Bovine serum albumin
CAA	Chloroacetamide
CIP	Calf intestinal alkaline phosphatase
CNS	Central nervous system
CNS	Crystallography and NMR System
CRP	C-reactive protein
ddH2O	Double distilled water
DIC	Disseminated intravascular coagulopathy
DMEM	Dulbecco's modified eagle's medium
DNA	Deoxyribonucleic acid
DTT	Dithiothreitol
ECL	Enhanced chemiluminescence
ECTB	Endovascular cytotrophoblast
EDTA	Ethylenediaminetetraacetic acid
ELISA	Enzyme linked immunosorbent assay
EMT	Epithelial-mesenchymal transition
EOP	Early-onset preeclampsia
FBS	Fetal bovine serum
Flk-1	fetal liver kinase-1
Flt1	Fms-like tyrosine kinase-1
fp	Forward primer
FSGS	Focal segmental glomerulosclerosis

GA-1000	Gentamicin sulfate-Amphotericin
GBM	Glomerular basement membrane
H2O	water
hEGF	Human Epidermal Growth Factor
HEK	Human embryonic kidney cells
HELLP	Hemolysis, elevated liver enzymes, low platelets
hFGF-B	Human fibroblast growth factor beta
HIF1-α	Hypoxia-inducible factor 1-alpha
HPR	Human haptoglobin Protein
HUVEC	Human umbilical vein endothelial cells
IF	immunofluorescent staining
IgG	Immunoglobulin G
IL	Interluekin
kDa	Kilodaltons
KDR	Kinase insert domain receptor
l	liter
LOP	Late-onset preeclampsia
MAP	Mitogen-activated protein kinase
mg	Miligram
min	Minutes
ml	Milimolar
mM	Mililiter
mmHg	Millimetre of mercury
mRNA	Massenger Ribonucleic acid
NaCl	Sodium chloride
NaCNBH3	Sodium cyanoborohydride
nm	Nanometer
nM	Nanomolar
NO	Nitric oxide

p Value	Probability
PAS	Periodic acidic Schiff
PBS	Phosphate-buffered saline
PCR	Polymerase chain reaction
PE	Preeclampsia
PECAM	Platelet endothelial cell adhesion molecule
PlGF	Placental growth factor
R3-IGF-1	Long arginine 3-IGF-1
ROS	Reactive oxygen species
RPM	Revolutions Per Minute
rp	reverse primer
scPlGF	Single-chain PlGF
scVEGF	Single-chain VEGF
SD	Slit diaphragm
SDS	Sodium dodecyl sulfate
sEng	Soluble endoglin
sFlt-1	Soluble fms-like tyrosine kinase-1
siRNA	Small interfering RNA
TEMED	Tetramethylethylenediamine
TGF-β	Transforming growth factor beta
Tris	Tris(hydroxymethyl)aminomethane
VEGFA	Vascular endothelial growth factor type A
VEGFR	Vascular endothelial growth factor receptor
WT-1	Wim's tumor supressor 1 protein

1. Abstract

Preeclampsia is a pregnancy-specific complication, occurring in 6 – 8 % of pregnancy cases, and is the leading cause of 76,000 maternal and 500,000 prenatal deaths per year worldwide (Redman and Sargent 2005). Due to the current lack of effective treatment options and its high prevalence, the development of novel and effective therapies for preeclampsia is of great importance ('Gestational Hypertension and Preeclampsia: ACOG Practice Bulletin Summary, Number 222' 2020). So far, there is no clear understanding of the pathophysiology of proteinuria and hypertension caused by preeclampsia, and animal models to study preeclampsia are debatable. Yet, it is well known that elevated sFlt-1 plasma levels, by scavenging VEGF and PlGF, lead to preeclampsia (Maynard et al. 2003; Levine et al. 2004). Pilot trials of apheresis therapy to eliminate sFlt-1 in patients with severe preeclampsia proved to be safe and effective (Thadhani et al. 2011). However, currently used platforms for sFlt-1 apheresis are unspecific, eliminating not only sFlt-1 but also other soluble proteins and factors.

The current thesis establishes a highly specific sFlt-1 apheresis set up through the generation of a VEGF-based ligand with enhanced binding characteristics for sFlt-1. This novel ligand enables adsorption of up to 80% of circulating sFlt1 with the highest specificity while additionally restoring angiogenic balance by liberating endogenous PlGF and VEGF. According to in *silico* molecular modeling, a single-chain VEGF165 dimer (scVEGF165) was generated, which multimerizes to tetra- and higher multimeric VEGF molecules with enhanced sFlt-1 binding characteristics. A short peptide linker hampers intrachain dimerization scVEGF165 to induce assembly, preferably as tetrameric molecules as visualized in negative staining electron microscopy. scVEGF165 multimers possess a 1.2-fold higher affinity for sFlt-1 as compared to the available antibodies or monomeric VEGF. Consequently, scVEGF165 multimers have the ability to competitively release sFlt-1-bound PlGF and, in particular, VEGF. In *ex vivo* adsorption experiments using serum samples from patients with preeclampsia, scVEGF165 multimers reduce sFlt-1 levels by 85% and increase PlGF and VEGF levels by 20- and 9-fold, respectively. This system is directly applicable for further testing in large animal models of preeclampsia, which is crucial to evaluate the effect of VEGF release on pregnancy.

Furthermore, in this thesis, a novel transgenic mouse model of preeclampsia that expresses soluble human sFlt-1, is characterized. Through inducible systemic expression of sFlt-1, hallmarks of preeclampsia, hypertension, and proteinuria are reproducible in this mouse model.

The findings described in this thesis will help to create a highly effective, targeted apheresis therapy for patients with preeclampsia. In addition, the presented mouse model will be an important tool for studies enhancing our understanding of renal physiology and pathophysiology of preeclampsia.

2. Zusammenfassung

Präeklampsie ist eine in 6 – 8% der Schwangerschaften auftretende Erkrankung und häufigste Ursache von 76.000 mütterlichen und 500.000 pränatalen Todesfällen weltweit (Sibai et al. 2005; Redman and Sargent 2005). Da aktuell keine spezifische Therapie für diese Erkrankung existiert, ist die Entwicklung effektiver Behandlungsmethoden von großer Bedeutung . Gegenwärtig ist die Pathophysiologie der mit einer Präeklampsie einhergehenden Proteinurie und Hypertonie nicht gut verstanden und bestehende Tiermodelle bilden die Erkrankung nur ungenau nach. Seit einigen Jahren ist bekannt, dass erhöhte Serumspiegel des löslichen VEGF-R1 (sFlt-1) im Kreislauf der Mutter zur Präeklampsie führen. sFlt-1 bindet VEGF und PlGF und unterbindet die trophische Wirkung dieser proangiogenen Faktoren auf die Endothelzellen (Maynard et al. 2003; Levine et al. 2004; Hagmann et al. 2012). Pilotstudien zur Entfernung von sFlt-1 aus dem mütterlichen Blut mittels Apherese bei Patienten mit schwerer Präeklampsie erwiesen sich als sicher und wirksam (Thadhani et al. 2011) Allerdings eliminieren die zur Verfügung stehenden Apheresesysteme sFlt-1 unspezifisch, d.h. immer zusammen mit andere löslichen Proteinen und Faktoren.

Im Rahmen dieser Forschungsarbeit wurde eine hochspezifische sFlt-1 Apheresesäule entwickelt, die bis zu 80% des zirkulierenden sFlt-1 adsorbiert und zudem das angiogene Gleichgewicht durch Freisetzung von PlGF und VEGF wiederherstellt. In-silico Modellierungen zeigten auf molekularer Ebene, dass multimere VEGF Moleküle, bestehend aus Dimeren von VEGF165 Einzelketten (scVEGF165), generiert werden können, die bessere Bindungseigenschaften für sFlt-1 besitzen als wildtyp VEGF 165. Ein kleiner Peptidlinker zwischen den monomeren scVEGF165 Sequenzen verhindert dabei die Dimerisierung innerhalb der jeweiligen Einzelketten, so dass die Bildung von tetrameren Makromolekülen begünstigt wird, die mittels Negativ-Kontrast-Elektronenmikroskopie visualisiert werden konnten. scVEGF165-Multimere besitzen eine 1,2-fach höhere Bindungsaffinität gegenüber sFlt-1 im Vergleich zu verfügbaren Antikörpern oder monomerem VEGF. Dies ermöglicht die kompetitive Freisetzung von sFlt-1-gebundenem PlGF und VEGF. *Ex vivo* Adsorptionsexperimente mit scVEGF165 Multimeren konnten die sFlt-1 Plasmaspiegel im Serum von Präeklampsie-Patientinnen um 85% reduzieren und die Plasmaspiegel von PlGF

und VEGF um das 20- bzw., 9-Fache erhöhen. Dieses Verfahren ist biokompatibel und kann unmittelbar in Großtiermodellen für Präeklampsie angewendet werden. Dies ist von großer Bedeutung, um den Effekt der Freisetzung von VEGF auf Mutter und Fetus zu untersuchen. Zudem wurde in dieser Forschungsarbeit ein Mausmodell der Präeklampsie charakterisiert, in dem humanes sFlt-1 transgen exprimiert wird. Nach einer systemischen Induktion der sFlt-1 Expression, konnten die typischen Merkmale der Erkrankung: Hypertonie und Proteinurie in diesem Mausmodell reproduziert werden.

Zusammenfassend leisten die Ergebnisse dieser Forschungsarbeit einen Beitrag für künftige Grundlagenforschung im Bereich der Nierenphysiologie sowie der Pathophysiologie der Präeklampsie und ermöglichen durch die Entwicklung eines spezifischen sFlt-1 Aphareseverfahrens einen wichtigen Schritt hin zur optimierten, zielgerichteten Therapie der Präeklampsie.

3. Introduction

3.1. Preeclampsia

Hypertension is considered one of the most frequent complications during pregnancy. It affects about 4.6% of all pregnancies worldwide (Abalos et al. 2013). Hypertensive pregnancy disorders encompass four major conditions, namely chronic hypertension, gestational hypertension, preeclampsia or eclampsia, and chronic hypertension, with superimposed preeclampsia. Among these complications, preeclampsia with a global prevalence of 6-8% per year, remains among the most common hypertensive disorders associated with pregnancy (Sibai et al. 2005; 'Report of the National High Blood Pressure Education Program Working Group on High Blood Pressure in Pregnancy' 2000).

Preeclampsia is diagnosed after the 20th week of gestation with new-onset hypertension above 140/90 mmHg (Giles et al. 2009) and presence of protein in the urine (proteinuria) above 300 mg/24 hours (or 300 mg/g creatinine in spot urine sample) (Carroll and Temte 2000). Other diagnostic signs include significant end-organ dysfunction such as liver failure, acute kidney injury, hematologic changes or central nervous system (CNS) related symptoms (e.g., headaches, visual disturbances, and paraesthesia). Advanced preeclampsia can lead to cerebral ischemia and seizures. By definition, the condition in which seizures or coma occurs due to preeclampsia is termed eclampsia (MacKay, Berg, and Atrash 2001; Katz, Farmer, and Kuller 2000). HELLP (hemolysis, elevated liver enzymes, low platelets) syndrome, renal failure, liver injury, cerebral haemorrhage and edema, pulmonary edema, hypertensive encephalopathy, disseminated intravascular coagulopathy (DIC), and thrombocytopenia are among other serious maternal clinical complications associated with advanced preeclampsia (Buchbinder et al. 2002; Haram, Svendsen, and Abildgaard 2009; Norwitz, Hsu, and Repke 2002). Together, preeclampsia and eclampsia encounter more than 50,000 maternal deaths per year globally (Young, Levine, and Karumanchi 2010). In addition, preeclampsia is considered a major risk factor for fetal demise. The rate of fetal stillbirth in severe preeclampsia is 21 per 1000 and in mild preeclampsia 9 per 1000 (Simpson et al. 2002). Moreover, preeclampsia increases the risk of fetal growth restriction, neonatal

thrombocytopenia, neonatal neutropenia, bronchopulmonary dysplasia in late-preterm infants (Backes et al. 2011).

Therefore, early diagnosis of preeclampsia is pivotal to both maternal and fetal health and survival.

Besides detecting previously non-existent hypertension and proteinuria, the sFlt-1/PlGF ratio as a clinical marker has been of great value in the diagnosis of preeclampsia. This screen-testing parameter was suggested by Verlohren et al. in 2011 and showed 85% sensitivity in detecting early preeclampsia. Currently available commercial tests measuring the PlGF/sFlt-1 ratio, in combination with uterine artery Doppler, have reached a sensitivity of 95% or even higher (Verlohren et al. 2012).

Based on clinical manifestations and laboratory values, "preeclampsia with severe features" can be differentiated. Preeclampsia is considered severe when the blood pressure exceeds 160/110 mmHg or when hepatic abnormalities (e.g., transaminases elevated >2 times the upper limit of normal), acute kidney injury, thrombocytopenia (<100.000 /µl), pulmonary edema, or symptoms of CNS dysfunction are present. In case of severe maternal and fetal complications, pre-term delivery is advised. Depending on the gestational week of onset of symptoms, preeclampsia can be classified into early-onset preeclampsia (EOP) or late-onset preeclampsia (LOP) (Wojtowicz et al. 2019; Kornacki and Skrzypczak 2008). Disease onset before the 34th gestational week is considered EOP, while onset after the 34th week is termed LOP ('Hypertension in pregnancy. Report of the American College of Obstetricians and Gynecologists' Task Force on Hypertension in Pregnancy' 2013). A rare form of preeclampsia is postpartum preeclampsia, where preeclampsia occurs 48 hours after childbirth (Munjuluri et al. 2005).

3.2. Preeclampsia - From past to present

In the fifth century, despite the lack of knowledge about preeclampsia and eclampsia, headaches and convulsions were recognized as bad signs for pregnancy by Hippocrates (Bell 2010). However, until the 15th century, the disease was not specified as a pregnancy disorder but rather as one of four types of epilepsy (Bell 2010; Chesley 1985). The Greek word ‘‘eclampsia’’, meaning ‘’sudden occurrence’’, was used for the first time in 1619 by Johannes Varandaeus in his Treatise on Gynaecology. It was Boissier de Sauvages, who in the 18th century could finally differentiate epileptic seizures from eclampsia. He believed that

eclampsia is an acute form of convulsion and a mechanism by which the body can eliminate its morbid elements, while epilepsy is a chronic condition with lifetime reoccurrence of convulsions (Bell 2010). During this era, depending on the severity of symptoms, blood-letting was commonly used and repeated as a treatment method for preeclampsia and eclampsia. Another treatment method suggested by Danman was using cold water on the face and warm baths to speed up the delivery while using opioids to help with women's irritations (Bell 2010).

In the late 18th century, it was believed that toxins found in meat were responsible for preeclampsia and eclampsia, and consequently, meat restricted diets were prescribed for women to prevent the disease (Chesley 1984). In 1843, John Lever, for the first time, introduced proteinuria as a symptom found in women with eclampsia. In the same year, Robert John et al. could associate early pregnancy symptoms like headaches, vision disturbances, and stomach aches with the later development of convulsions in pregnant women (Bell 2010). Finally, in 1978 the term pre-eclampsia was defined by Vaquez and Nobecourt as a pregnancy-specific disorder and an early state of eclampsia, in which clinical symptoms like proteinuria, edema, and headaches are observed, and the chance of developing convulsions is increased. Between 1960 and 1986, several scientists compared the placenta of women who died from preeclampsia with normal placentas and reported significant differences in morphology, trophoblast cells, and blood vessels in preeclamptic placentas (Brosens, Robertson, and Dixon 1967; Brosens, Robertson, and Dixon 1972; Gerretsen, Huisjes, and Elema 1981; Khong et al. 1986). In 1983, for a short time, it was believed that a worm-like parasite was responsible for the pathogenesis of preeclampsia and eclampsia. However, six years later, Roberts et al. proposed a theory that is now the basis of modern research concerning the etiology of preeclampsia. Together with his colleagues, he introduced preeclampsia as an endothelial disorder, claiming that the injured placenta releases an unknown pathogenic factor into the blood circulation, triggering a systemic effect in the body of women with preeclampsia (Roberts et al. 1989).

Since then, much fundamental research has been performed to increase understanding of the pathophysiology of preeclampsia. In recent years an imbalance of angiogenic and anti-angiogenic factors in the maternal circulation - the latter originating from the placenta - has been identified as the source of generalized endothelial dysfunction in the mother (Levine et al. 2006; Sibai et al. 2005; Veerbeek et al. 2015).

3.3. Pathophysiology of preeclampsia

In a normal pregnancy with successful placentation, invasive placental cytotrophoblasts reach out into the maternal uterine wall, where they induce branching of maternal veins, vasodilation, and remodeling of the maternal arterioles. This process is necessary for connecting the maternal circulation to the intervillous space of the placenta and thus increasing maternal blood flow into the placenta. For the spiral arteries to remodel as a response to cytotrophoblast invasion, epithelial cells have to lose their smooth muscle cell phenotype and convert to mesenchymal cells to be able to dilate – a process that is known as epithelial-mesenchymal transition (EMT). In preeclampsia, cytotrophoblasts are believed to induce incomplete remodeling of maternal arterioles, leading to insufficient perfusion of the placenta and placental ischemia (Fig. 1). Impaired placental perfusion is believed to be the cause of a hypoxic uterine environment, the presence of anti-angiogenic factors, and inflammatory response in the mother leading to maternal arterial hypertension. The mechanisms by which cytotrophoblast EMT contributes to the course of preeclampsia is still unclear (Sun et al. 2011; Pennington et al. 2012; Madazli et al. 2000)

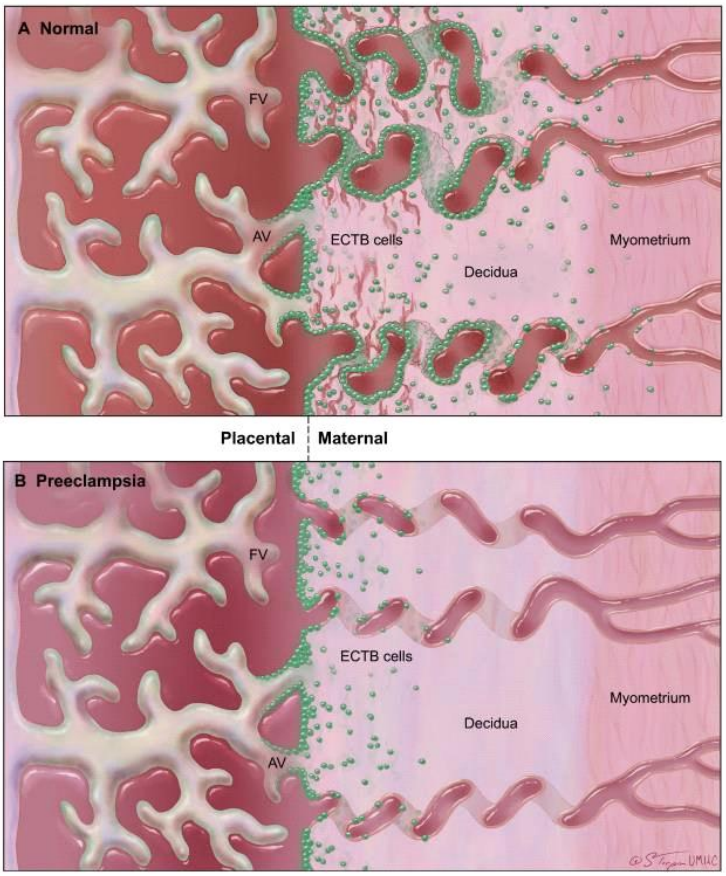

Figure 1: Invasion of cytotrophoblast cells (ECTB) in normal pregnancy and preeclampsia. (Pennington et al. 2012)

3.4. Renal pathology in preeclampsia

One of the common hallmarks of preeclampsia is proteinuria. Proteinuria is defined as a loss of more than 300 mg of plasma proteins a day through the urine and is due to a defect of glomerular filtration (Carroll and Temte 2000).

During the process of glomerular filtration, the kidney generates primary urine from the blood to eliminate metabolic waste, electrolytes, and excess water. The primary urine is further processed in the tubular system of the kidney before the urine is excreted into the bladder. By definition, glomeruli are tufts of small blood capillaries that are surrounded by the Bowman's capsule. The highly complex filtration barrier consists of three main layers that selectively filter fluids and macromolecules based on their size (cut-off 30-50 kDa) and charge. Those layers are endothelial cells, glomerular basement membrane (GBM), and podocytes (Lote 1986).

Endothelial cells, with their anionic glycocalyx, coat the luminal surface of glomerular capillaries and create unique pore-like structures known as fenestrae. These pores are between 50-100 nm in diameter and facilitate plasma flow while preventing the filtration of blood cells (Lote 1986).

Podocytes are greatly specialized epithelial cells that cover the outer surface of glomerular capillaries via their densely packed primary and secondary foot processes. The adjacent interdigitating foot processes of podocytes are bridged by a unique and specialized cell-to-cell junction known as the slit diaphragm (SD). The gap between two podocytes at the SD is about 40 nm wide and is formed by specialized transmembrane and scaffold proteins like nephrin, and podocin. Mutations in the genes *NPHS1* (encoding nephrin) and *NPHS2* (encoding podocin) result in severe proteinuria, and a serious condition of nephrotic syndrome with histologic scarring of the glomeruli called focal and segmental glomerulosclerosis (FSGS) (Kestila et al. 1998; Boute et al. 2000; Huber et al. 2001).

The GBM is synthesized by endothelial cells and podocytes and resides between the two cell types. The GBM is 300 nm thick and consists of collagen IV, laminin, and heparan sulfate (Davidson et al. 2015). In 1970 it was believed that the GBM contributes to the filtration

barrier mainly by its charge selectivity (Brenner, Hostetter, and Humes 1978; Kanwar, Danesh, and Chugh 2007), however later *in vitro* studies on the isolated GBM were unable to confirm this theory (Kanwar, Danesh, and Chugh 2007; Bolton, Deen, and Daniels 1998). Recent studies show that a complex interaction between the actin cytoskeleton of podocyte's foot processes, mechanical compression of the GBM itself, and SD length affect protein permeability of the GBM (Butt et al. 2020).

In preeclampsia, proteinuria is accompanied by a decrease in the glomerular filtration rate. After termination of pregnancy, proteinuria remits within 3 - 8 weeks. Studies have shown a loss of both size- and charge-based selectivity of the glomerular filtration barrier in preeclampsia (Moran et al. 2003). Although histological examination of preeclamptic human kidney tissue is limited due to ethical concerns of conducting studies on pregnant women, there are several studies that describe the general morphology of glomerular lesions in human kidney samples of preeclampsia patients using light microscopy. Glomeruli of patients with preeclampsia are enlarged in size, the capillary lumen exhibits reduced amounts of blood and endothelial and mesangial cells appear hypertrophic. These morphological changes can also be focal (Spargo et al. 1976; Fisher et al. 1981; Pollak and Nettles 1960). In biopsies taken two weeks postpartum, deposition of fibrin in glomeruli has been reported (Morris et al. 1964). Electron microscopy confirmed glomerular endotheliosis and loss of endothelial fenestrae (Mautner et al. 1962). Despite evident proteinuria, in most cases, podocyte's foot processes appeared relatively intact (Karumanchi et al. 2005).

3.5. The role of soluble factors in preeclampsia

Before the year 2000, there were several studies suggesting that circulating factors are responsible for maternal systemic endothelial dysfunction. However, there was no evidence of a specific soluble factor that could cause endothelial dysfunction and proteinuria. In a series of experiments, Vuorel et al. in 2000 and Zhou et al. in 2002 could show that the protein soluble fms-like tyrosine kinase-1 (sFtl-1) is upregulated in the amniotic fluid and the placenta of women with preeclampsia, however at this time, there was no clear link between this finding and the systemic effects caused by elevated sFlt-1 levels in preeclampsia (Zhou et al. 2002; Vuorela et al. 2000).

It was Maynard et al. that could associate excess sFlt-1 in the maternal circulation with the pathophysiology of preeclampsia for the first time. By profiling gene expression of placental tissues of women with preeclampsia, they were able to identify sFlt-1 as an anti-angiogenic factor that is strikingly upregulated in the placenta of patients with preeclampsia. The increase in sFlt-1 levels correlated with the endothelial dysfunction in mothers with preeclampsia as well as the decrease of free vascular endothelial growth factor (VEGF) and placental growth factor (PlGF), two angiogenic factors in the maternal circulation, referring a constant trophic signal to endothelial cells. By administering sFlt-1 to pregnant rats, Maynard et al. were able to induce symptoms of preeclampsia like hypertension and proteinuria. Furthermore, injecting VEGF and PlGF rescued endothelial dysfunction in the rat model (Maynard et al. 2003).

In another study by Sugimoto et al., antibodies against VEGF were able to induce glomerular endothelial damage and proteinuria in non-pregnant mice (Sugimoto et al. 2003). In addition, Eremina et al. have reported the development of glomerular endotheliosis and proteinuria in non-pregnant mice upon 50% reduction of podocyte-derived VEGF (Eremina et al. 2008). Furthermore, there are clinical reports of preeclampsia-like symptoms, i.e., proteinuria and hypertension, in patients who received VEGF antagonists, e.g., bevacizumab, for cancer therapy (Eremina et al. 2008; Patel et al. 2008).

As previously mentioned, differentiation of placental cytotrophoblast cells is one of the key stages in proper placental perfusion. There are studies that directly link pathogenic sFlt-1 upregulation in preeclampsia with abnormal placental perfusion and hypoxia. It has been shown that the administration of sFlt-1 to cultured primary cytotrophoblast cells can interfere with their differentiation and invasion (Zhou et al. 2002). Besides, blocking VEGF inhibited the differentiation of cytotrophoblast cells to endothelial cells (Ng et al. 2004).

Several studies indicated significant upregulation of the hypoxia-inducible factor 1 (HIF1-α) in the placenta of preeclamptic patients. HIF1-α is a well-known transcription factor that regulates VEGF and FLT-1 gene expression (Caniggia et al. 2000; Rajakumar et al. 2003; Gerber et al. 1997; McKeeman et al. 2004).

Although endothelial cells and monocytes can also be a potential source for sFlt-1 expression during preeclampsia, studies comparing sFlt-1 concentrations in the uterine vein and uterine

artery indicated that the sFlt-1 levels are significantly higher in veins, suggesting that the placenta is the major origin for sFlt-1 production in preeclampsia (Cerdeira et al. 2019).

Physiologically, the concentration of sFlt-1 is elevated in every normal pregnancy. However, in preeclampsia, this elevation is more pronounced (Maynard et al. 2003). In addition, increased sFlt-1 levels are present in pregnancies with a higher risk of developing preeclampsia, such as in twin pregnancies, where maternal circulating sFlt-1 levels, as well as sFlt-1/PlGF ratios, are twice as high compared to singleton pregnancies. In twin pregnancies, the elevation of sFlt-1 levels is not believed to be due to an increase in sFlt-1 mRNA levels but due to higher placental mass (Maynard et al. 2008; Bdolah et al. 2008). Contrarily, in mothers who smoke, the incidence of developing preeclampsia is lower than in non-smokers. In smokers, a lower chance for developing preeclampsia has been linked to lower circulating sFlt-1 levels (Powers et al. 2005; Levine et al. 2006; Caniggia et al. 2000). Upon delivery, maternal sFlt-1 levels go back to normal, and systemic clinical manifestations of preeclampsia improve as well.

Placenta-derived soluble endoglin (sEng) is another soluble factor whose upregulation is associated with preeclampsia. sEng is the truncated splice variant of endoglin, which is a part of the cell surface TGF-β receptor complex (Venkatesha et al. 2006). It has been reported that cytotrophoblasts harvested from the placenta of women with preeclampsia in culture express higher sEng levels compared to normal cytotrophoblast cells. In addition, *in vitro* data shows inhibition of capillary tube formation by this protein (Gu, Lewis, and Wang 2008). Venkatesha et al. have studied the role of sEng in pregnant rats with vascular damage mediated by sFlt-1 through coadministration of sFlt-1 and sEng. They demonstrated that sEng could enhance the damage caused by sFlt-1 and induce severe preeclampsia-like symptoms as well as HELLP syndrome *in vivo* (Venkatesha et al. 2006). Similar to sFlt-1, elevated concentrations of sEng remit after delivery. Circulating levels of both sFlt-1 and sEng increase in early disease stages, even before the development of clinical symptoms (Rana et al. 2007). Therefore, it is suggested that both soluble factors induce similar downstream signaling pathways in the course of preeclampsia.

3.6. VEGFR1 (Flt-1) and VEGFR2 (KDR) and their isoforms

Flt-1 and KDR are both tyrosine kinase receptors that bind to VEGFA with high specificity. Upon VEGFA binding, KDR becomes activated by tyrosine transphosphorylation. Experiments on KDR knock-out mice proved that KDR activation is essential for endothelial development and maintenance (Shalaby et al. 1995). In contrast, FLT-1 acts as a decoy receptor modulating KDR signaling by scavenging VEGFA (Mac Gabhann and Popel 2007). This interaction is implicated e.g., in embryonal vasculogenesis. The dispensability of tyrosine kinase signaling via FLT-1 has been investigated in the study of Hiratsuka et al., who demonstrated largely unaltered vascular development in mice with deletion of the tyrosine kinase domain of FLT-1 (Kappas et al. 2008; Hiratsuka et al. 1998).

Binding characteristics and affinities of VEGFA to FLT-1 and KDR receptors differ. According to the study from Park et al., FLT-1 has a higher affinity of KD=10-20 pM to VEGFA than KDR with KD= 75-125 pM (Park, Keller, and Ferrara 1993), yet a study published in 1997 by Wiesmann et al. comparing VEGFA binding to KDR in monomeric and dimeric states showed that dimeric KDR binds more tightly to VEGFA than FLT-1 and monomeric FLT-1 has a 100-fold higher binding affinity to VEGFA than monomeric KDR (Woolard et al. 2004; Wiesmann et al. 1997).

FLT-1, also known as Flt-1, is a tyrosine kinase cell surface receptor, which is usually found on the surface of endothelial cells, fibroblasts, smooth muscle cells, and macrophages. FLT-1 is expressed in tissues such as the kidney, liver, heart, brain, and placenta. FLT-1 signaling is vital for angiogenesis, cell proliferation, migration, and cell survival (Dawson et al. 2009). In the absence of its specific ligands, FLT-1 remains in monomeric conformation and is inactive. Upon binding to VEGFA, VEGFB, and PlGF, the kinase receptor gets dimerized and activated by autophosphorylation of its intracellular tyrosine residues. Although in 1997 Wiesmann et al. showed that domain 2 of Flt-1 is sufficient for binding to VEGFA (Wiesmann et al. 1997). In 2004, Woolard et al. reported that the binding site of Flt-1 to VEGFA consist of extracellular immunoglobulin-like domains 2 and 3 (Woolard et al. 2004).

In another context, FLT-1 can also act as a decoy receptor of VEGFA signaling and thereby regulate and control vasculogenesis and vascular morphogenesis. Upon ligand binding and differential post-translational palmitoylation, the membrane FLT-1 can act as an intrinsic receptor that negatively regulates vascular morphogenesis (Boucher et al. 2017).

Alternative splicing of Flt-1 mRNA yields a 100 kDa glycoprotein called soluble Flt-1 (sFlt-1). sFlt-1 comprises the conserved ligand-binding domain while the intracellular kinase domain and membrane-spanning domain are absent (Kendall and Thomas 1993; Kappas et al. 2008). Hence this secreted protein is able to act as a decoy for VEGFA, VEGFB, and PlGF modulating signal processes via these growth factors.

So far, eight splice variants of human Flt-1 have been identified, seven of which lack the complete transmembrane domain (amino acid position 759 – 780) and the intracellular domain (Szalai et al. 2015).

VEGF receptor 2 is also known as kinase insert domain receptor (KDR) in humans and fetal liver kinase-1 (Flk-1) in mice. KDR binds to VEGFA, VEGFC, and VEGFD and plays an important role in angiogenesis, vascular development, and permeability. The kinase activity of KDR mediates MAP kinase and PI3K/AKT1 signaling pathways (Terman et al. 1992). VEGF-mediated activation of KDR at the surface of endothelial cells is required for physiologic endothelial function. VEGF-signaling promotes proliferation, migration, and survival of endothelial cells and regulates vascular permeability (Holmes et al. 2007). Specifically, VEGF-signaling via KDR on endothelial cells controls the production of the vasodilator nitric oxide (NO). In preeclampsia, NO levels are reduced in patient's serum, suggesting its contribution to arterial hypertension and endothelial damage (Seligman et al. 1994). Similar to Flt-1, the binding of KDR to VEGFA is facilitated by the extracellular immunoglobulin-like domains 2 and 3 of this receptor (Fuh et al. 1998; Munaut et al. 2012). KDR isoforms 2 and 3 lack the transmembrane domain and can act as soluble regulators of VEGFA, C, and D by limiting the abundance of free growth factors at the cell surface (Holmes et al. 2007).

In preeclampsia, the circulating levels of soluble FLT-1 and KDR are altered differently during the term of pregnancy and after delivery. Soluble FLT-1 (sFlt-1) levels increase during gestation and drop dramatically after delivery of the placenta, while soluble KDR levels are lower in preeclampsia compared to healthy pregnancies and stay low after delivery. Therefore, it is likely that the soluble FLT-1 is of placental origin, whereas the soluble KDR originates from endothelial cells (Munaut et al. 2012; Holash et al. 2002).

3.7. VEGF-Trap

Soluble FLT-1 and KDR have been of interest in cancer therapy due to their antiangiogenic function and restriction of cancer cell invasion. In 2002, Holash et al. designed a novel molecule that blocks VEGF-mediated angiogenesis in cancer, termed VEGF-Trap. VEGF-Trap (aflibercept) is generated by fusing the second Ig domain of VEGFR1 and the third Ig domain of VEGFR2 together to the Fc domain of human IgG1 (Holash et al. 2002). The dissociation constant of VEGF trap to VEGF ligand is about 1 pmol/L (Presta et al. 1997). Primarily, administration of VEGF trap completely abrogated hypertension in rats one to three days before intravenous injection of VEGF (Konner and Dupont 2004). Currently, VEGF-Trap has shown promising efficiency in several clinical studies to be used in cancer therapy and proved to be safe and effective in combination with radio- and chemo-therapies (Teng et al. 2010).

3.8. VEGF family

Vascular endothelial growth factor type A (VEGFA) is most extensively characterized among the members of the platelet-derived growth factors (PDGF) family. Besides VEFGA, VEGFB, VEGFC, VEGFD, the group of VEGF-related polypeptides comprises virus-encoded VEGFE, snake venom-derived VEGFF, and PlGF. All of these proteins naturally function as homodimers (Ogawa et al. 1998; Yamazaki et al. 2009; Iyer and Acharya 2011). As cystine knot proteins, VEGF dimers are connected by two intermolecular disulfide-bonds (Poltorak, Cohen, and Neufeld 2000).

VEGFA, is encoded by the *VEGFA* gene, located on chromosome 6 of the human genome. Several splice variants of VEGFA have been identified, increasing the complexity of this protein. Isoforms include VEGF121, VEGF165, VEGF189, and VEGF206 (Holmes and Zachary 2005). The first 151 N-terminal residues are conserved within all splice variants of VEGFA. In addition, they all share six common residues at the C-terminus. The receptor activation and binding domain consist of 110 amino acids. The other main domains involve a cell surface heparin-binding domain comprised of 44 amino acids and a 24 amino acid domain that facilities binding to the extracellular matrix (Fig. 2) (Keyt et al. 1996; Poltorak, Cohen, and Neufeld 2000; Robinson and Stringer 2001). Alternative splicing of VEGFA modulates its binding ability to VEGF receptors, heparan sulfate and neuropilins. For instance, VEGF206 and 189 isoforms are known to bind to neuropilins, and heparan sulfate while VEGF 121 does not.

In addition, different isoforms are known to exhibit different binding affinities for the same receptors. Based on Nano-BRET quantifications from Peach et al., the VEGF165 isoform shows a higher binding affinity to KDR than any other isoform. Isoform 165 also is reported to be the most abundant one of all isoforms in mammals (Peach et al. 2018; Houck et al. 1991). Mamer et al., by comparing more practiced isoforms under comparable physiological conditions, showed that VEGF121 has a weaker binding to KDR than VEGF165 (Mamer, Wittenkeller, and Imoukhuede 2020).

In 1996 Keyt et al. characterized the FLT-1 binding surface of VEGFA, utilizing charge-reversal mutagenesis studies. Later, some of the characterized residues were reported as binding surfaces of the KDR to VEGFA by Muller et al. This study revealed domains 2 and 3 as important locations extending along the VEGFA dimer interface that serve as binding epitopes for KDR Domain 4, 5, and 7 (Keyt et al. 1996; Poltorak, Cohen, and Neufeld 2000; Markovic-Mueller et al. 2017). The same year Wiesmann et al. generated the first crystal structure of the VEGFA-FLT-1 receptor complex. Based on the observation that five out of seven residues important for KDR binding are located within the interface of FLT-1 in a 3D structural model, Wiesmann et al. suggested that the VEGF binding sites to its receptors 1 and 2 are very similar to each other (Wiesmann et al. 1997).

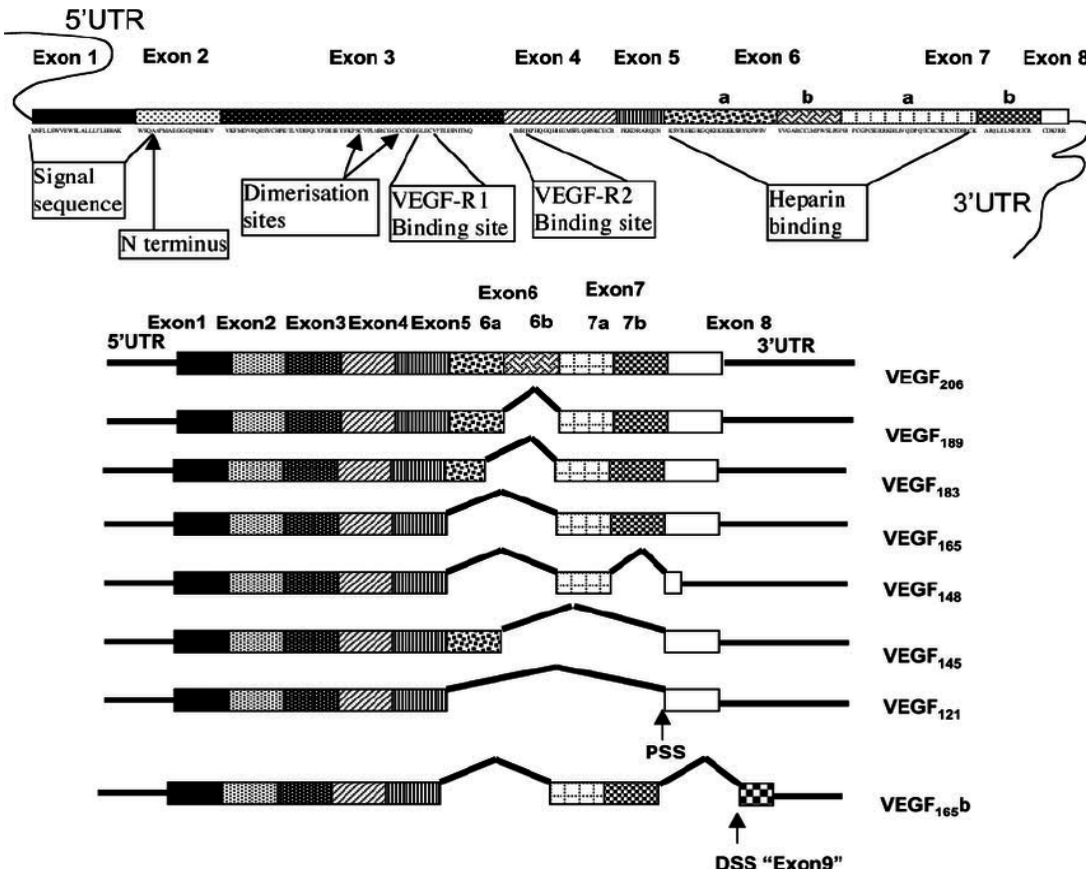

Figure 2: VEGFA domains and isoforms. (Woolard et al. 2004)

There is contradictory data on VEGF serum levels of patients with preeclampsia in different studies, which is most likely due to different measuring techniques and their ability to detect bound and free VEGF. For instance, in a study using an immunofluorometric assay, the levels of serum VEGF are reported to be higher in patients with preeclampsia versus healthy and non-proteinuric hypertensive pregnant women (Baker et al. 1995; Seligman et al. 1994). Yet, VEGF levels quantified by this technique are not limited to free VEGF but also include total serum VEGF. In other studies, where enzyme-linked immunosorbent assay (ELISA) against free VEGF was performed, free levels of VEGF in the serum of preeclamptic patients were found to be significantly decreased when compared to serum in normotensive pregnancies (Chielie et al. 2020).

Placental growth factor (PlGF) is another member of the VEGF family, which is mainly expressed in the placenta and in lower extents in the lung, liver, and heart (Maglione et al. 1991). The gene encoding for PlGF is located on chromosome 14 and can be spliced into four different variants: PlGF1, 2, 3, and 4. Isoforms 2 and 4 contain cell membrane-associated

heparin-binding domains (Yang et al. 2003; Hauser and Weich 1993). Predominantly, PlGF functions in the form of homodimers, however, natural heterodimers of VEGFA-PlGF were also reported. Whether these heterodimers confer pro- or anti-angiogenic effects is not clear (Birkenhager et al. 1996). PlGF binds to its specific receptors FLT-1 and neuropilin receptor-1, while, unlike VEGFA, it is unable to bind to KDR (Terman et al. 1994).

In a normal pregnancy, PlGF levels increase after 11 weeks of gestation and continue to increase until week 30 to about 140 pg/ml before they decrease. In contrast, sFlt-1 levels continuously increase throughout gestation. In preeclampsia, placental levels of PlGF in pregnant women are abnormally low for their gestational age, most likely due to abnormal placentation or due to scavenging of circulating sFlt-1 (Chappell et al. 2013). This low PlGF rate is detectable even before the appearance of signs of the disease as early as the second trimester of pregnancy. Therefore, in pregnant women, an elevated sFlt-1/PlGF ratio is used as a biomarker to predict the onset of preeclampsia (Agrawal et al. 2019). Clinically, in pregnant women with suspected preeclampsia, sFlt-1/PlGF ratio lower than 38 is considered as the absence of preeclampsia (Zeisler, 2016).

3.9. Treatment of Preeclampsia

Currently, there is no causal treatment for preeclampsia. In many cases, preterm delivery remains the only available effective treatment for these patients. Besides delivery, physicians manage the patient's symptoms by using medication. Since untreated hypertension can lead to severe cardiovascular, renal and cerebral complications, it is vital to treat high blood pressure in pregnant women with drugs such as methyldopa or labetalol (Berzan, Doyle, and Brown 2014). Another medication that is commonly used to manage preeclampsia or eclampsia is magnesium sulfate. Magnesium is shown to be beneficial for relieving cerebral vasospasms and elevates the convulsive threshold in eclampsia (Sadeh et al. 1989). Low doses of aspirin, started before 16 weeks of gestation, have been shown to decrease fetal mortality by 14% and the risk of preeclampsia by 17% (Duley et al. 2007). In a more recent study to prevent preeclampsia (ASPRE trial), women at high risk of developing preeclampsia were treated with 150mg aspirin per day from 11 to 36 weeks of gestation. These women had a significantly lower chance of developing preterm preeclampsia compared to their control group (Rolnik et al. 2017). In studies on rat models, PARP inhibitors have been effective in restoring the angiogenic balance and decreasing endothelial dysfunction, which might be of

therapeutic value in the future, although side effects have to be considered (Walsh et al. 2012). In addition, downregulation of placental sFlt-1 expression using stabilized siRNA has improved proteinuria and hypertension in a baboon model (Turanov et al. 2018).

Previously, Thadhani et al. established the first pilot study of adsorption therapy for retaining sFlt-1 from the maternal circulation. Their method is based on adsorption of positively charged sFlt-1 from maternal circulation by negatively charged dextran sulfate matrix. A total of twenty women with severe early preeclampsia were treated with dextran sulfate apheresis in two independent studies for the duration of 14 to 21 days. Apheresis treatments were applied in several sessions and proved to be safe to mother and fetus as well as effective, reducing 20-25% of circulating sFlt-1 per treatment. Interestingly, proteinuria was reduced significantly after each session. Although not powered for outcomes, this trial showed beneficial effects of sFlt-1 adsorption with regard to prolongation of pregnancy by 2 to 4 weeks, giving the fetus more time to mature and develop. After birth, no anomalies or complications were reported in the neonates. In addition, the results showed the trend, that the infants of moms who got dextran sulfate apheresis treatment had superior respiratory outcomes. (Thadhani et al. 2011; Thadhani et al. 2016).

Meanwhile, specific apheresis systems have been developed. Antibody-based adsorption of sFlt-1 in preeclampsia is currently investigated in a phase II trial. Recently, Trapiella-Alfonso et al. pioneered an *in vitro* study on VEGF-based apheresis of sFlt-1. The group developed a column comprising biotinylated bacterial expressed VEGF95 immobilized on magnetic beads. The truncated isoform of VEGF (VEGF95) could efficiently capture sFlt-1 from serum and liberate PlGF, reducing the sFlt-1/PlGF ratio in the serum of patients with preeclampsia by 68% (Trapiella-Alfonso et al. 2019).

4. Thesis aims

1. Design and characterization of affinity enhanced ligands for sFlt-1 to establish a competitive sFlt-1 apheresis system, which specifically and efficiently eliminates sFlt-1 and liberates endogenous VEGF and PlGF to enhance efficiency and tolerability of treatment.

Given the fact that angiogenic imbalance is the main cause of endothelial dysfunction and maternal systemic symptoms in preeclampsia, previously, there was a therapeutic approach implementing dextran sulfate apheresis to prolong gestation by clearing positively charged sFlt-1 from the serum of the patients. Yet this approach was not free of downsides. Dextran sulfate binds sFlt-1 nonspecifically. That means that by applying the serum to the column, not only sFlt-1 but all other positively charged molecules in the plasma could potentially be absorbed by the column, some of which might be necessary for mother and fetus. Besides, since binding to dextran sulfate beads takes place through the positively charged Ig domains of sFlt-1 and spare the ligand binding site of sFlt-1 (Thadhani et al. 2011), the binding between sFlt-1 and its ligands VEGF and PlGF will stay intact and thus eliminate endogenous VEGF and PlGF.

Currently, some pharmaceutical companies are developing an antibody-based apheresis approach for sFlt-1. In this system, monoclonal antibody against sFlt-1 is immobilized on the Sepharose matrix. The antibody specifically binds sFlt-1 in the shaft region of the receptor. Currently, his apheresis system undergoes clinical evaluation in a phase II trial. However, in principle, this setup, alongside specifically and efficiently eliminating sFlt-1 from the patients' circulation, might also increase the risk of initiating immunological side effects due to the full-length human IgG that is contained. In addition, since the antibody is not directed to the VEGF-binding site, endogenous VEGF and PlGF complexed with sFlt-1 will be eliminated as well.

A competitive apheresis approach can potentially eliminate sFlt-1 while liberating the growth factors VEGF and PlGF. The first proof of concept of competitive sFlt-1 apheresis was published recently where a bacterial expressed truncated VEGF isoform (VEGF-95) was able to clear sFlt-1 with high specificity while liberating PlGF.

In this thesis, we aim to extend the concept of competitive sFlt-1 further and generate the first clinically applicable apheresis system that, beside high specificity and efficiency in sFlt-1 clearance, is able to liberate plasma PlGF and VEGF.

2. Introduction of a suitable animal model for studying the renal pathophysiology of preeclampsia and testing novel therapeutic concepts *in vivo*.

The glomerular phenotype of preeclampsia is unique among glomerulopathies. Commonly in preeclampsia, nephrotic range proteinuria subsides within a few weeks after delivery, whereas in other glomerulopathies, recovery of proteinuria even after effective therapies takes for months. The mechanism of proteinuria which is generally conceived as podocyte disease with long time to recovery in the other glomerulopathies seems to be triggered by the endothelium in preeclampsia. Knowledge on the cross-talk between endothelial cells and podocytes as well as the direct contribution of endothelial cells to the filtration barrier is sparce. A mouse model of sFlt-1 mediated proteinuria as it is seen in preeclampsia could help to better understand glomerular pathophysiology of preeclampsia and even more so glomerular physiology of podocyte-endothelial-crosstalk.

Due to the complex pathophysiology of preeclampsia, which involves fetal trophoblast cells and maternal endometrial and endothelial cells, and also considering the differences in placentation in the class of mammals, finding a proper *in vivo* model that recapitulates preeclampsia seen in humans have been challenging.

So far, the majority of animal studies on preeclampsia are based on rat models, where the uterine arteries are manipulated to cause placental ischemia or mouse models, in which systemic symptoms of preeclampsia are induced by external application of recombinant sFlt-1 (Carter 2020; Li et al. 2007; Turanov et al. 2018; Makris et al. 2016; McCarthy et al. 2011).

In this thesis, we aim to introduce an inducible mouse model of transgenic expression of human sFlt-1, that represents renal manifestations of preeclampsia, enables us to study the renal pathophysiology of preeclampsia, and potentially allows to test novel therapeutic approaches *in vivo*.

5. Materials and Methods

5.1. Materials

5.1.1. Chemicals/reagents/solutions

Table 1: List of chemicals, reagents and solutions

Name	**Product no.**	**provider**
1-Step™ Ultra TMB-ELISA Substrate Solution	34028	Thermo Fisher
37% formaldehyd solution	4979.1	Th. Geyer GmbH
acid disodium salt dihydrate (EDTA)		
Agarose	16116	Thermos Fisher
Ammonium persulfate (APS)	A1142,0250	Applichem
Ammonium sulfate	3746	Carl Roth
Ampicillin sodium Salt	RO/K0291.000100	Th. Geyer GmbH
beta-Mercaptoethanol	A1108,0025	LABOMEDIC GmbH
Bouinsche Lösung	HT10132-1l	Sigma
Bovine Serum Albumin	A9418	Sigma
BS3 (bis(sulfosuccinimidyl)suberate)	21586	Thermo Fisher
Calcium chloride	RO/HN042.00050 0	Th. Geyer GmbH
Collagen II, Bovine	A1064401	Invitrogen
Complete protease inhibitor tabl. EDTA-free (PIM)	11873580001	Roche
Coomassie brilliant blue G-250	161-0400	Bio Rad
D1000 DNA Ladder	5067-5586	Agilent
D1000 Sample Buffer	5067-5602	Agilent
Dimethyl Sulfoxide (DMSO)	A3672,0100	AppliChem
Dithiothreitol (DTT)	R0862	Thermo Fisher
dNTP Set, 100mM Solution	R0182	Thermo Fisher Scientific
dNTPs	R0182	Thermo Fisher
Dulbecco's Modified Eagle Medium (DMEM)	D6429	Sigma
EDTA	E5134	Sigma
EGMTM-2 Endothelial Cell Growth Medium-2 BulletKit	CC-3162	Lonza
Ethanol 96% v/v partially denatured technical grade	2128000.072	PanReac AppliChem
Ethanol absolute	9065	Carl Roth
Ethidiumbromide solution 1%	2218	Carl Roth
Ethylenediaminetetraacetic acid	60-00-4	Sigma
Ethylenediaminetetraacetic acid disodium saltdihydrate (EDTA)	E5134	Sigma

Fetal Bovine Serum (FBS)	10270-106	Gibco
fuGENE HD Transfection reagent	E2311	Promega
GeneRuler 1kb DNA Ladder	SM0311	Thermo Fisher
GeneRuler 50bp DNA ladder	SM0372	Thermo Fisher Scientific
Glycerol	3783	Carl Roth
Glycine	3908.3	Carl Roth
Heparin	3862340	Rotexmedica
Histomount	HS-103	National Diagnostics
Hydrochloric acid	7332.1	Carl Roth
Hydrochlorid acid 2 N	T134	Carl Roth
Incidin Plus	3011520	Ecolab
Isopropanol	5752.3	Carl Roth
Kanamycin sulfate	K400	Sigma
Ketamine hydrochloride solution (Ketavet)	K-002	Merck
LB-Agar	X965	Carl Roth
LB-Medium	X964	Carl Roth
Loading dye solution (6X)	R0611	Thermo Fisher Scientific
Magnesium Chloride	1.05833.0250	Merck
Magnesium chloride hexahydrate	105833	Merck
Magnesium sulfate heptahydrate	P027	Carl Roth
Matrigel	356231	BD Bioscience
Mayer’s Hematoxylin Solution	MHS1	Sigma
Methanol	4627	Carl Roth
1MOPS	M1254	Merck
N,N,N´,N´tetramethylethylenediamine (TEMED)	2367	Carl Roth
Normal donkey serum (NDS)	017-000-121	Dianova
PageRuler plus prestained protein ladder	26619	Thermo Fisher Scientific
Paraformaldehyde (PFA)	P6148	Sigma
PBS Dulbecco Powder	L182-50	Biochrom
Periodic Acid 99%	3257	Carl Roth
Polyacrylamide	T802	Carl Roth
Potassium Chloride	6781	Carl Roth
ProLong Gold antifade reagent with DAPI	8961 S	New England Biolabs
Protease inhibitors	11697498001	Roche
Pure acetic acid 99% - 100%	7332	Carl Roth
Pure acetic acid 99% -100%	7332	Carl Roth
REDTaq® ReadyMix™ PCR Reaction Mix	R2523	Sigma
RNase-free water Ultra-Pure	10977-035	Invitrogen
RNase-free water Ultra-Pure	10977-035	Invitrogen
Schiff's Reagent	1.090.330.500	VWR
SDS pellets	CN30	Carl Roth
Sodium azide	S2002	Sigma
Sodium Chloride	S5886	Sigma

Sodium dodecyl sulfate (SDS) pellets	CN30	Carl Roth
Sulfuric Acid (H2SO4)	339741	Merck
Thiazole orange	17519	AAT Bioquest
Tris Base	T1503	Sigma
Tris Hydrochlorid (HCl)	9090.3	Sigma
TRIS hydrochloride	T3253	Merk
Triton X-100	108603	Merk
Triton X-100	A4975,1000	Applichem
Trizma Base	T1503	Sigma
Trypsin sor mass spectrometery	T6567	Sigma
Trypsin-EDTA solution (1X)	T3924	Sigma
Tween®20	3472	Caesar & Lorentz
Urea	V125	Sigma
Vectashield Mounting Medium with DAPI	H1200	Vector Laboratories
Water PCR Reagent	R2523	Sigma
Xylol >98%	371.5	Geyer

5.1.2. Buffer/solution

Table 2: List of buffers and solutions

Name	Composition
1% Triton-X 100 buffer	20 mM Tris-HCl pH 7.5 1% (v/v) Trition-X 100 50 mM NaCl 50 mM NaF 15 mM Na4P2O7 Complete protease inhibitors (PIM)
Anesthesia	6,8 ml 0.9% NaCl 1 ml 100mg/ml Ketamine 0.4 ml Xylazine
Base Solution	25 mM NaOH 0.2 mM EDTA pH 12
Binding buffer for streptactin-XT sephorase	50 mM Tris-HCl 150mM NaCl pH 8.0
Blocking solution for staining	5% (v/v) NDS in 1x PBST
Blocking solution for solid phase ELISA	2mM CaCl2 3% (v/v) BSA in TBS
Cell Freezing Solution	45% (v/v) FBS 45% (v/v) DMEM or RPMI-1640 10% (v/v) DMSO
Colloidal Coomassie Stock Solution	755 mM (NH4)2SO4 2.55% (v/v) Phosphoric acid 0.1% (w/v) Coomassie brilliant blue G-250
Colloidal Coomassie Solution	80% Colloidal Coomassie Stock solution 20% (v/v) Methanol
Demasking Tris-EDTA buffer	10 mM Tris-HCl 1 mM disodium EDTA 10% (v/v) TWEEN-20 pH 9.0
Elution Buffer	50 mM Tris-HCl 150mM NaCl 50mm biotin in NaOH pH 8.0
Fixing solution for Coomassie	25% (v/v) Isopropanol 10% (v/v) Acetic Acid

High Salt Washing Buffer	50mM Tris-HCl 1M NaCl pH 8.0
Laemmli Sample Buffer (2x)	100 mM Tris 4% (w/v) SDS 20% (v/v) Glycerol Bromophenol Blue 100 mM DTT pH 6.8
Laemmli Sample Buffer (5x)	250 mM Tris 10% (w/v) SDS 50% (v/v) Glycerol Bromophenol Blue 250 mM DTT pH 6.8
Mass Spectrometry Digestion Buffer	2 M Urea 50mM HEPES 50 mM Choloroacetamin (CAA) pH 8.0
Mass Spectrometry Elution Buffer	2 M Urea 50mM HEPES 5mM DTT pH 8.0
Mass Spectrometry Wash Buffer 1	50 mM Tris (pH7.5) 150 mM NaCl 5% (v/v) Glycerol 0.05% (v/v) NP-40
Mass Spectrometry Wash Buffer 2	50 mM Tris 150 mM NaCl pH 7.5
Neutralization Solution	40 mM Tris-HCl pH 5
Phosphate Buffered Saline (PBS)	137 mM NaCl 2.7 mM KCl 10 mM Na2HPO4 2 mM KH2PO4
Regeneration Buffer	50mM NaOH in H2O
Running Buffer	25 mM Tris 192 mM Glycine 0.1% (w/v) SDS
Stacking Gel	250 mM Tris 5% (v/v) PAA 0.2% (w/v) SDS pH 6.8

PBST	1 mM CaCl 0.5 mM MgCl2 1% Triton-X in 1 x PBS
Coupling Buffer for CNBr Sepharose	100 mM NaHCO3 150mM NaCl pH 8.3
SOC Medium	2% (w/v) Tryptone 0.5% (w/v) Yeast Extract 8.6 mM NaCl 2.5 mM KCl 20 mM MgSO4 20 mM Glucose
TAE (1x)	40 mM Tris 20 mM Acetic Acid 1 mM EDTA pH 8.5
TBS	50 mM Tris-HCl 150 mM NaCl, pH 7.6
TBST	2.5 % (v/v) tween-20 in TBS pH 7.6
Transfer Buffer	25 mM Tris 188 mM Glycine 0.1% (w/v) SDS
Wash Buffer for Solid phase ELISA	2mM CaCl2 in TBS pH 7.6
Wash Buffer for Western Blot	30 mM Tris 300 mM NaCl 0.3% (v/v) Tween-20 pH 7.5

5.1.3. Kit/Assay

Table 3: List of kits and assays

Name	**Product Number**	**Provider**
AminoLink™ Plus Coupling and Immobilization Resin	20394	Thermo Fisher Scientific
CNBr-Activated Sepharose™ 4 Fast Flow Affinity	17098101	GE Healthcare
Creatinine Assay Kit	Cay500701-480	Biomol
GeneJet Gel Extraction Kit	K0692	Thermo Fisher Scientific
GeneJet Plasmid Miniprep Kit	K0503	Thermo Fisher Scientific
GoTaq® DNA Polymerase	M3001	Promega
Human PlGF Quantikine ELISA Kit	DPG00	R&D systems
Human VEGF Quantikine ELISA Kit	SVE00	R&D systems
Human VEGFR1/Flt-1 Quantikine ELISA Kit	SV100C	R&D systems
Q5® Hot Start High-Fidelity DNA Polymerase	M0493	New England Biolabs
REDTaq® ReadyMix™PCR reaction mix	R2523	Sigma Aldrich
T4 DNA Ligase	M0202	New England Biolabs

5.1.4. Antibodies and enzymes

Table 4: List of antibodies and enzymes

Name	**product Number**	**Provider**
Alexa Fluor® 488 AffiniPure Donkey Anti-Guinea Pig IgG (H+L)	2340472	Dianova/Jackson ImmunoResearch
Alkaline Phosphatase, Calf Intestinal (CIP)	M0290	New England Biolabs
Anti-Human Beta-Tubulin antibody	T0198	Sigma Aldrich
Anti-Human p44/42 MAP kinase antibody	9102	Cell Signaling
Anti-Human phospho-p44/42 MAP kinase antibody	4370	Cell Signaling
Anti-Human phospho-VEGFR2 antibody	AF1766	R&D systems
Anti-Human VEGFR2 antibody	55B11	Cell signaling
Anti-Mouse CD31 (PECAM) antibody	AF3628-SP	R&D systems
Anti-Mouse IgG1, HRP conjugated	A90-105P	Biomol
Anti-Mouse IgG-Fc Fragment, HRP conjugated	A90-131P	mol
Anti-Mouse Nephrin antibody	20R-NP002	Fitzgerald
Anti-Wilms Tumor Protein (wt1) antibody	ab89901	Abcam
BamHI-HF	R3136	New England Biolabs
BglII	R0144	New England Biolabs
Cy3-AffiniPure Donkey α-Rabbit IgG (H+L)	711-165-152	Dianova/Jackson ImmunoResearch
Cy™3 AffiniPure Donkey Anti-Goat	705-165-147	Dianova/Jackson ImmunoResearch
Dpn1	R0176 S	New England Biolabs
Goat-anti-mouse IgG-HRP conjugated	115-035-003	Dianova/Jackson ImmunoResearch
Goat-anti-rabbit IgG-HRP conjugated	111-035-003	Dianova/Jackson ImmunoResearch
MluI	R0198S	New England Biolabs
MluI-HF	R3198S	New England Biolabs
NheI-HF	R3131	New England Biolabs

5.1.5.Material

Table 5: List of materials

Name	Product Number	Provider
10 cm dish for agar plates	82.1472.001	Sarstedt
8-Lid chain	65.989.002	Sarstedt
8-Lid chain lids, flat	65.989.002	Sarstedt
Blotting paper (Type BF4,580 x 580)	732-4094	VWR
Cell culture dish (96-wellF-Form)	655180	Greiner BioOne
Cell culture dishes (10-cm)	430167	Corning
Coverslips (round 18 mm no. 1.5)	CB00180RAC	Menzel Gläser
Crymold® standard	4557	Sakura
Cryovials 1,2ml PP	479-3221	VWR
Cytiva Whatman™ Grade 2V Folded Qualitative Filter Papers	09-832C	Fisher Scientific
Discofix®-3	4098102	Braun
Econo-Column® Chromatography Columns, 1.5 × 15 cm	7374156	Biorad
Fast thermal cycling plates 96well	4346907	Applied Biosystem
Fisherbrand™ Regenerated Cellulose Dialysis Tubing	21-152-3	Fisher Scientific
Glass cuvette	631-9511	VWR
Histosette® I	M499-11	Simport
Low temperature freezer cryo vials	10018-758	VWR
Marienfeld Superior™ Lamelles couvre-objets	111600	Thermo Scientific
Micro tubes (1.5ml)	72.690.001	Sarstedt
Millipore Immobilon-P transfer membranes	T831.1	Carl Roth
Nunclon cell culture flask, 80 cm2, straight neck, filter cap	178905	Thermo Scientific
Polypropylene conical tube (15 ml)	734-0451	VWR
Polypropylene conical tube (50 ml)	734-0448	VWR
PTFE Tubing	20531	Merck
Rotiabo®-syringe filters, 0.22µm	P666.1	Carl Roth
Rotiabo®-syringe filters, 0.45µm	P667.2	Carl Roth
Safe Lock 1.5ml Eppendorf tubes	301 23 328	LMS
Stripettes (10 ml)	4101	LMS
Stripettes (25 ml)	4251	LMS
Stripettes (5 ml)	4051	LMS
SuperFrost®/Plus microscope slides	H867.1	Th.Geyer Group
Syringe (1ml)	7392/2007	BD
TC-Plate 6 weel, Standard F	7478811	Starstedt
TipOne (0.1-10 µl XL), sterile	S1110-3810-c	Starlab
TipOne 101-1000µl graduated, sterile	S1111-2831-c	Starlab
TipOne 1-200µl beveled, sterile	S1111-1816-c	Starlab
Tissue culture dish with 20mm Grid	353025	Falcon

Venofix® Safety 21 G 3/4''	4056520-01	Braun
Weighing tray 100ml	611-9169	VWR
Weighing tray 300ml	2159.2	Carl Roth

5.1.6. Equipment

Table 6: List of the equipment

Name	Model/Product no.	Provider
Analogue tube roller	D-8400	Neolab
Autoclave	V-150	Systec
Avanti centrifuge	J-301	Beckman
BioPhotometer	6131	Eppendorf
Centrifuge (refrigerated)	Z216MK	Hermle
Confocal microscope LSM/Axiobserver Z1	LSM 710	Zeiss
Cryostat	CM1850 UV	Leica
Dumont #5 forceps	14098	WPI
Dumont #55 forceps	14099	WPI
FiveEasy Plus pH meter FP20-Std-Kit	30266628	Mettler Toledo
Forceps (for coverslips)	232-0111	VWR
Fusion Solo	60-FU-SOLO	PeqLab
Hamilton syringe (50 µl Typ 705)	549-1155	VWR
Heatingblock	TH 21	Ditabis
Hood	21928	Kojair
Horizontal electrophoresis system size L	401214	PeqLab
Horizontal electrophoresis system size S	40-0708	PeqLab
Incubator (agarose)	BD 115	Binder
Incubator (bacteria)	BD 115	Binder
Incubator (cell culture)	MCO-20AIC	Sanyo
JuLI Br live cell analyzer	91-JUBR04	PeqLab
Multipette® M4	613-2890	VWR
Microcentrifuge	5421	Eppendorf
Microtome	RM2235	Leica
Minicentrifuge	521-2844	VWR
Mini-PROTEAN® Tetra Handcast Systems	1658000FC	Biorad
Mithras multimode microplate reader	LB 940	Berthold Technologiies
Multichannel pipet	316-3706	VWR
Multifuge	4KR	Heraues
Nanodrop spectrophotometer	1000	PeqLab
Odyssey CLx		Li-COR
Operating scissor	501754	WPI
Pipetboy	613-4438	Integra
Pipettes: Research plus 3-Pack Option 1 (0,5-10µl,10-100µl, 100-1000µl)	613-1143	Eppendorf
Power supply	700-0115	VWR
Power supply	EV231	consort
Shaker	SSL3	Stuart
Slidescanner	SCN400	Leica
Suction pump	181-0067DE	VWR

Suction pump (cell culture)	HLC	DITABIS
Thermal cycler	070-601	Biometra
Thermal cycler	GE4832T/GE4852T	Bio-center
UV Transilluminator system	Ti5	Biometra
Vannas scissors	500086	WPI
Vortex mixer	444-1372	VWR
Water bath (for paraffin sections)	HI1210	Leica

5.1.7.Software

Table 7: List of software

Name	Version	Provider
Adobe Illustrator CS4	14.0.0	Adobe
Adobe Photoshop	11	Adobe
Finch TV	1.4.0	Geospiza Inc.
FusionCAPT	15.16	Vilber Lourmat
GraphPad Prism 8	8.4.3	GraphPad software Inc.
ImageJ/Fiji	1.52p	Wayne Rasband
ImageScope	12.3.2.8013	Aperio
ImageStudio	5.2	LI-COR
Microsoft Office Suite	2016	Microsoft
Nanodrop	3.7	Thermo Scientific
Serial Cloner	2.6.1	SerialBasics
ZEN software	2009	Zeiss

5.1.8.Online Software

Table 8: List of online software

Name	Website
Benchling	https://www.benchling.com/
Ensembel.org	http://www.ensembl.org/index.html
NCBI	http://www.ncbi.nlm.nih.gov/
NCBI Double Digest Finder	https://www.neb.com/tools-and-resources/interactivetools/double-digest-finder
NCBI Primerblast software	http://www.ncbi.nlm.nih.gov/tools/primer-blast/
NCBI Pubmed	http://www.ncbi.nlm.nih.gov/pubmed
Reverse Complement	https://www.bioinformatics.org/sms/rev_comp.html
Tm Calculator	https://tmcalculator.neb.com/#!/main

5.1.9. Cloning Primers

Table 9: List of cloning primers

Name	**sequence 5'→3'**
moVEGF165 forward	5-'ACAGCTAGCGCTCCTATGGCTGAAGGCGG-3'
moVEGF165 reverse	5'-TGTGGATCCCCGTCTGGGCTTATCGCAGC-3'
scVEGF165 forward	5'-ACAGCTAGCGCTCCTATGGCTGAAGGCGG-3'
scVEGF165 reverse	5'-TGTGGATCCCCGTCTGGGCTTATCGCAGC-3'
moPlGF forward	5'-ACAGCTAGCCTGCCTGCTGTTCCTCCTC-3'
moPlGF reverse	5'-TGTGGATCCCTCTACGAGGCACGGCGTCG-3'
scPlGF forward	5'-ACAGCTAGCCTGCCTGCTGTTCCTCCTC-3'
scPlGF reverse	5'-TGTGGATCCCTCTACGAGGCACGGCGTCG-3'
VEGF-M39R forward	5-AAAGCTGCAGCACCCATGGCAGAAGGAGGAG-3'
VEGF-M39R reverse	5'-ACACGTCTCTAGACATCTCTGAACTTCACCACTTCGTG-3'
VEGF-M39K reverse	5'-ACACGTCTCTAGACATCTTCGAACTTCACCACTTCGTG-3'
VEGF-M39K reverse	5'-ACACGTCTCTAGACATCTTCGAACTTCACCACTTCGTG-3'
VEGF forward	5'-ACACGTCTCTGTCTATCAGCGCAGCTAC-3'
VEGF reverse	5'-CAACGTCTCCCCTGATGAGATCGAGTAC-3'
VEGF-I67D forward	5'-CAACGTCTCGAGTACGATTTCAAGCCATCCTGTGTGCC-3'
VEGF-I67E forward	5'-CAACGTCTCGAGTACGAATTCAAGCCATCCTGTGTGCC-3'
VEGF-I67D reverse	5'-TTTGGATCCCCGCCTCGGCTTGTCACATCTG-3'

5.1.10.Genotyping Primers

Table 10: List of genotyping primers

Name	**sequence 5'→3'**
Col1a1 reverse	TGG TTT CTT TGG GCT AGA GG
Col1a1 forward	CCA TCC CAA CAA TAC ATC ACA
sFlt-1 forward	CAAGGACGTAACTGAAGAGG
sFlt-1 reverse	TTTCTTCCCACAGTCCCAAC
Tpbpa_Cre_Forward	CAATTTACTGACCGTACACC
Tpbpa_Cre_Reverse	TCCCCAGAAATGCCAGATTAC
ROSA-rtTA-common	AAGGGAGCTGCAGTGGAGTA
ROSA-rtTA-wt rev	CCGAAAATCTGTGGGAAGTC
ROSA-rtTA-mutant rev	TCATCAAGGAAACCCTGGAC

5.2.Methods

5.2.1.Nucleic acid analysis

5.2.1.1. Amplification of DNA using polymerase chain reaction (PCR)

For cloning, the PCR Q5® High-Fidelity DNA Polymerase kit was used according to manufacturer's instructions. Cloning primers are indicated in table 5.9. All components of the reaction were assembled on ice as following:

Table 11: Components of PCR reaction for DNA amplification

Component	**Reaction volume**	**Final concentration**
5X Q5 Reaction Buffer	10 µl	1X
10 mM dNTPs	1 µl	200 µM
10 µM Forward Primer	2.5 µl	0.5 µM
10 µM Reverse Primer	2.5 µl	0.5 µM
Template DNA	variable	< 1,000 ng
Q5 High-Fidelity DNA Polymerase	0.5 µl	0.02 U/µl
5X Q5 High GC Enhancer	(10 µl)	(1X)
Nuclease-Free Water	ad 50µl	

Reactions were transferred into a preheated thermocycler and the following protocol was run:

Table 12: Thermocycler program of PCR reaction for DNA amplification

step	**Description**	**Temperature (°C)**	**Time**	**Repeats**
1	Polymerase activation	95°C	2 min	
2	Denature	95°C	20 s	X 35
3	Annealing	Recommended primer Tm °C	10 s	
4	Extension	70°C	15 s/kb	
5	Final extension	70°C	2 min	
6	Hold	4°C	∞	

5.2.1.2. Cloning and mutagenesis of PlGF and VEGF165

Human placenta library was used for designing and amplification of moVEGF165 (NP_001165097; aa:27-191) and moPlGF (NP_001193941; aa:19-149). Specific PCR primers containing NheI and BamHI restriction, listed in table 9, were used for amplification of DNA fragments into a sleeping beauty transposon expression vector which has previously been

modified by group of the Prof. Manuel Koch. The vector bears an N-terminal BM40 signal peptide sequence and a C-terminal thrombin cleavage site. For facilitating purification, a double Strep II purification tag is located at the C-terminal directly after the thrombin cleavage site.

For cloning scVEGF165 and scPlGF, customized double-stranded linear DNA fragments were ordered in the form of GeneArt String DNA fragment from ThermoFisher Scientific, Germany. The double-stranded DNA fragments consist of two sets of amino acid sequences from VEGF165 (NP_001165097; aa:27-191) and PlGF (NP_001193941; aa:19-149). The sequence for the signal peptide was removed from the second monomer, and the two monomers were connected to each other via a linker with 14 amino acids, GSTSGSGKSSEGKG. Cloning sites for NheI and BamHI enzymes were added at the terminus of each fragment. To optimize cloning, similar cloning nucleotide sequence sites within the dimer sequence were exchanged in a way to conserve representing amino acid sequence. Specific PCR primers listed in table 9 was used to amplify the fragments, which were later cloned into the noted modified sleeping beauty transposon expression vector.

Golden Gate assembly system was used for the generation of mutation within moVEGF165. Four mutations, M39R, M39K, I67D, and I67E, were generated. For each mutant, a set of primers containing three PCR primers which are listed in table 9, was used. The final DNA fragment was the result of the combination of three smaller fragments, two of which contained the desired mutations. The assembly of three fragments was done utilizing Esp3I endonuclease. Like other previously explained constructs, the mutants were also cloned into the same modified sleeping beauty transposon expression vector via NheI and BamHI restriction sites.

5.2.1.3. Enzymatic Digestion

Enzymatic digestion of Plasmids, vectors, and PCR fragments were performed using restriction enzymes from New England BioLabs (NEB) or fast digest enzymes from ThermoFisher Scientific. For enzymatic digestion reactions, the following conditions were applied:

Table 13: Components of NEB enzymatic reaction

Component for NEB enzymes	**Amount**
Plasmid/PCR product	2 µg/27 µl
NEB buffer	3 µl
Restriction Enzyme (5U/µl)	0.5 µl
H2O	ad 30 µl

Table 14: Components of enzymatic reactions using fast digestion enzymes

Component for Fast digest enzymes	**Amount**
Plasmid/PCR product	400 ng/µl
Fast digestion buffer	10 µl
Restriction Enzyme (5U/µl)	1,5 µl each
H2O	ad 100 µl

Digestion reactions were mixed, centrifuged, and incubated at 37°C for 1 hour or overnight for optimal outcome. Digested vectors were treated with 1,5 µl calf intestinal alkaline phosphatase (CIP, NEB) for 30 min to remove 5'-phosphate groups from the DNA before storing them at 4°C.

5.2.1.4. Agarose gel electrophoresis

For analysis of DNA, samples were premixed with 6X DNA loading dye before running on a 1% or 2% (for small PCR products) agarose gel containing thiazole orange DNA-binding dye (Sigma-Aldrich) in 1X TAE buffer. In order to estimate the size of the DNA fragments on the gel, in each run, samples were loaded together with either 1 kb DNA ladder for Plasmids or 50 bp DNA ladder for PCR products (NEB). DNA was visualized using an Intas UV Trans-illuminator system. If required, excited desired bands were cut using a scalpel under UV or blue light for unstable PCR products.

5.2.1.5. DNA purification

DNA samples were purified using the GeneJET Gel Extraction Kit according to the manufacturer's instructions.

5.2.1.6. DNA Ligation

Ligation of PCR products into the vector systems was performed using T4 DNA ligase (ThermoFisher Scientific) together with normal or Rapid ligation buffer (ThermoFisher Scientific) according to manufacturer's instructions.

Table 15: Components of enzymatic reaction for DNA ligation

Component for NEB enzymes	**volume**
10X T4 DNA ligase /5X fast ligation Buffer	4,2 µl / 2 µl
T4 DNA Ligase	0,5 µl
Digested plasmid	1.5 µl
Insert fragment	1.5µl
H2O	ad 15 µl

Reactions were incubated at room temperature for 12 minutes (using fast ligation buffer) or 1 hour (using regular ligation buffer).

5.2.1.7. Bacterial heat shock transformation and plasmid isolation

60% of the ligation or control ligation reaction was added to 25µl of heat competent bacteria cells (E.coli DH10B T1 phage Resistant). The transformation was carried out by incubation of samples at 42°C for 45 seconds, followed by immediate incubation on ice for 2 minutes. 175µl of SOC medium was added to the bacteria and incubated at 37°C for 1 hour at a 900 rpm shaker in order to allow their regeneration. Finally, 80µl of bacteria were plated on ampicillin containing LB agar plate and incubated in a Heraeus B12 function line incubator, at 37°C, overnight. The following day, several bacterial colonies were picked and allowed to proliferate in 5ml LB medium supplemented with 100µg/ml ampicillin overnight at 37°C. Plasmid DNA was isolated and purified from 3ml of bacteria using the GeneJET Plasmid Miniprep Kit according to the manufacturer's instructions.

5.2.1.8. DNA Sequencing

Correct insertion of the plasmids was verified using automated Sanger sequencing offered by Microsynth, Lindau, Germany. 40-100 ng/µl plasmid DNA was premixed with 2pmol/µl

sequencing primers in H2O for a total volume of 10µl before sending samples for sequencing. Sequence readings were assessed using Benchling (https://benchling.com), FinchTV, and serial cloner windows software.

5.2.2. Cell culture

All cell culture work was performed under completely sterile conditions under a laminar-flow hood. For maintenance, the cells were incubated in a humidified incubator with 5% CO2 at 37°C.

Table 16: List of cell lines used in this thesis

Cell line	**Cell-type**	**Organism**	**Origin**
HEK293	embryonic kidney	human	ATCC
HUVEC	endothelial	human	ATCC

HEK 293 (human embryonic kidney) cells were cultured in Dulbecco´s Modified Eagle Medium (DMEM/F-12 + Glutamax, Invitrogen) supplemented with 10% FBS. For passaging, after washing cells with 1XPBS pre-warmed PBS, 1ml of trypsin was added to the cells and incubated at 37°C until the cells detached from the cell culture dish surface. For stopping trypsinization, 9 ml of DMEM medium containing 10% FBS was added to the cells. Finally, the desired number of cells were transferred to fresh culture dishes.

Collagen II coated six-well plates were used for culturing HUVECs (Human umbilical vein endothelial cells) at passage 3 with a maximum of 80% confluency. The cells were culture using a special medium for endothelial cells, Endopan 3 kit medium which contains 5% FBS, hydrocortisone, VEGF, hFGF-B, R3-IGF-1, ascorbic acid, hEGF, GA-1000 (Pan biotech, Bavaria, Germany). For maintaining low passage numbers, half of the cells were frozen each time they reached confluency. For passaging, cells were washed with 1X PBS and incubated with 1ml of trypsin at room temperature for 1 minute until the cells were no longer adherent. For stopping trypsinization, Dulbecco´s Modified Eagle Medium supplemented with 10% FBS was used. After centrifugation at 500rpm for 5 minutes and removing the supernatant, the desired number of cells were cultured in new collagen II coated, pre-warmed dishes. For starvation of HUVECs, cells were cultured with Endopan 3 medium supplemented with 3% FBS and without

additive growth factor supplemented for 24 hours. On the next day, cells were stimulated with the appropriate recombinant proteins as indicated and incubated at 37°C for 10-60 minutes, depending on the experiment.

5.2.2.1. Freezing and thawing cells

For freezing, cells were washed with pre-warmed 1X PBS prior to the addition of 1ml trypsin. After stopping trypsinization by adding 9 ml cell culture DMEM medium supplemented with 10% FBS, cells were centrifuged for 5 minutes at 500 rpm. The supernatant was discarded, and the cell pellet was resuspended in 1 ml of freezing medium containing 50% of the respective cell culture medium, 40% FBS, and 10% DMSO. The cell suspension was quickly transferred into a cryotube and placed in a freezing chamber to allow the slow temperature reduction of the cells to -80°C. For thawing the cells, cryotubes were placed into a 37°C water bath while keeping the lid over the water surface. Before full defrosting, cells were resuspended into 1ml of pre-warmed cell culture medium and immediately transferred into a fresh cell culture plate containing the appropriate volume of warm cell culture medium.

5.2.2.2. Transfection and protein production of designed constructs

For recombinant protein production, stable HEK293 EBNA cell lines were generated employing the sleeping beauty transposon system. Briefly, expression constructs were transfected into the HEK293 EBNA cells using the FuGENE® HD transfection reagent (Promega GmbH, Madison, USA) in DMEM/F12 supplemented with 6% FBS. After selection with puromycin, cells were expanded in triple flasks and induced with doxycycline. The supernatant of the cells was harvested every three days.

For the production of heavy proteins, the cell culture medium was exchanged with labeled media for three passages before inducing the protein production as well as during protein production. The labeling medium was prepared by supplementing a lysine and arginine-free DMEM media with 7% dialyzed FBS, 164 mg/ml lys 8, and 84 mg/ml arg 10.

5.2.2.3. Cell proliferation and viability assay

Passage 13 HUVEC cells were seeded onto a 96 well plate at a decreasing density, from 250,000 to 50,000 cells per well, and incubated in a CO2 incubator at 37°C for 24 hours. After one day of starvation, cells were treated with 25nM of the respective recombinant protein for 4 hours. To measure the viability of the HUVEC cells, MTT Cell Proliferation Assay kit (Cayman Chemical, USA) was used according to the manufacturer's instructions. In brief, 10µl MTT reagent was added to the cells on an orbital shaker and incubated for the duration of 4 hours in a 37°C 5% CO2 incubator until dark formazan crystals were formed. The crystals were dissolved by adding 100µl of crystal dissolving solution to each well and incubation for 16 hours. The absorbance of each sample at 570 nm was measured using a microplate reader. Quantification analysis was done using GraphPad PRISM 8 windows software.

5.2.2.4. Immunostaining of HUVEC cells

HUVEC cells passage 14 or 15 were cultivated on a glass coverslip until they reached 50% confluency. After starving the cells for one day, cells were treated with the respective recombinant protein for 4 hours. Cells were washed with 1x PBS and immediately fixed with 4% PFA for 10 minutes at room temperature. The fixation solution was washed off the cells three times with 1x PBS and blocked by adding 3% BSA for 30 minutes at room temperature (RT). Permeabilization was performed by incubation of the cells with 0.1% Triton X-100 in PBS for 1 hour at RT. Subsequently, cells were incubated with the respective concentrations of primary antibodies (Table 4) overnight at 4°C, followed by incubation with specific secondary antibodies for 1 hour at RT. Coverslips were mounted on the slide using mounting medium Prolong Gold containing DAPI. Images were acquired using a Leica SP8 confocal microscope with a 63X/1.4 oil immersion objective and LAS X 3.1.5 windows software.

5.2.2.5. Analysis of VEGF signaling using western blot

HUVEC cells were cultured in Starlab's six-well culture plates until they reached 80% confluency. Cells were starved for two days prior to treatments. Cells treated with conventional endothelial medium represented positive controls while cells on starvation medium served as a negative control. For treatments with recombinant proteins, cells were cultured in an endothelial medium containing all the supplements except for VEGF; instead, 40nM of the recombinant VEGF variants were added to 1ml of cell suspension. After incubation for a duration of 2 hours at 37°C, cells were lysed as a whole by applying 2x

laemmeli buffer directly to the wells. After Western blotting, membranes were stained with antibodies against phosphorylated VEGR2, KDR, and beta-tubulin.

5.2.2.6. Wound-healing assay

To measure the extent of migration upon treatment with VEGF variants, HUVEC cells were cultured in 24 well plates coated with collagen until they reached full confluency. The following day, cells were starved for two days, and a linear scratch was made in the center of the well, using a sterile pipet tip. After washing cells with PBS to remove the floating cell debris, HUVECs were treated with 40µM of the desired recombinant proteins while cells maintained on starving medium served as a negative control. The movement of the cells was captured using an EVOS microscope in intervals of 20 minutes for a duration of 20 hours. Quantification of captured images was performed by using the MiToBo Scratch Assay Analyzer plugin tool of the Fiji windows software.

5.2.2.7. Tube-like structure formation assay

48well cell culture plates were coated with growth factor-free Matrigel TM BM matrix (BD science). To this aim, prior to the assay, pipet tips and cell culture plates were precooled at 4°C. Matrigel was defrosted and brought to 4°C. 100µl of cool Matrigel was pipetted into each well on ice while avoiding bubble formation, creating a striated surface. The plates were incubated at a temperature of 37°C for one h until the Matrigel solidified. HUVECs were seeded on top of the surface of the Matrigel at a density of 50,000 per well. Cells were incubated to grow for one day with standard Lonza endothelial culture media. The next day, media was exchanged with starvation media containing 3% FBS for 24 h. Starved cells were treated with proteins for an additional 16 h. Tube-like structures were documented by applying bright-field microscopy using a JuLi microscope. Analysis of the tube length was performed manually using Fiji windows software.

5.2.3. Protein Biochemistry

5.2.3.1. Molecular modeling of recombinant proteins

This technique was done by Prof. Stetefeld without the contribution of the writer of this thesis and is cited at the end of the paragraph.

The linker was modelled using PyMOL 2.2 software and analyzed for structural restraints. The high-resolution crystal structure of VEGF-A in complex with VEGFR-1 domains D1-6

(pdbcode: 5T89) was used as a modeling template. The implemented single-point mutations of arginine (Arg) 39 and aspartic acid (Asp) 67 were subject to gradient energy minimization in the crystallography and NMR system. The lowest energy structures of the single-point mutant version were subject to 500 cycles of unrestrained Powell minimization. Harmonic restraints were imposed on the target molecule (2 kcal/mol) with increased weight (25 kcal/ mol). Protein structure and model assessment tools were used to verify the quality of the modeled structure (Matin et al. 2020).

5.2.3.2. Purification of recombinant proteins

A eukaryotic expression system using HEK293 EBNA cell lines was utilized for the production of recombinant proteins. An optimized sleeping beauty transposon system was stably introduced to HEK293 EBNA cells via transfection. For transfection, 1,8 µg desired DNA together with 0,2 µg of the transposase plasmid and 6µl FuGENE® HD transfection reagent (Promega GmbH, Madison, USA) was incubated for 15 min at RT and dropwise added to a 70% confluent HEK293 EBNA cell in a 6cm dish and incubated overnight at 37 °C. The cell culture medium sued for protein production was DMEM/F12 supplemented with 7% FBS. After three days, the transfected cells were selected using 0.5 µg puromycin. Upon confluency, the cells were distributed in triple flasks and treated with 0.5 µg/ml doxycycline for induction of protein expression. Every three to five days, the supernatant was exchanged and collected for the desired duration. In order to avoid the proliferation of cells more than confluent, 3 mM Na-butyrate was added to the medium, and FBS was reduced to 2%. The collected medium containing the secreted recombinant proteins were filtered via a paper filter and purified via Strep-Tactin®XT (IBA Lifescience, Göttingen, Germany) resin according to the manufacturer's instruction. Proteins were eluted by 1-5 ml biotin containing TBS-buffer (IBA Lifescience, Göttingen, Germany) in 5 fractions, and aliquots containing purified proteins were stored at -80°C. Protein quantification was performed using a Biophotometer device (Eppendorf, Model 613).

5.2.3.3. SDS-polyacrylamide gel electrophoresis

In order to analyze and separate proteins according to their molecular weight, an SDS page was performed. To that aim, gel cassettes were hand-cast prior to experiments. For each cast plate, first, 6 ml of Resolving Buffer was mixed with 0.15% TEMED and 0.1% APS and was poured into the cassette, with a layer of isopropanol covering the running gel creating an even surface. After completion of polymerization, stacking gel premixed with 0.15% TEMED and

0.1% APS was added on top of the running gel, and a ten-well comb was placed onto the stacking gel and allowed to solidify. Before loading, gels were assembled in a Mini-PROTEAN® Tetra Handcast Systems (Biorad), and a 1X running buffer was filled into the chamber of the system. Samples were loaded together with 3µl of pre-stained protein ladder (ThermoFisher). Electrophoresis was applied to the samples with 70V for 30 minutes, followed by 20 milliamps per gel for one hour and 45 minutes.

5.2.3.4. Colloidal Coomassie Blue staining

For checking the protein purification pattern, 5µl of the cell supernatant before and after protein purification, as well as 5µl of the washing buffer and all elution fractions, were collected. Samples were diluted in 5µl H2O and mixed with 10µl of 2x laemmeli buffer.

For urine samples, after centrifugation, 1 µl of supernatant was diluted in 9µl of H2O and mixed with 10µl of 2X laemmeli buffer.

Samples were cooked for 5 minutes at 95°C and loaded on a 10% Sodium Dodecyl Sulfate Polyacrylamide (SDS) gel electrophoresis. SDS gels were fixated using 30ml fixation solution for 30 minutes on a shaker at RT. After washing the gels with tap water, gels were incubated in a 30ml colloidal Coomassie brilliant blue solution that was pre-activated by the addition of 6ml methanol overnight at RT on a decolorization shaker. The next day, de-staining of the gels was performed using tap water for 16 hours at RT. Images from the gels were acquired using the Odyssey CLx image scanning device.

5.2.3.5. Western blotting

For visualization, proteins on the SDS-gel were transferred to a Millipore Immobilon-P polyvinylidene difluoride (PVDF) membrane. Membranes were activated with methanol for 3 seconds and washed with transfer buffer prior to transfer. The transfer sandwich was assembled by placing the first filter paper soaked with transfer buffer, PVDF membrane, SDS-gel, and a second filter paper while avoiding bobble formation. By applying an electrical field with a constant 12V current for 1 hour and 20 minutes, the electrotransfer of proteins from the SDS gel to the membrane was achieved. Afterward, the membrane was blocked with 25 ml of 5% BSA dissolved in SDS-washing buffer for 1 hour at RT. After washing the membrane three times with washing buffer, the respective primary antibody (Table 4, diluted in wash buffer) was applied to the membrane and allowed to incubate at 4°C overnight. Next, the membrane was washed three times with washing buffer, and an HPR-conjugated secondary

antibody with the dilution of 1:5000 was applied to the membrane for 1 hour at RT. Excess secondary antibody was washed off from the membrane with washing buffer, and membranes were developed using 200µl Clarity Western ECL detection solution (Bio-Rad Laboratories, US). Images were acquired using Fusion Solo chemiluminometer and fusion-CAPT windows software.

5.2.3.6. Negative stain electron microscopy

This technique was done by Dr. Morgelin without the contribution of the writer of this thesis and is cited at the end of the paragraph.

The structure of monomeric and dimeric VEGF was visualized by negative staining electron microscopy as described previously (Bober et al. 2010). Briefly, samples were incubated on carbon-coated grids for 1 min, washed and then stained with 0.75% uranyl formate for 1 min. Grids were rendered hydrophilic by glow discharge at low pressure in air. Specimens were examined in a Philips/FEI CM 100 TWIN transmission electron microscope operated at 60 kV accelerating voltage. Images were recorded with a side-mounted Olympus Veleta camera with a resolution of 2048 x 2048 pixels and the ITEM acquisitions software (Matin et al. 2020).

5.2.3.7. Solid phase binding assay

For ELISA style binding assays, a 96 well ELISA plate (Thermo Scientific, Denmark) was coated with 0.5 µg recombinant VEGF or PlGF or VEGF mutants in TBS overnight at 4°C as negative control wells were loaded with only BSA. After two times wash with TBS containing 2mM CaCl2, the wells were blocked for 1-2 hours with 5% MP/TBS/2 mM CaCl2. After three more washing steps, an increasing concentration of VEGF-Trap ranging from 0,1 to 750 nM was added to the wells. Detection of the ligand-receptor complex was done by the addition of an HRP-conjugated antibody which binds to the Fc domain of the VEGFR1/R2 trap. Luminescence OD 450nM was measured using a spectrophotometer (Thermo Scientific, Multiskan GO, Finland).

5.2.3.8. Generation of specific VEGF/PlGF columns

Immobilization of the recombinant protein on Strep-Tactin®XT matrix (IBA Lifescience, Göttingen, Germany) was performed on Polyprep® chromatography columns (Bio-Rad Laboratories, USA) according to manufacturer's instructions. The recombinant proteins

containing a strep-tag were incubated with the recommended amount of resin in TRIS 50 mM, NaCl 150mM, pH=8 overnight.

For immobilization of a recombinant protein on Cyanogen bromide activated resin (Merck, Germany) on Polyprep® chromatography columns (Bio-Rad Laboratories, USA), the proteins were dialyzed in coupling buffer containing 100mM NaHCO3, 500mM NaCl, pH=8.3 for two days. Beads were activated with 30 ml cold 1mM HCl for 15 min. The recommended amount of resin was incubated with the dialyzed proteins overnight at 4°C. The unbound surface of the beads was blocked by Tris-HCl 0.1M for 2 hours at RT.

For immobilization of a recombinant protein on an agarose matrix (AminoLink™ Plus Immobilization Kit, Thermo Fisher Scientific, USA), the manufacturer's instructions were followed. Briefly, recombinant proteins were incubated in coupling buffer pH=10, added to the resin, and incubated for 4 hours with 50mM NaCNBH3 in coupling buffer, pH=7.2. Blocking of the unbound surface of the resin was performed by incubation with 50mM NaCNBH3 in a quenching buffer.

In all cases, protein concentrations were measured before and after the coupling to determine the coupling efficiency. An equal concentration of around 500 mg/ml from each recombinant protein was used for immobilization to the corresponding resin.

5.2.3.9. VEGF, PLGF and sFlt-1 measurements

Quantification of Human sFlt-1, free VEGF, and PlGF concentrations was utilized by specific commercial ELISA kits (R&D Systems, Minneapolis, USA) according to the manufacturer's instruction. Quantification of colorimetric ELISAs was performed using a spectrophotometer (Thermo ScientificMultiskan GO, Finland). Data analyzing was facilitated with GraphPad Prism 9 software.

5.2.3.10. Precipitation of strep-tagged proteins from flow-through

After treatment of patient serum samples with the generated apheresis columns, the flow-through was collected and exposed to Strep-Tactin®XT (IBA Lifescience) beads as positive control recombinant strep-tagged VEGF was manually added to the flow-through. The beads were washed two times with TRIS 50 mM, NaCl 150mM, pH=8, 30µl. To elute the bound proteins from the bead, samples were boiled with 2x Laemmle buffer at 90°C. Analysis of the

results was done using SDS polyacrylamide gel electrophoresis, and immunoblots were stained with strep-tag-specific antibodies.

5.2.4. Determination of sFlt-1 isoforms via mass spectrometer

After validation of labeling efficiency of produced VEGF165, heavy VEGF165 molecules were immobilized on agarose matrix (AminoLink™ Plus Immobilization Kit, Thermo Fisher Scientific, USA). Serum of different patients was applied to the generated columns, and sFlt-1 removal in the flow-through was validated using the VEGFR1 ELISA Kit (R&D Systems, Minneapolis, USA). Afterward, the beads were washed several times using wash buffer of the AminoLink™ Plus Immobilization Kit, and an on-bead digestion affinity purification mass spectrometry protocol was performed. In brief, DTT was added to the beads to a final concentration of 5mM and incubated at 55°C for the duration of 30 minutes, followed by the addition of CAA to a final concentration of 40mM and incubation for 30 minutes at RT in the dark. After centrifugation for 10 minutes at 20,000 g, the supernatant was transferred into a fresh tube and stored at -20 °C prior to a targeted measurement of sFlt-1 by the Proteomics Core Facility of CECAD, Cologne.

5.2.5. Mouse experiments

All the mouse lines for this thesis were housed based on standardized specific pathogen-free conditions in the in vivo Research Facility of the University of Essen. All mouse experiments were carried out within the guideline frame provided and approved by the LANUV NRW (Landesamt für Natur, Umwelt und Verbraucherschutz Nordrhein-Westfalen/State Agency for Nature, Environment and Consumer Protection North Rhine-Westphalia) -Tierantragsnummer at LANUV is G1265/12, G1644/17, and G0364/17.

5.2.5.1. Genotyping of mice

Genotyping was performed using extracted DNA from ear or tail biopsies of mice. To this aim, tissue biopsies were incubated in 60 µl of Base solution at 95°C for 30 minutes. By the addition of 60µl of neutralization solution, the reaction was stopped. For the PCR reaction Mix, REDTaq® Ready MixTM, or GoTaq® Green Master Mix was used. The specific primer sequences used are listed under table 10. Detailed genotyping protocols are listed in the tables below (Table 17, 18).

Table 17: Reagents and program for genotyping hsFlt-1 transgene

hsFlt-1		**PCR program:**
ddH2O	8.5	
5x GoTag	11	95°C 5 min
Forward primer (10 pmol/µl)	1,5	94°C 45 sec
Reverse primer (10 pmol/µl)	1,5	60°C 45 sec
DNA	2,5	72°C 1 min
Total volume	25	goto step 2 and repeat 40 times
		72°C 5 min
		8°C forever

Table 18: Reagents and program for genotyping Rosa 26 rtTA transgene

Rosa 26 rtTA		**PCR program :**
ddH2O	11	
REDTaq® ReadyMix™PCR reaction mix	11	95°C 3 min
		94°C 30 sec
Forward primer (10 pmol/µl)	0,25	61°C 1 min
Reverse primer (10 pmol/µl)	0,25	72°C 1 min
DNA	2,5	goto step 2 and repeat 53 times
Total volume	25	72°C 2 min
		8°C forever

5.2.5.2. Whole animal perfusion, blood withdrawal and kidney collection

Animals were fully anesthetized via intraperitoneal injection of Ketamine/Xylazine using a 30-gauge needle. The anesthesia was administered for 0,1ml/10g mouse body weight. Using a standard scissor, the skin was opened up, exposing the chest cavity and heart. Prior to perfusion, blood withdrawal directly from the heart was performed using heparin containing needle. Blood samples were centrifuged at 11,000rpm for 10 minutes. Extracted plasma from the supernatant was stored at -20°C. For perfusion, a 30-gauge needle connected to cold PBS was inserted to the apex of the left ventricle while immediately cutting the right ventricle using surgical Vannas scissors. After allowing the blood to flow out of the animal for about 5-10 minutes, kidney tissues were collected and kept in 4% formalin at 4°C overnight. The next

day samples were immersed in cold PBS and processed via tissue processor in the Center of Pathology, University Hospital Cologne. Completely dehydrated samples were embedded in paraffin blocks for conservation.

5.2.5.3. Immunostaining of kidney tissues

For immunostaining, paraffin-embedded tissues were cut in 3µm thick sections via a hand section microtome (RD-495, China). The tissues were demasked prior to antibody staining by incubation in Tris-EDTA pH=9.0 at 110°C for 10 minutes. Blocking was performed by incubation with 3% fetal bovine serum overnight at 4°C. The next day, kidneys were then treated with primary antibodies overnight at 4°C. The dilutions used for anti-CD31/PECAM 1 polyclonal goat antibody was 1/1000, for anti-Nephrin polyclonal Guinea pig antibody was 1/200 and for anti-WT1 monoclonal rabbit antibody was 1/1000 in blocking solution. After several washing steps, respective secondary antibodies corresponding to each primary antibody were diluted in Tris pH=8 and incubated with the tissues for 1 hour. As a control for staining, the tissues were stained only for the secondary antibody. Kidneys were embedded with Prolong Gold antifade DAPI. Analysis and quantification of the pictures were obtained by a confocal immunofluorescence microscopy (SP8 confocal microscope, Leica Microsystems) on a 63x magnification.

5.2.5.4. Histochemical analysis of kidney tissues

For conventional light microscopy, harvested kidney tissues embedded in paraffin were cut in the section of 2µm via a hand section microtome (RD-495, China). Prior to the staining, tissues were rehydrated by 5 min incubation in a serial descending ethanol concentration, and after the staining, samples were dehydrated by incubation into ascending ethanol concentrations. Tissues were embedded with histomount and coverslips prior to imaging via a Leica SCN400 Slide Scanner on a 40x magnification.

5.2.5.5. Periodic Acid-Schiff staining

Rehydrated kidney tissues were incubated for 10 minutes in 0.9% periodic acid (Carl Roth, Germany) under a laminar flow hood. Then they were immersed in Schiff reagent (Merk Millipore, Germany) for 10 minutes. Finally, they were stained with Mayer's hematoxylin solution (Sigma Aldrich, United States) for 2 minutes prior to dehydration.

5.2.5.6. Acid- Fuchsin Orange G staining

Rehydrated kidney tissues were fixed by cooking the tissues with Bouin solution at 70°C for 1 hour. Staining started by incubation of the samples with Weigert's hematoxylin (Carl Roth, Germany) for 5 minutes, followed by immersing the tissues in a solution of 4% HCl, 63% ethanol for 10 seconds. Afterward, the tissues were incubated in 1% phosphomolybdic acid for a duration of 5 minutes before staining with AFOG solution for 10 minutes.

5.2.5.7. Determination of Albumin to Creatinine Ratio (ACR)

A Mouse Albumin ELISA kit (ICL/Dunn Labortechnik, Asbach, Germany) was utilized for measuring the concentration of mouse Urinary albumin. Urine samples were quickly centrifuged prior to the assay. 1 µl of urine samples were diluted 1:100000, and the concentration of albumin was determined according to the manufacturer's instruction. For measuring the concentration of Urinary creatinine, 1:20 dilution of urine samples was used in a colorimetric assay, and the creatinine levels were measured according to the Creatinine Assay Kit (Cayman Chemical, Michigan, USA) manufacturer's instruction. The albumin to creatinine ratio was calculated after adjusting the units.

6. Results

6.1. Molecular modeling and structural analysis of VEGF165 and PlGF mutants

In order to stablish an efficient, competitive sFlt-1 apheresis system, the most important step is to generate a biomolecule with a higher binding affinity for sFlt-1 than the natural ligands of the soluble receptor.

There is a considerable amount of literature on the crystal structure, function, and interactions between VEGF variants and their receptors available. Based on this information, two strategies were defined to increase the binding affinity of VEGF165 to sFlt-1: (1) substitution of amino acid residues in the binding motif of VEGF165 by site-directed mutagenesis and (2) connecting monomeric VEGF165 sequences to form higher-order homo-multimers of VEGF165 with the idea to gain better accessibility of the binding sites during apheresis.

In order to optimize the binding affinity of VEGF165 to sFlt-1 by targeted mutations, *in-silico* modeling of the VEGF165/sFlt-1-complex was performed by employing a CNS algorithm. According to the algorithm, the substitution of two uncharged amino acids (methionine and isoleucine) located at the ligand-receptor binding interface by charged amino acids (lysine/arginine and glutamic acid/aspartic acid, respectively) was predicted to increase the affinity of VEGF165 to sFlt-1. According to the prediction, exchanging methionine to lysine/arginine results in a positively charged guanidine anchor on the ligand that faces the negatively charged binding motif located on the receptor (Fig. 3, A). Replacing isoleucine with glutamic acid/aspartic acid forces a negative charge on the ligand that could stabilize the binding complex by forming a salt bridge with the positively charged lysine residue located at the opposite receptor site (Fig. 3, B). Subsequently, four different mutants of VEGF165 were generated, and sFlt-1 affinity was quantified as the equilibrium dissociation constant (KD) by ELISA style binding assay.

As a second strategy, single-chain VEGF165 dimers were generated to force VEGF monomers into multimerization. Based on the unique structural features of intermolecular disulfide

bonds in VEGF and PLGF, we were able to engineer higher-order multimers that bind to sFlt-1 with enhanced affinity.

It is well-known that monomeric VEGF consists of the growth factor cystine knot structural motif with three disulfide bridges. Two disulfide bridges stabilize an eight-residue-containing ring, while the third bridge passes through the ring. These bridges stabilize four-stranded central beta-sheets, extending from the cystine knot motif (Muller et al. 1997). In nature, VEGF as a dimer consists of (mostly) two identical monomers that are located antiparallel to each other and are linked via two covalent intramolecular disulfide bridges. The dimer is the active configuration of VEGF and can unfold the receptor binding sites (Muller et al. 1997). In the designed construct, two VEGF165 monomers were linked via a 14 amino acid linker to form single-chain VEGF dimers (scVEGF165). These dimers were tagged by a cleavable double strep tag to facilitate purification (Kowarz, Loscher, and Marschalek 2015) (Fig. 3, C). The short 14 amino acid linker interferes with the formation of the conventional side-to-side, antiparallel structure of the VEGF dimer. This forces an open structure of two VEGF165 monomers within a scVEGF165 molecule that allows the formation of multimers between more scVEGF165 molecules bound together via disulfide bridges (in the form of tetramers or multimeric chains) (Fig. 3, C+D).

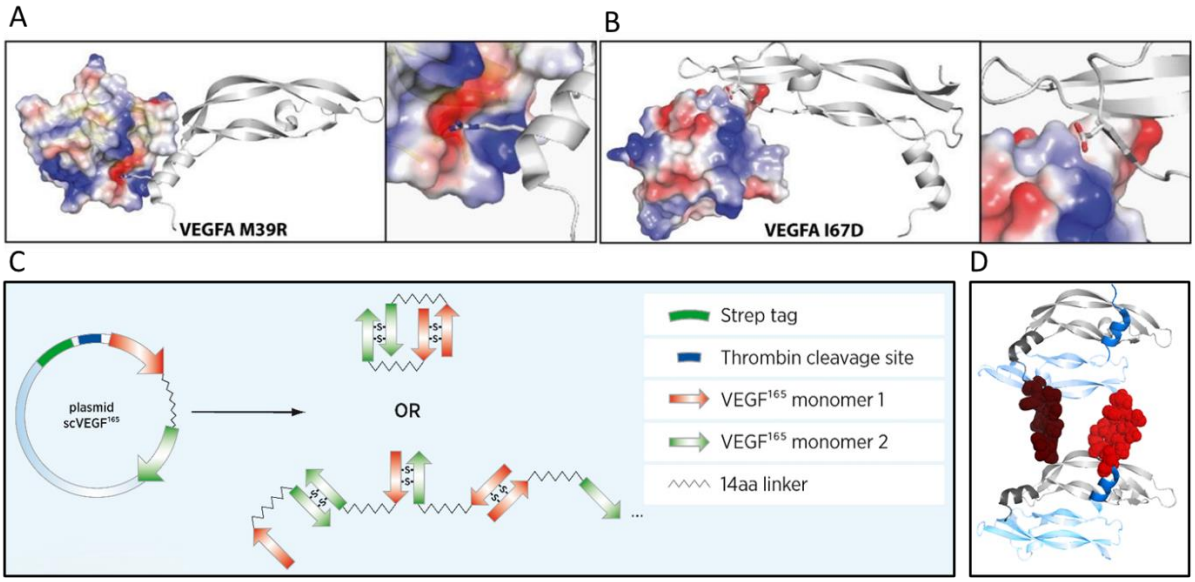

Figure 3: Molecular engineering and modeling of VEGF mutants (Matin et al. 2020). **A+B)** Schematic overview from the composite model of VEGF165/Flt-1 (domain D1-6) complex, shown in band and ribbon structures, representing the electrostatic surface potential at the binding surface of the two proteins. Color code Blue represents the positively charged regions, whereas color code red indicates the negatively charged regions. Based on gradient energy reduction predictions, improved VEGF165 binding could be achieved with the point mutations at the ligand-binding site M39R or M39K and I67D or I67E, which is represented as a stick model.

Forcing M39R mutation adds a positively charged guanidine anchor imposing the negative regions alongside the receptor biding motif (A), whereas point mutation I67D located at the þ-meander of VEGF165 builds an electrovalent bond with K223 residue of Flt-1 (B). **C)** Schematic cartoon of scVEGF165 expression plasmid and several potential routes of assembly into VEGF165 multimers. Possible intermolecular conformations are linked via disulfate bridges. **D)** Band and ribbon illustration of two superimposing single-chain VEGF165-dimers forming a tetramer. Dark and light red spheres represent the 14aa linker.

Since in a clinical setting, eukaryotic post-translational modifications (like glycosylation) might be needed for the proper function of proteins, and specific bacterial post-translational modifications may cause immunogenicity in eukaryotic environments (Kuriakose, Chirmule, and Nair 2016). In order to avoid the side effects of bacterial post-translational modifications in our clinical application, eukaryotic expression systems were employed for the production of recombinant proteins. The described recombinant mutants together with strap tagged PlGF and scPlGF (single-chain PlGF, composed of two PlGF monomers linked with the previously described 14 amino acid linker) were expressed as secreted proteins in HEK cells and purified under physiologic conditions from the supernatant (Fig. 4)

Since the expressed recombinant growth factors should be able to induce MAP kinase signaling cascade via KDR receptors (Narasimhan et al. 2009), the biological function of the recombinant proteins was assessed by staining for phosphorylated ERK 1 /2 signal as a marker for activated Map kinase signaling pathway in experiments using cultured HUVEC cells (Fig. 5). While starved cells showed reduction in phosphorylated ERK 1 /2 signal, recombinant monomeric as well as single-chain VEGF and PlGF showed activation of the MAP kinase signaling pathway.

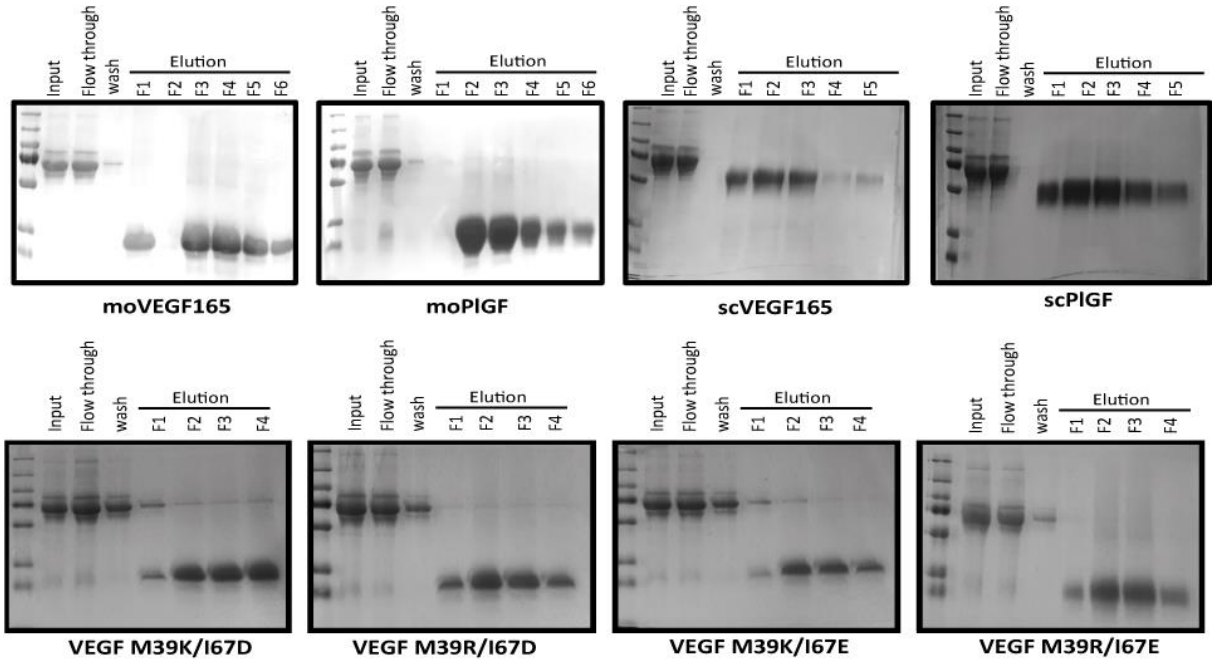

Figure 4: Coomassie staining of recombinant protein purification (Matin et al. 2020). Culture media supernatant of the cells stably expressing a recombinant monomeric or single-chain VEGF and PlGF, as well as the VEGF variants bearing the point mutations, were harvested and purified via Strep-Tactin purification resin. Supernatant medium is referred to as input. After washing the resin in the wash sample, no recombinant protein can be found, whereas a distinct and robust purification pattern in the Elution fractions is detectable (F1-F4/6).

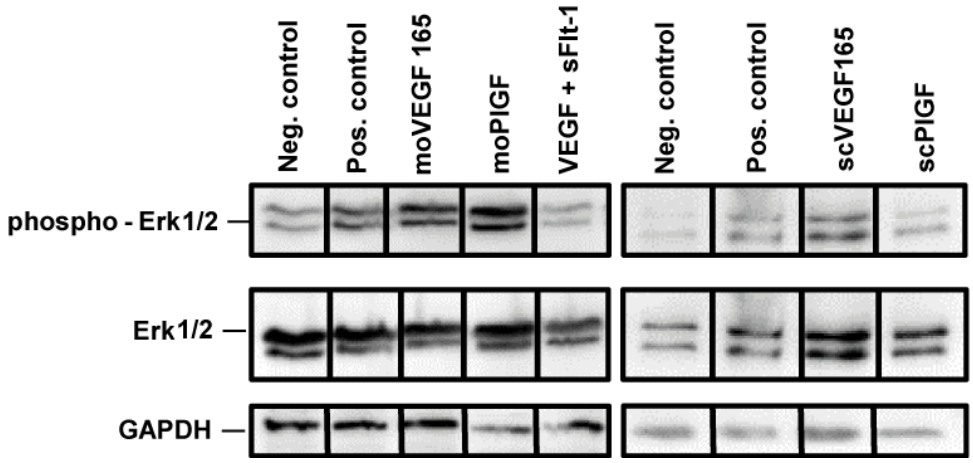

Figure 5: Assessment of molecular characteristic and function of recombinant sFlt-1, monomeric and single-chain VEGF, and PlGF (Matin et al. 2020). Activation of MAP-kinase pathway was evaluated in the starved HUVEC cells treated with the recombinant monomeric and single-chain VEGF and PlGF as well as sFlt-1 to approve functionality of these recombinant proteins. Cells treated with VEGF and PlGF variants were able to activate MAP-kinase transduction detected by immunoblot analysis using specific phosphorylated ERK1/2 antibody, whereas cells treated with sFlt-1 showed a reduction in the signal for phosphor-Erk1/2. Equal loading of the samples was referenced by staining against GAPDH and total Erk1/2 antibodies.

Utilizing negative staining electron microscopy enabled us to visualize the molecular structure of scVEGF165 and compare it to the structure of VEGF165 (Fig. 6). Monomerically expressed VEGF165 proteins formed instant dimers and appeared as dumbbell-shaped dimeric complexes under electron microscopy. In contrast, as expected, the scVEGF165 formed mostly clover-leaf-shaped complexes representing tetrameric structure with 2:2 configuration.

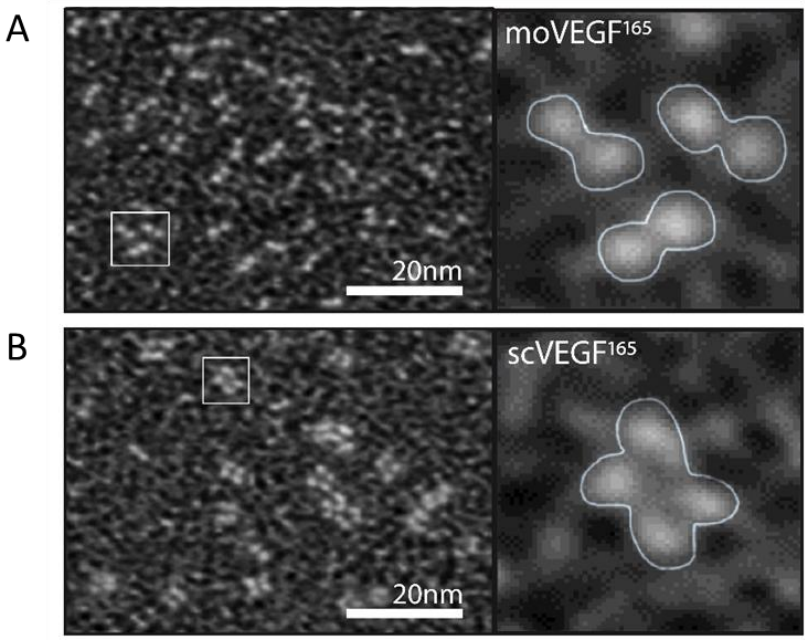

Figure 6: Negative staining electron microscopy revealing the molecular structure of scVEGF165 vs. moVEGF165 (Matin et al. 2020). Molecular configuration of purified recombinant moVEGF165 appeared as mostly dimeric dumbbell-shaped structures together with few monomeric dot-like structures **(A)**, whereas scVEGF165 configuration appeared as mostly tetrameric clover leaf-liked shapes together with few dumbbell-shaped single scVEGF165 molecules **(B)**. To facilitate the observation, a representative molecule was magnified and outlined on the right side of the picture.

6.2. Point mutations at binding motifs of VEGF165 to sFlt-1/Flt-1 do not enhance binding affinity

After successfully generating the recombinant proteins, the impact of VEGF165 mutational alterations at the VEGF-sFlt-1 binding region was studied. For measuring the alteration in binding affinity and static binding capacity of VEGF165 mutants compared to wildtype VEFG165, a serial dilution of VEGF-Trap was applied to the fixed VEGF165 mutants in an ELISA style binding assay (Fig. 7). Quantifications revealed that in contrast to the prediction of *in silico* modeling, bearing mutations at the binding site of VEGF165-sFlt-1 does not enhance the binding characteristics of VEGF165, and the dissociation constant remains unaltered compared to wildtype VEGF165.

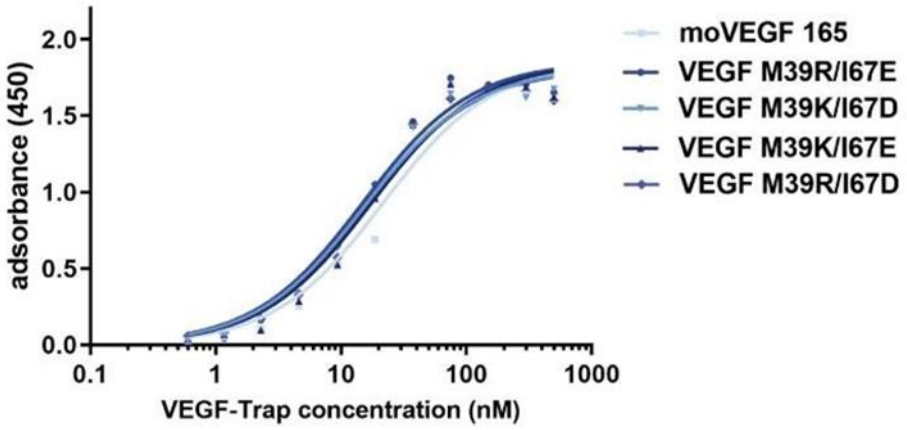

Figure 7: Biochemical characterization of VEGF165 mutants. Vs. moVEGF165 (Matin et al. 2020). The binding affinity of VEGF165 isoforms was quantified using a gradient concentration of VEGF-Trap in an ELISA-style binding assay. The equilibrium dissociation constant (Kd) is defined by the curve. Mutation in the VEGF165 binding site to Flt-1 didn't affect their binding affinity and static binding capacity when compared to the wildtype moVEGF165. Each depicted value is the average of three experimental triplicates (n=3).

6.3. scVEGF165 enhances sFlt-1/Flt-1 binding affinity

Next, we studied the binding characteristics of scVEGF165 as well as scPlGF and compared them to their wildtype forms. Once again, a solid ELISA-like assay utilizing VEGF-Trap was used for quantification of the equilibrium dissociation constant (Kd). As previously reported, moVEGF165 represented a 2-fold greater affinity when compared to moPlGF (Christinger et al. 2004). Interestingly, scVEGF165 displayed an 11% higher binding affinity to the receptor in comparison to moVEGF165. Moreover, looking at the binding assay curve, scVEGF165 showed a higher binding capacity compared to moVEGF165 as well. However, forcing multimerization did not change the binding characteristics of PlGF significantly (Fig. 8). Therefore, in this thesis, scVEGF165 would be used for further studies of proof-of-concept in our clinical applications.

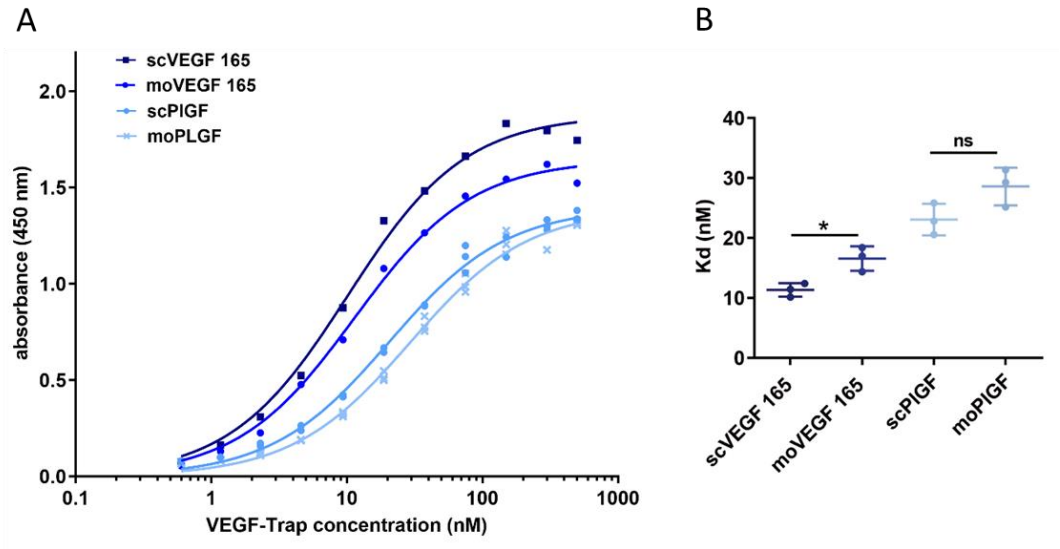

Figure 8: Biochemical characterization of VEGF165 and PlGF monomers vs. single-chain (Matin et al. 2020). **A)** The binding affinity of VEGF165 and PlGF monomers vs. single-chain was quantified using a gradient concentration of VEGF-Trap in an ELISA-like binding assay. The equilibrium dissociation constant (Kd) is defined by the curves. Each depicted value is the average of three experimental triplicates (n=3). **B)** Kd graph, comparing the binding affinities quantified for each molecule. The averages of standard deviations from three individual experiments are plotted. scVEGF165 represents the lowest Kd or the highest binding affinity. *P<0.018; ns: P>0.05.

6.4. Comparing VEGF signaling in HUVEC cells treated with scVEGF165 and moVEGF165

We have further investigated the functional characteristics of scVEGF165 compared to monomeric VEGF165 (moVEGF165) to see whether cells behave differently in the presence of scVEGF165 or moVEGF165. We have utilized human umbilical vein endothelial cells (HUVEC) since these cells express both VEGF receptor 1 (Flt-1) and VEGF receptor 2 (KDR) at their surface. After one day of serum starvation, cells were exposed to equal amounts of moVEGF165 or scVEGF165 for 4 hours while maintaining the control group on starvation. In order to visualize and quantify the VEGF signaling pathway, cells were directly stained with phospho-KDR specific antibody and lysates analyzed by SDS-PAGE and immunoblot using phosphor-KDR and total KDR antibody. While starved HUVEC cells showed no activated KDR receptor, cells treated with moVEGF165 showed activation of KDR receptors at their surface. Interestingly, cells treated with scVEGF165 exhibited a stronger and locally enhanced signal for phosphorylated KDR receptors at their surface (Fig. 9, A). Activation of the KDR receptor in cells treated with scVEGF165 and moVEGF165 appeared not to be significantly different in western blot analysis (Fig. 9, B).

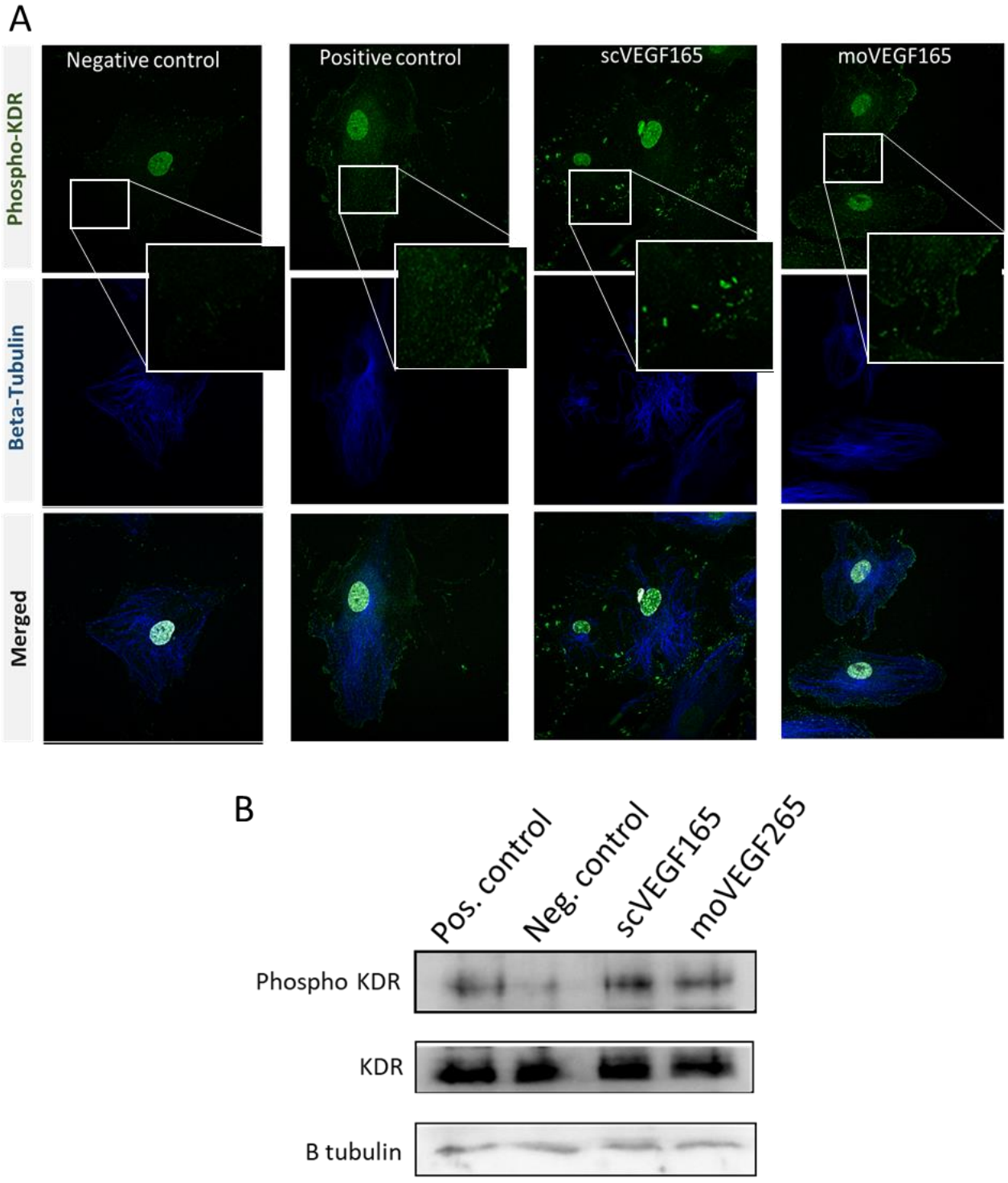

Figure 9: Difference in VEGF signaling in cells treated with scVEGF165 compared to moVEGF165. **A)** Higher activation and clustering of KDR receptor on the surface of HUVEC cells treated with scVEGF165 in comparison to moVEGF165, visualized by staining the cells with phospho-KDR antibody. **B)** Western blot analysis of HUVEC cells treated with scVEGF165 or moVEGF165 stained for phosphorylated KDR. Total cell KDR is visualized by staining against KDR antibody, while β-Tubulin serves as the loading control.

6.5. scVEGF165 and moVEGF165 induce similar cell proliferation and migration patterns

Functional activity of scVEGF165 and moVEGF165 with regard to cell proliferation and migration was assessed in cultured HUVEC cells. After two days of serum starvation, densely cultured HUVEC cells were treated with moVEGF165 and scVEGF165. A wound-healing experiment was used to test the ability of cells to migrate. Cells treated with scVEGF165 showed a slightly faster wound closure (Fig 10, A+B). However, discrimination between migration and proliferation is not precisely possible in this assay. In addition, proliferation assays were performed in starved HUVEC cells cultured in densities ranging from 0 to 300000. The cells were treated with recombinant scVEGF165 and moVEGF165, and the production of active metabolic indicator-purple formazan was measured using a colorimetric commercial MTT migration assay kit. Cells treated with scVEGF165 showed a slight increase in proliferation (Fig 10, A+B) and an increased purple formazan signal (Fig 10, C). However, changes in both assays were not statistically significant.

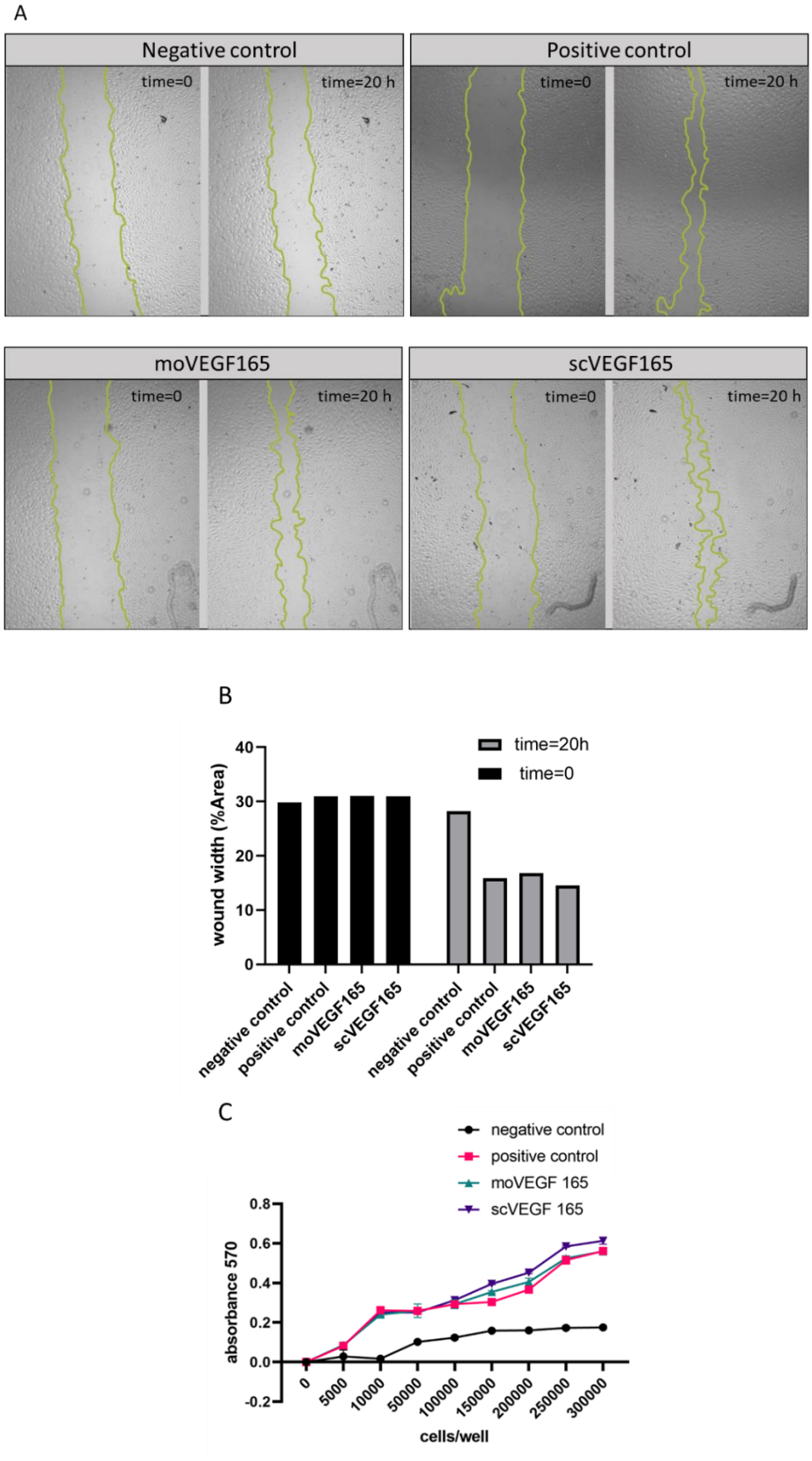

Figure 10: MTT assay absorption curve of cells treated with moVEGF165 vs. scVEGF165. A) migration of cells treated with scVEGF165, moVEGF165, and commercial VEGF165 before and after 20 hours of treatment. Magnification 4X. **B)** quantification of cell-free area, marked with yellow in section A, before and after 20 hours

of treatment. **C)** MTT absorption at 570 nm of different cell densities ranging from 0 to 300,000 cells per 96 well plate after 4 hours of treatment with recombinant proteins.

6.6. scVEGF165 promotes angiogenesis similar to moVEGF165

To test whether recombinant scVEGF165 and moVEGF165 trigger the formation of capillary-like tubular structures in endothelial cells, we performed a tube-like formation assay. HUVECs were cultured on a growth factor-free Matrigel, representing an extracellular matrix needed for the organization of tubes. After culturing and serum starvation of cells, the cells were treated with recombinant moVEGF165 or scVEGF165. Tube networking was quantified by measuring tube length, which is the distance between two nodes. Cells treated with wildtype VEGF served as positive control while starved cells served as a negative control. Indeed, the lack of growth factors in the starved control cells inhibited tube formation. Tube length parameters were comparable for the fully formed tube structures triggered by wildtype VEGF and recombinant moVEGF165. Although quantification of tube length from three experimental replicates revealed a slight increase in tube length under scVEGF165 treatment compared to moVEGF165, the difference was not significant, suggesting similar angiogenic effect cause my moVEGF165 and VEGF165 (Fig 11 A+B).

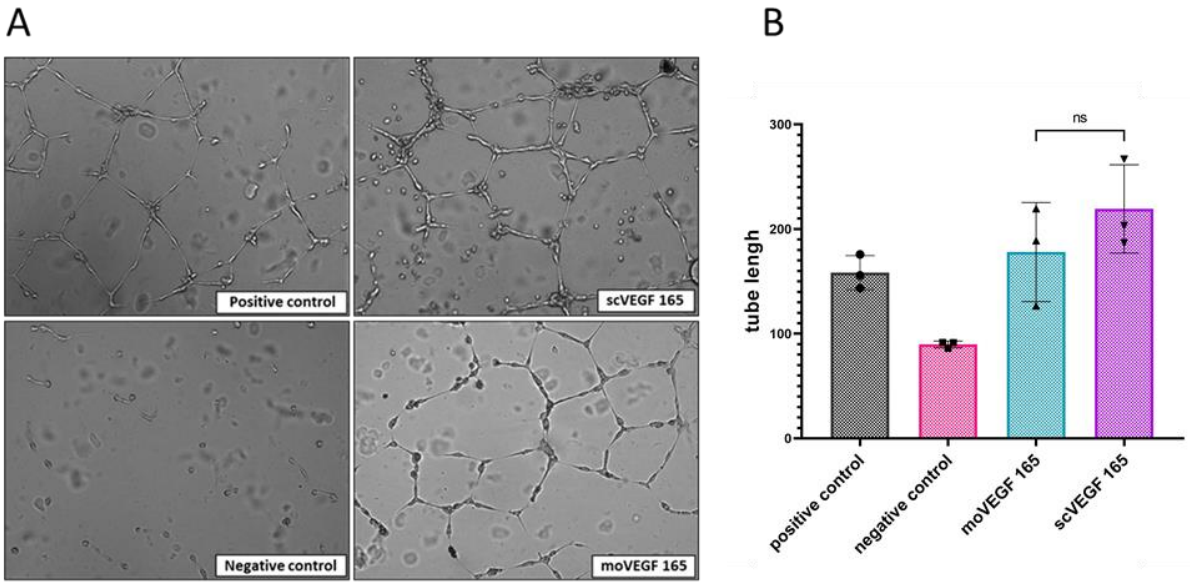

Figure 11: The effect of recombinant VEGF on endothelial cell tube formation. A) Representative picture of tube formation in cells treated with wildtype VEGF, moVEGF165, and scVEGF165. In the growth factor-free condition of negative control, no tube was formed. scale bar = 200µm. **B)** Quantification of tube length as measured by the distance between two neighboring nodes. Each dot represents the mean of tube length measured in one experimental replicate.

6.7. Assessing different substrate matrices and validating the stability of sFlt-1 capturing apheresis columns

In therapeutic applications, biomolecules are coupled to Sepharose or aldehyde-activated agarose inert matrices. These matrices are able to form covalent bonds with the linked biomolecule and thereby reduce the chance of leakage. Other non-covalent strategies, such as avidin-based interactions, have a greater chance of immunogenicity when used for in vivo purposes (Brunger et al. 2007). In order to optimize the matrix with regard to binding dynamics of the apheresis column, we immobilized moPlGF and moVEGF165 as well as scVEGF165 on three different matrices, namely Streptactin, cyanogen bromide activated Sepharose or aldehyde-activated agarose. Adsorption of recombinant sFlt-1 spiked into human serum samples was quantified using a commercial sFlt-1 ELISA kit. We observed significant clearance of sFlt-1 in all the coupled resins. However, the greatest sFlt-1 clearance in a single run with 84.4% was achieved by the column with immobilized scVEGF165 using aldehyde-activated agarose as the matrix (Fig. 12, A). Therefore agarose-based immobilization was used for further experiments. Furthermore, the stability of the scVEGF165-based agarose column was tested over a duration of 1 to 90 days after production of the column, and no substantial loss of binding was observed (Fig. 12, B).

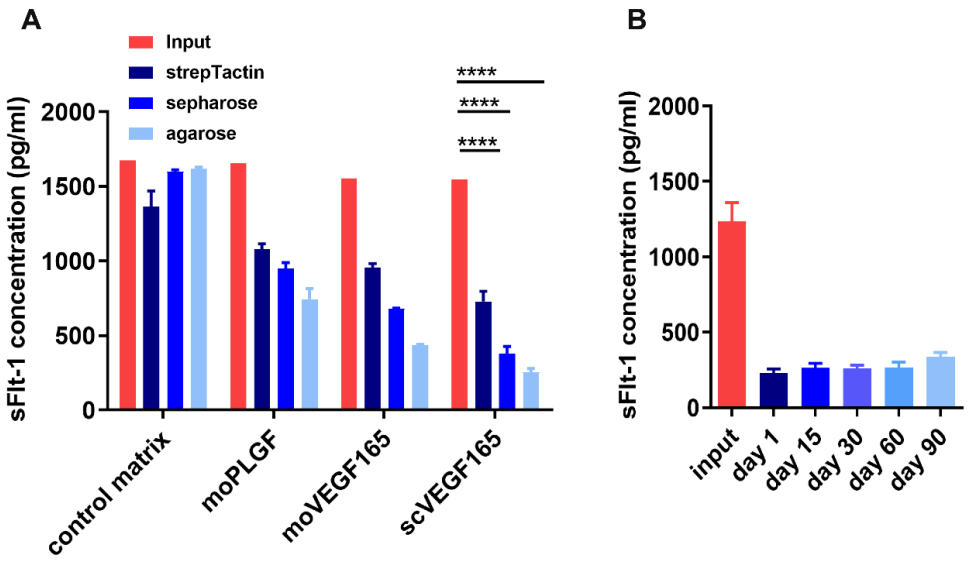

Figure 12: Capturing sFlt-1 using different ligands and matrices (Matin et al. 2020). **A)** Comparison of Strep-Tactin XT, CNBr-activated Sepharose, and amino-linked agarose matrices, equipped with equivalent doses of recombinant moPlGF, moVEGF165, or scVEGF165, to find the best apheresis configuration. For all three capturing molecules, coupling to amino-linked agarose generated the best yield of sFlt-1 reduction from human blood in a single run. The averages and standard deviations from three different experiments are plotted (****p< 0.0001). **B)** Longitudinal stability studies on sFlt-1 adsorption were performed within the duration of 90 days (1, 15, 30, 60, and 90). Columns used in this experiment showed promising stability even after storage at 4°C for 90 days with a slight reduction in efficiency.

6.8. Characterizing different sFlt-1 capturing ligands using the preeclampsia patient's serum

Next, we immobilized different sFlt-1 capturing molecules on an aldehyde-activated agarose-based matrix. The concentration of loaded proteins on the matrix was equally calculated, and the efficiency of coupling was measured after immobilization (Table 19). The capturing molecules included recombinantly expressed moVEGF165, scVEGF165, moPlGF, scPlGF, and a commercially available specific Flt-1 antibody. Concentrations of sFlt-1, free VEGF, and PlGF were measured by specific commercial ELISA kits for each protein before and after applying the serum samples to the respective column in a single run.

Whereas there was no evident change in sFlt-1, VEGF, and PlGF levels in control columns, clearance of sFlt-1 with the engineered columns depended on the specific ligand (Fig. 13). With moVEGF165 as ligand, 77.2% of serum sFlt-1 was cleared, which is comparable to the clearance results of using the sFlt-1 antibody. As expected, the least effective sFlt-1 reduction with 46.2% belonged to moPlGF. PlGF columns were unable to compete and release the serum's in-complex VEGF (Fig. 13, C). Antibody columns were unable to release both VEGF and PlGF (Fig. 13, B+C). Interestingly, single-chain VEGF dimers (scVEGF165) boasted an sFlt-1 reduction of 89.9% (Fig. 13, A) while simultaneously releasing large amounts of VEGF and PlGF in a single run (Fig. 13, B+C). Comparable to our previous results, single-chain PlGF (scPlGF) molecules were not able to significantly increase sFlt-1 clearance as well as VEGF and PlGF release compared to moPlGF (Fig. 13, A).

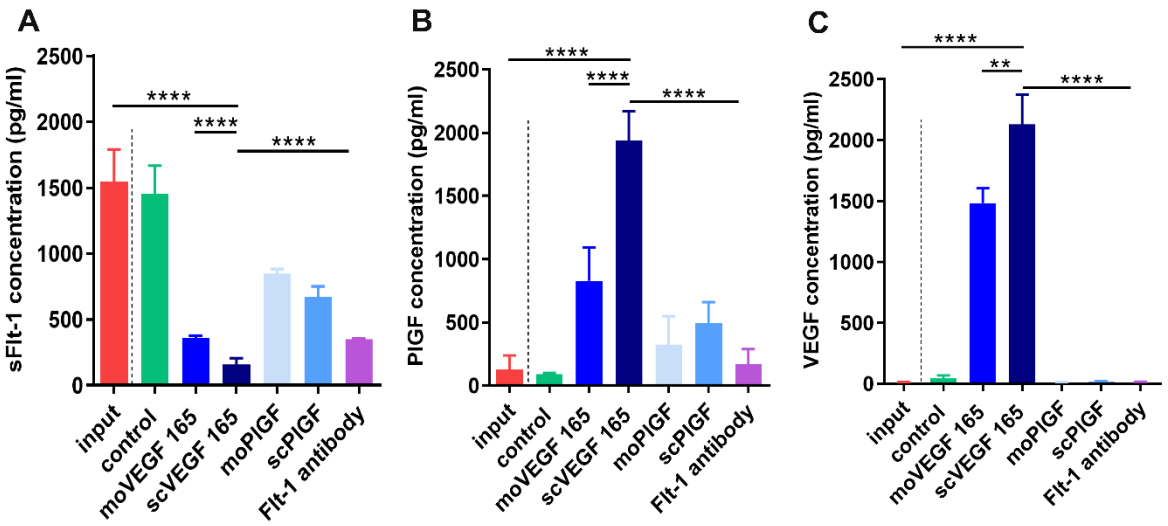

Figure 13: Characterizing the sFlt-1 ligands utilizing patient serum (Matin et al. 2020). **A)** all columns containing immobilized VEGF and PlGF variants, as well as the Flt-1 specific antibody, were able to reduce serum sFlt-1. Among all the columns, scVEGF165 with $p<0.0001$ showed the greatest efficiency in sFlt-1 reduction. **B)** As for the liberation of PLGF, the most pronounced PlGF release was achieved engaging the scVEGF165 column ($p<0.0001$). sFlt-1 antibody column failed to release any serum PlGF. **C)** VEGF liberation was only observed in moVEGF165 and scVEGF165 columns, with scVEGF165 showing more pronounced release ($p<0.0001$) compared to moVEGF165($p=0.0017$). PlGF and sFlt-1 columns failed to release any serum VEGF.

Table 19: Representative list of concentrations from proteins before and after immobilization on the resin to determine the coupling efficiency (Matin et al. 2020)

Protein name	**[Protein](µg/ml) before coupling**	**[Protein](µg/ml) after coupling**	**percentage**
mo $VEGF^{165}$ coupled agarose	519,1	0,192	99,96
mo $VEGF^{165}$ coupled CnBr	518,9	0,124	99,97
mo $VEGF^{165}$ coupled StrepTactin	518,5	0,187	99,96
moPlGF coupled agarose	487,9	0,161	99,967
moPlGF coupled CnBr	490	0,117	99,97
moPlGF coupled StrepTactin	489,2	0,158	99,96
mo $VEGF^{165}$ coupled agarose	513	0,113	99,977
sc $VEGF^{165}$ coupled agarose	538	0,189	99,96
VEGF DR coupled agarose	523	0,154	99,97
moPlGF coupled agarose	512	0,139	99,97
scPlGF coupled agarose	524	0,143	99,97
Flt-1 antibody coupled agarose	543	0,182	99,96

In clinical apheresis applications, leakage of the adsorbent is a great concern. We excluded doubts about leakage of recombinant VEGF or PLGF by taking advantage of the Strep-tag on the recombinant proteins. After running the serum samples over the competitive apheresis columns, Strep-tagged proteins were precipitated in the flow-through of serum samples. We analyzed the precipitated proteins by directly cooking the beads before SDS-PAGE and immunoblot with Strep-tag specific antibody. No evidence for the presence of recombinant VEGF or PlGF could be detected on immunoblot. The quantitative ELISA for Strep-tagged VEGF and comparing it to VEGF approves these data (Fig. 14, A+B).

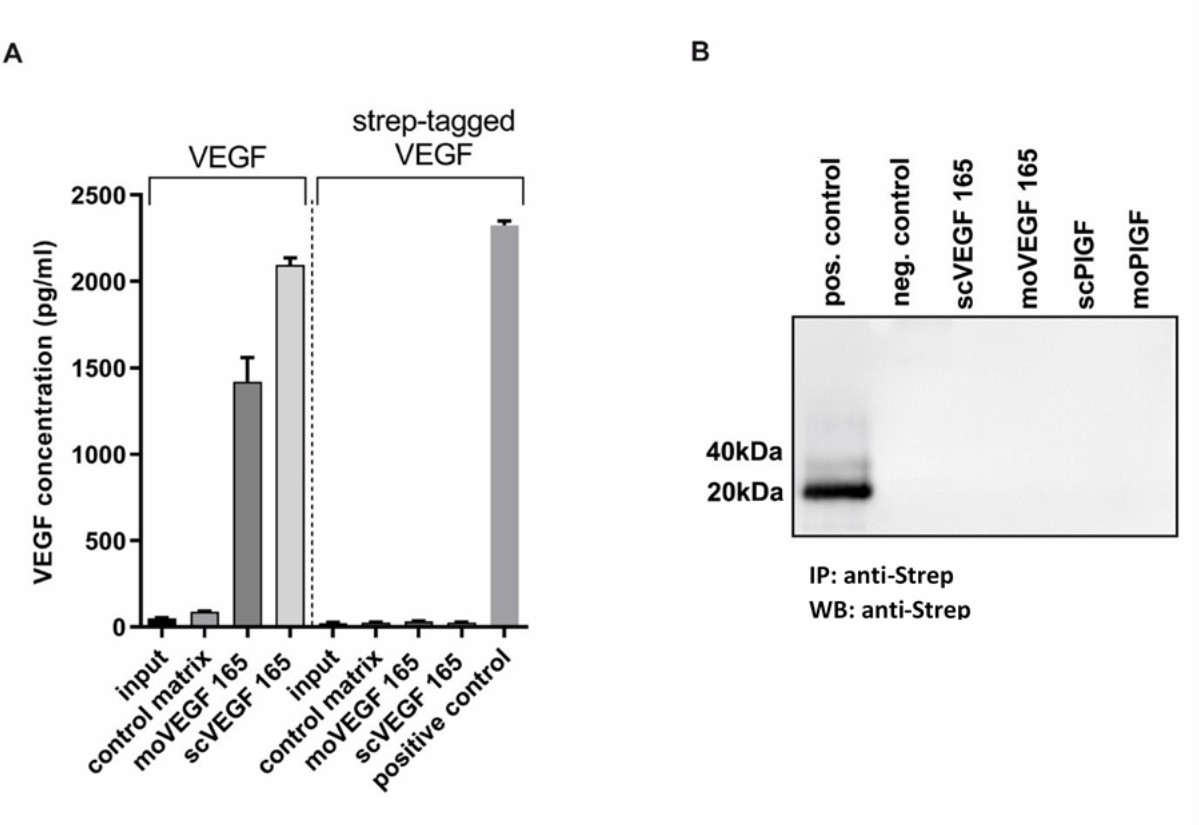

Figure 14: The robustness and stability of immobilization on agarose columns (Matin et al. 2020). **A)** Graph represents two different quantitative ELISAs performed on the flow-through of scVEGF165 column, on the left side of the panel VEGF ELISA and on the right side of the panel strep-tag ELISA. The graph indicates the detection of a high amount of free VEGF while detecting no strep-tagged scVEGF165. As a positive control, recombinant Strep-tagged scVEGF165 with a concentration of 2300 pg/ml was manually added to the flow-through. **B)** immunoblot analysis of precipitated proteins in the flow-through samples, treated with competitive apheresis using Strep-tag specific antibody. Unlike the positive control, no protein containing a strep tag could be detected on immunoblots.

6.9. Initial sFlt-1 plasma levels determine the amount of VEGF release

In order to investigate whether initial sFlt-1 levels affect the efficiency of the treatment and whether the amount of VEGF-release is linked to sFlt-1 clearance, we characterized the relationship between sFlt-1 clearance and VEGF liberation in serum samples with varying initial sFlt-1 levels. Descending serial dilutions of serum samples (D1-D5) were run over identical scVEGF165 apheresis columns. The serum sample belonged to a patient with severe early preeclampsia with initial sFlt-1 levels of 14,000 pg/ml. sFl-1 clearance was measured by a commercial-specific sFlt-1 ELISA. A great percentage of sFlt-1 in the diluted samples was cleared by the apheresis column (81.8 - 89.7%). Meanwhile, the reduction of the undiluted sample was only 47.2%. Most likely, this effect is due to saturation of the mini columns with an overall matrix volume of 200 µl (Fig. 15, A). VEGF release was quantified by performing specific VEGF ELISA on the flow, though. We observed that the released VEGF levels correlate with initial sFlt-1 levels (Pearson correlation: R=0.83) as well as with sFlt-1 clearance (R=0.96) (Fig. 15, B). These data suggest that apheresis via scVEGF165 columns indeed liberates endogenous VEGF from sFlt-1 binding. In addition, for future clinical applications, personalized treatment regimes modifying, e.g., treatment duration and efficiency of apheresis (ligand density), can be adapted based on initial sFlt-1 levels.

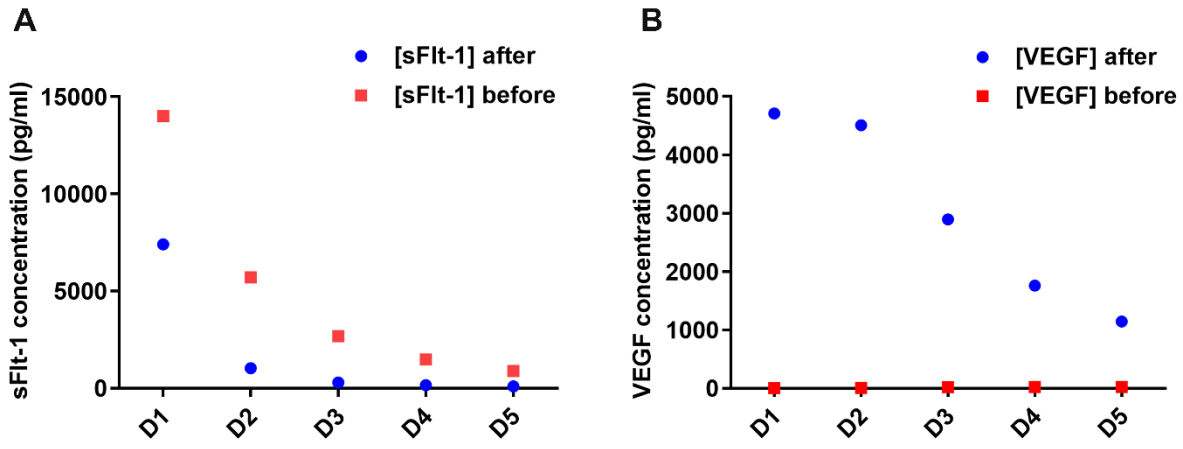

Figure 15: Graph showing the correlation of VEGF release with sFlt-1 reduction (Matin et al. 2020). A serial dilution (D1-D5) of a patient sample with similar initial sFlt-1-levels of 14000pg/ml was subjected to scVEGF165-apheresis. **A)** sFlt-1 is lowered by 87.4% in all dilutions (mean). The sFlt-1 decrease in the undiluted sample is 47.2 percent. **B)** VEGF liberation is influenced by the initial sFlt-1 levels as well as the efficiency of sFlt-1 removal.

6.10. Validation of scVEGF165-based apheresis in independent patient samples

To validate the previous results in a larger patient cohort, we performed sFlt-1 apheresis on ten independent patient samples from women with different severity of preeclampsia (according to clinical presentation and sFlt-1/PlGF ratio) at varying gestational ages. A single run over scVEGF-based agarose column was sufficient for a mean sFlt-1 reduction of 88% in all the samples (median 92.2%; SD 5.27) (Fig. 16, A). PlGF levels increased at a mean of 20-fold when compared to initial levels (median 14.6-fold; SD 5.40) (Fig. 16, B). VEGF levels increased with a mean of 9.1-fold compared to their initial levels (median 8.7.; SD 4.15) (Fig. 16, C).

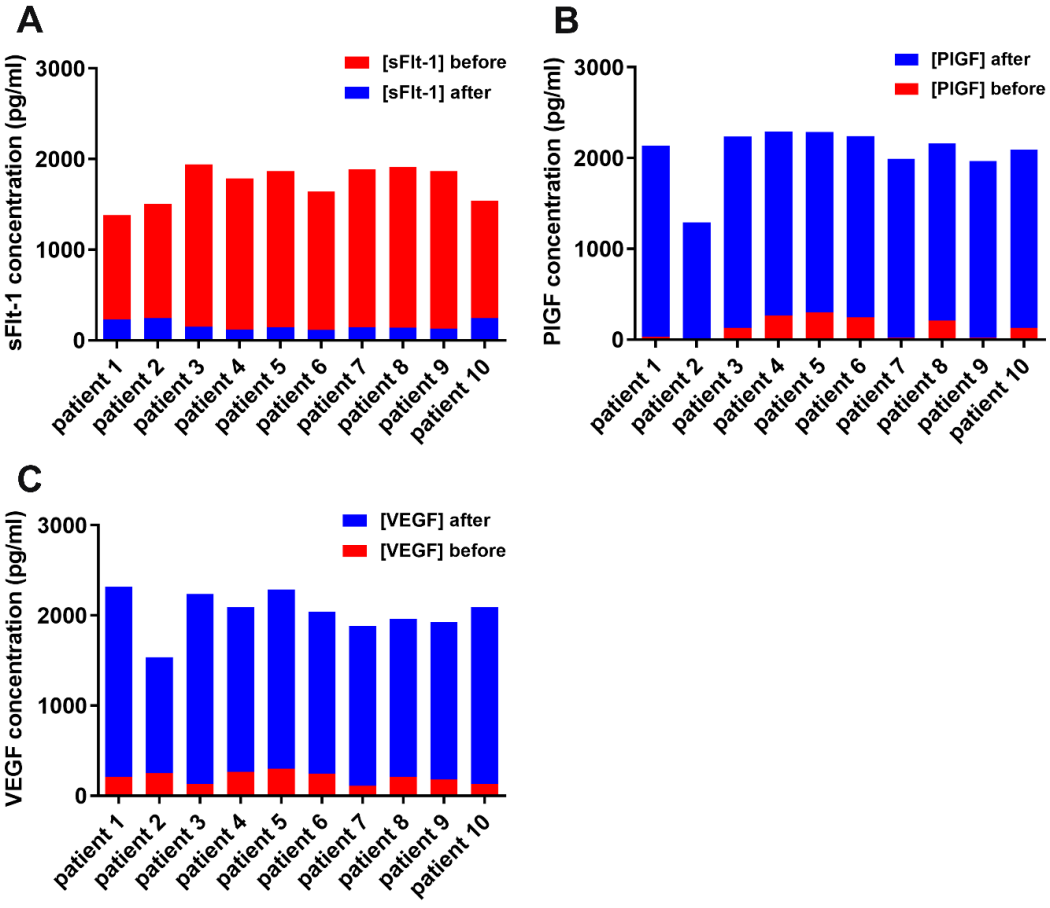

Figure 16: Validating the function of the scVEGF165 apheresis column using several patient samples (Matin et al. 2020). scVEGF165 apheresis was used to treat serum samples from 10 preeclampsia patients. Before (red) and after (blue) adsorption, the levels of sFlt-1, free PlGF, and free VEGF were assessed by ELISA. **A)** In all serum samples, sFlt-1 was lowered by an average of 88 percent (median 92.2 percent; SD 5.27%). **B)** PlGF release was measured as 20-fold (median 14.6; SD 5.40), and **C)** VEGF release was measured as 9.1-fold (median 8.7; SD 4.15) compared to starting values.

6.11. Characterization of sFlt-1 isoforms in samples of patients with varying severity of preeclampsia

In order to study the abundance of different sFlt-1 isoforms in the plasma of patients with preeclampsia and to investigate whether there is a correlation between disease severity and the predominant sFlt-1 isoform, we analyzed serum samples of patients at different stages of preeclampsia (Table 20). After absorption of sFlt-1 from patients' serum using the scVEGF165 agarose column, we subjected the adsorbate on agarose beads to an on-bead protein digestion protocol followed by identification of sFlt-1 unique peptides via mass spectroscopy. Knowing the characteristics of different sFlt-1 isoforms, we were able to identify several sFlt-1 peptides using a targeted measurement approach. In all patients, most of the detected peptides were commonly found in all the Flt-1 isoforms 2, 3, and 4. Only for Flt-1 isoform 3, also known as sFlt-1-14, a single unique peptide was identified, DQEAPYLLR (Table 21). However, due to high similarities between the sFlt-1 isoforms, and the abundance of detected sFlt-1 peptides belonging to all isoforms, this approach was not valid to discriminate between isoforms for diagnostic purposes.

Table 20: List of the patients with preeclampsia used in this experiment (Matin et al. 2020)

Patient No.	**Patient 1**	**Patient 2**	**Patient 3**	**Patient 4**	**Patient 5**
Abbreviation	PE 1	PE2	PE3	PE4	PE5
PE stage	severe PE	Sever PE	Fulminate PE	Fulminate PE	Late PE
Proteinuria	10g/g	1,2 g/g	300mg/g	300 mg/g	N/A

Table 21: Mass spectrometry measured data from the identified sFlt-1 peptides from the serum of patients with preeclampsia

Protein Accession	Peptide Sequence	PE 1 total area	PE 2 total area	PE 3 total area	PE 4 total area	PE 5 total area
P17948-2	TNYLTHR	4.25E+06	7.92E+06	4.49E+06	4.18E+05	1.25E+07
P17948-2	AFPSPEVVWLK	1.76E+06	5.60E+06	1.89E+06	6.80E+04	8.94E+05
P17948-2	DGLPATEK	1.91E+06	6.88E+06	3.68E+06	3.65E+05	1.16E+07
P17948-2	GYSLIIK	8.99E+05	3.16E+06	1.85E+06	2.86E+05	1.94E+06
P17948-2	AVSSFPDPALYPLGSR	1.82E+07	5.03E+07	2.92E+07	4.48E+06	5.14E+07
P17948-2	IESITQR	2.90E+06	1.07E+07	8.94E+06	1.22E+06	1.62E+07
P17948-2	DVTWILLR	8.36E+05	1.23E+06	6.77E+05	1.68E+05	1.93E+06
P17948-3	TNYLTHR	4.25E+06	7.92E+06	4.49E+06	3.55E+05	1.25E+07
P17948-3	AFPSPEVVWLK	1.76E+06	5.63E+06	1.89E+06	6.80E+04	8.94E+05
P17948-3	DGLPATEK	1.91E+06	7.05E+06	3.68E+06	5.33E+06	1.18E+07
P17948-3	GYSLIIK	9.03E+05	3.66E+06	1.85E+06	2.86E+05	2.02E+06
P17948-3	AVSSFPDPALYPLGSR	1.82E+07	5.03E+07	2.92E+07	4.48E+06	5.14E+07
P17948-3	IESITQR	2.98E+06	1.12E+07	9.75E+06	1.70E+06	1.74E+07
P17948-3	DVTWILLR	8.36E+05	1.23E+06	6.78E+05	1.68E+05	1.93E+06
P17948-3	**DQEAPYLLR**	6.62E+06	1.10E+07	6.97E+06	1.55E+06	2.46E+07
P17948-4	TNYLTHR	4.25E+06	7.92E+06	4.49E+06	3.55E+05	1.25E+07
P17948-4	AFPSPEVVWLK	1.76E+06	5.63E+06	1.89E+06	6.80E+04	8.94E+05
P17948-4	DGLPATEK	1.91E+06	7.05E+06	3.68E+06	5.33E+06	1.18E+07
P17948-4	GYSLIIK	9.03E+05	3.66E+06	1.85E+06	2.86E+05	2.02E+06
P17948-4	AVSSFPDPALYPLGSR	1.82E+07	5.03E+07	2.92E+07	4.48E+06	5.14E+07
P17948-4	IESITQR	2.98E+06	1.12E+07	9.75E+06	1.70E+06	1.74E+07

6.12. Finding a versatile animal model for preeclampsia

Animal models are indispensable for the further study the pathophysiology of preeclampsia and the evaluation of therapeutic approaches. In a cooperation project, we characterized transgenic mice overexpressing human sFlt-1 in an inducible system. These mice bear transgenic rtTA at the ROSA locus, which enables the induction of transgene sFlt-1 on the Col1A1 locus upon doxycycline treatment. Mice receiving sucrose treatment (here referred to as dox control) and mice lacking the transgenic hsFlt-1 allele served as wildtype controls. The systemic induction of sFlt-1 in mice was performed at mid-pregnancy 10.5 dpc. The experimental animals were sacrificed at the end of pregnancy at 18.5 dpc for histologic analysis.

6.13. Overexpression of hsFLT-1 in mice affects glomerular morphology and function.

Renal tissues harvested from mice at 18.5 dpc were subjected to conventional light microscopy. In glomeruli of mice overexpressing hsFlt-1, endothelial cells appeared swollen and capillary lumen were occluded. This histologic finding is called endotheliosis and is pathognomonic for anti-angiogenic states such as in preeclampsia. To visualize fibrosis in kidney sections, we employed AFOG staining. In wildtype mice as well as dox control mice, glomerular morphology was regular (Fig. 17). In mice expressing sFlt-1, stronger blue staining of basement membranes and glomerular mesangial areas represents more fibrosis as compared to controls (Fig 17, A). Analysis of urinary albumin/ creatinine ratio (ACR) was performed to assess glomerular function. Mice expressing sFlt-1 showed elevated ACR compared to the control groups, suggesting that overexpression of sFlt-1 is sufficient to cause damage to the glomerular filtration barrier (Fig. 17, B).

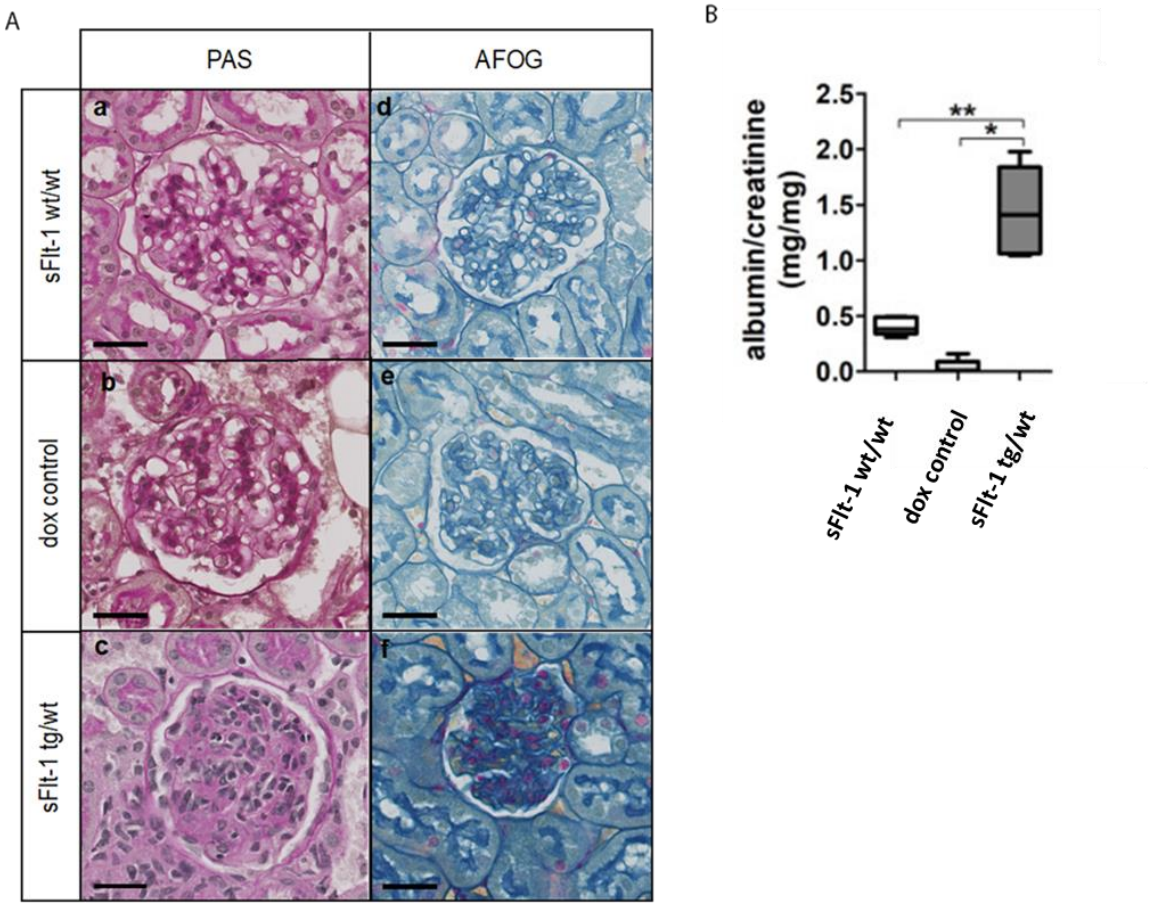

Figure 17: Histologic analysis of kidney tissue (Vogtmann et al. 2021). **A)** Histological analysis of mice at day 18.5 post coitum. Unlike sFlt-1 wt/wt mice and dox control mice, mice with ubiquitous overexpression of human soluble fms-like tyrosine kinase 1 (hsFLT1) demonstrated glomerular endothelial cell hypertrophy and mesangial expansion leading to occlusion of the capillary lumen. In addition, these mice demonstrated glomerular lesions represented by rich collagen staining. Scale bar: 80µm. **B)** Albuminuria of hsFLT1/rtTA mice was quantified by determination of the urinary albumin/creatinine ratio (n=5 for each condition). Mice with ubiquitous overexpression of hsFlt-1 showed a significantly higher albumin/creatinine ratio compared to control mice (P value= 0.0089).

6.14. Potential involvement of both endothelial cells and podocytes in proteinuria in mice overexpressing hsFLT-1

Further characterization of kidney sections from mice overexpressing sFlt-1 was done by performing immunofluorescence staining using specific antibodies against renal tissue markers. Double labeling was achieved by employing distinctly labeled secondary antibodies to the following primary antibodies: Nephrin antibody served as a marker for the slit diaphragm, PECAM (CD31) served as a marker for endothelial cells, and WT-1 was used as a marker for podocyte cells. In mice carrying sFlt-1 negative Col1A1 alleles as well as in dox control animals, Nephrin staining showed the classic garland appearance representing the fine slit-diaphragm located on the outer aspect of the capillary tuft. The latter is stained by anti-PECAM antibody marking endothelial cells in close proximity of the slit diaphragm staining without direct overlay (Fig. 18, A). Staining for WT-1 marks nuclei of podocytes and allows for quantification of podocyte number per glomerulus (Fig. 18, B). In contrast, stainings on renal sections of mice overexpressing sFlt-1 showed diminished Nephrin, WT-1, and PECAM signals. The garland-like signal of Nephrin is lost, and immunoreactivity appears discontinuous and patchy. Similarly, PECAM is not detectable on the whole capillary loop circumference. Lastly, WT-1 is positive in fewer cells per glomerular cross-section as compared to wildtype control as well as dox control animals. These data suggest that an increase in serum sFlt-1 negatively impacts the main cell components of the filtration barrier by damaging endothelial cells and podocytes, resulting in loss of slit diaphragm integrity and in disturbance of the glomerular filtration barrier.

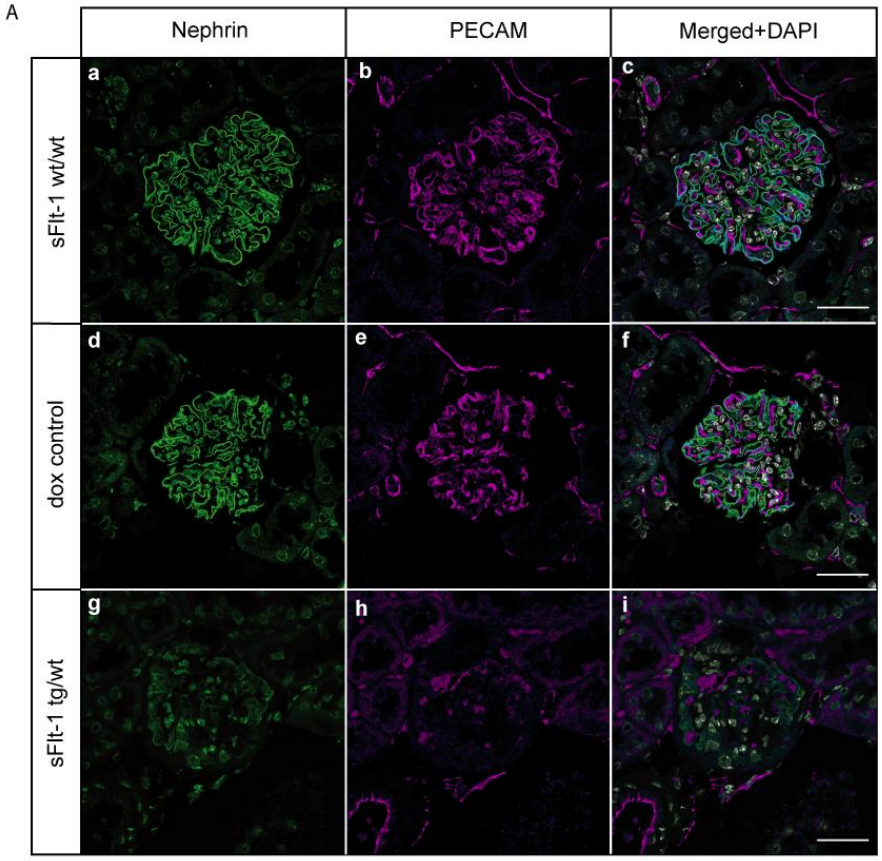
A
Nephrin
PECAM
Merged+DAPI
sFlt-1 wt/wt
dox control
sFlt-1 tg/wt
a
b
c
d
e
f
g
h
i

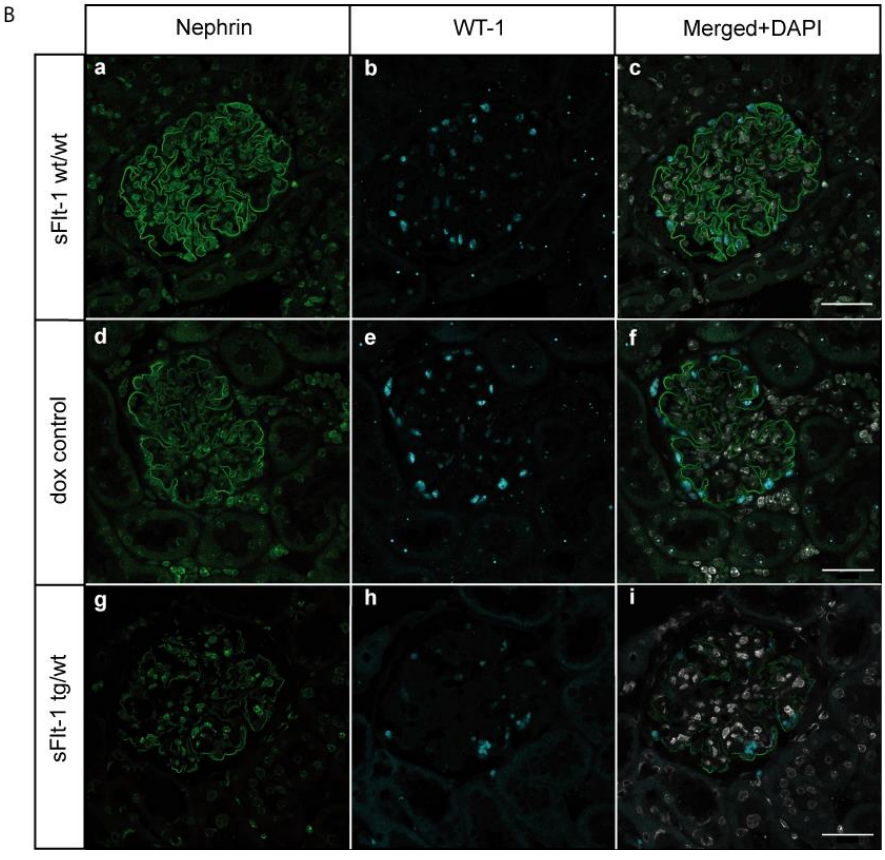
B
Nephrin
WT-1
Merged+DAPI
sFlt-1 wt/wt
dox control
sFlt-1 tg/wt
a
b
c
d
e
f
g
h
i

Figure 18: Immunofluorescence staining of glomeruli (Vogtmann et al. 2021). **A)** Double staining of glomeruli with slit diaphragm marker Nephrin (a, d, g) and endothelial cell marker CD31/PECAM (b, e, h). Compared to control mice, ubiquitously hsFlt-1 expressing mice show reduced Nephrin (g) and CD31/PECAM staining (h). **B)** Double staining of glomeruli with Nephrin antibody (a, d, g) and for podocyte-specific transcription factor WT-1 (b, e, h) showing reduced Nephrin and WT-1 staining. Scale bar: 200µm.

7. Discussion

Despite all advanced research and progress in the field, preeclampsia is still considered a global threat to the infants and the health of pregnant women. Therefore, a treatment for preeclampsia that is both specific and effective is an absolute medical need.

It is well understood that circulating sFlt-1 causes angiogenic imbalance leading to preeclampsia. However, it is critical to understand and consider the complex physiology behind preeclampsia before designing novel therapies. Previous studies have proven the benefits of leveling angiogenic imbalance through the systemic infusion of VEGF121 or PlGF in animal models (Makris et al. 2016; Li et al. 2007). Furthermore, in baboon preeclampsia models, sFlt-1 overexpression in the placenta was reduced by stabilized siRNA (Turanov et al. 2018). Yet, any systemic medical or pharmaceutical intervention for preeclampsia that can potentially influence the expression of sFlt-1 must be weighed with caution. According to *in vivo* studies on elegant mouse models, in the placentas of pregnant mice, VEGF is produced as a response to placental hypoperfusion and ischemia. Conversely, sFlt-1 derived from trophoblast cells on the fetal side of the placenta scavenges VEGF and shields the fetus against maternal VEGF. As reported by this study, maternal sFlt-1 is essential for the maintenance of VEGF function on endothelial cells while locally blocking angiogenesis at the decidua. Therefore, interfering with sFlt-1 expression may expose the fetus to harmful levels of maternal VEGF (Clark et al. 1998).

As of now, after proof of safety and efficacy of sFlt-1 adsorption by nonspecific dextran sulfate apheresis in patients with preeclampsia (Thadhani et al. 2011; Thadhani et al. 2016), the concept of refined and specific extracorporeal elimination of circulating sFlt-1 is the more appealing treatment choice.

7.1. Designing VEGF mutants to increase the binding affinity of VEGF to sFlt-1

In our study, we aimed to design a therapeutic intervention for preeclampsia that enables clearance of pathogenic sFlt-1 from the patients' plasma while at the same time liberating initially sFlt-1-trapped endogenous VEGF and PlGF. We hypothesize that this intervention will efficiently re-establish the angiogenic balance in the circulation of patients suffering from preeclampsia, ameliorate maternal symptoms and thus prolong pregnancy to benefit fetal development.

Generation of single-chain VEGF dimers to fixate a dimeric VEGF molecule was previously described for VEGF121 isoform by Papo et al. in 2002 (Papo et al. 2011). They connected two optimized VEGF121 isoforms using a 42 base pair linker to create a homodimer. The linker is a glycine-rich, 14 residues (GSTSGSGKSSEGKG) peptide. This linker is designed to avoid unspecific interactions between VEGF and the VEGFR2 (KDR) receptor. According to the crystal structure of VEGF121, the binding domain of VEGF121 to KDR in dimeric conformation is located where the C terminus of one monomer meets the N terminus of the other monomer. Therefore, the DNA sequence coding for the linker was placed in between the sequence of two monomers to encode the single-chain VEGF121 as a homodimer that mimics the wildtype VEGF121 dimer. Papo et al. expressed single-chain VEGF121 in yeast. Their study showed that post translational modifications, which differ in the yeast expression system, like e.g., glycosylation patterns, had no effect on VEGF activity. Single-chain VEGF121 exhibited a comparable effect stimulating endothelial cell proliferation as wildtype VEGF121 dimers.

When designing single-chain VEGF dimers, it is crucial to consider several parameters. As previously mentioned, one is to use a linker that averts unspecific internal and external interactions. Another critical parameter is the size of the monomers in their secondary structure. VEGF121 and VEGF165 differ by 44 amino acids in length. Insertion of the mentioned 14 amino acid linker is long enough for VEGF121 to form an intramolecular dimer within the single-chain VEGF sequence similar to the wildtype. The linker enables the two VEGF121 monomers to form an antiparallel side-by-side configuration. However, the identical linker for the bigger isoform VEGF165 is too short in length to allow for intramolecular dimer assembly. Applying the same linker between two VEGF165 monomers will limit the freedom

of monomers to be placed side-by-side and forces an open configuration on them. The open structure of VEGF165 dimers facilitates attraction and binding of two adjacent open scVEGF165 dimers, forming tetramers. Potentially, these structures can also extend to form higher-order multimers.

We do not have an exact explanation on why scVEGF165 can enhance the binding affinity to sFlt-1. We speculate that the three-dimensional structure of this multimeric molecule spaced binding sites due to steric effects allowed more efficient binding. In addition, the molecule's orientation in the vicinity to the ligand might be more efficient for binding in the scVEGF165 dimer molecule. According to the cooperativity rule, the first step of binding a dimeric protein to its ligand is similar to the reaction of binding a monomeric protein to its ligand. However, if the binding of the first monomer to the ligand affects the binding of the other monomer positively or negatively, this second reaction is faster or slower than the first reaction. A dimeric protein with an occupied binding site might also have a faster or slower dissociation reaction. There are several hypotheses proposed to explain the positive, cooperative effect. One is conformational changes caused by the first ligand-receptor binding that progressively changes the affinity of the unoccupied site. This hypothesis gets more complex in the case of the multimeric proteins, where each subunit in a bound or unbound state might allow a unique conformational change that affects the whole system differently (Lefurgy et al. 2012).

In the future, it would be interesting to see whether binding characteristics alter upon generation of heterodimers within a scVEGF and whether engaging different monomeric variants in a single-chain VEGF could intensify the binding affinity to sFlt-1, and consequently increase in VEGF/PlGF release.

Like most cultured endothelial cells, HUVECs bear both Flt-1 and KDR at their cell surface, which are essential for normal vascular development (Sato et al. 2000). However, according to the study from Zeng et al. in 2001, KDR is responsible for the proliferation and migration of the human umbilical vein endothelial cells (Zeng et al. 2001). Therefore, we investigate the signaling pathway of KDR activation. Upon stimulation of cells with recombinant growth factors, cells treated with scVEGF165 showed a higher signal for phosphorylated ERK1/2 and MAP kinase activation than cells treated with wildtype VEGF. To our surprise, when staining PFA-fixed cells for phosphorylated KDR, accumulation of active KDR was observed as patches at the surface of cells treated with scVEGF165 while stimulation with wildtype VEGF showed

a homogenous granular pattern of KDR activation throughout the cell surface. These data suggest an increased reactivity of the endothelial cells to scVEGF165. Whether scVEGF165 promotes higher expression of KDR at the cell surface or solely promotes accumulation of existing surface KDR through multimeric VEGF molecules available for binding to KDR, cannot be resolved by immunostaining. In immunoblot analysis, the response of the cells to scVEGF165 and moVEGF165 treatment represented by phospho-KDR signal was not different. These data suggest that scVEGF165 clusters KDR receptor at the cell surface and does not increase its expression.

We further analyzed the effect of scVEGF165 on proliferation and migration patterns in the HUVEC cells treated with scVEGF165 and moVEGF165. However, our data failed to provide proof of a clear signal concerning scVEGF165-induced proliferation and migration of HUVECs. However, one should consider that our data has been obtained from cultured endothelial cells that differ in morphology and function dependent on different cell passages and culturing conditions. HUVEC cells lose their ability to migrate after around ten passages. Since the cells were starved before the introduction of growth factors, starvation may influence the kinetic activity of the cells in early passages differently than cells in later passages. Moreover, the quality of the recombinant proteins and the age and storage conditions of the stimulants can effectively influence the experimental outcome. Ideally, these experiments should be performed simultaneously using the same early cell passage, treated under the same conditions, employing stimulants with comparable quality. Furthermore, saturation of the receptor at the cell surface is another important factor that should not be neglected. We followed the previously published mitogen concentrations and recommended duration of starvation and treatment for our experimental settings. We could improve the experimental conditions by testing several different doses of stimuli, different treatment durations and measuring the activation of KDR using phospho-proteomics prior to the main experiments.

Furthermore, the dissociation constant in our study for monomeric and single-chain VEGF165 was measured in vitro under basic kinetic parameters. When employing these proteins to cell culture models, it is essential to consider that dissociation constants in steady states will not be defined by simple relations of association rate divided by dissociation rate, but rather other kinetic parameters like proteolysis, protein synthesis, monomer and dimer degradation rates

and dilution, will also affect the binding affinity and consequently the cell's response to the stimuli.

7.2. Choosing the proper matrix for the clinical application of sFlt-1 aphesis

The concept of plasma exchange was created as early as 1914 by Abel et al. for returning the red blood cells to donors after retaining the plasma (McCullough et al. 2021). Since then, apheresis has been performed to treat many different diseases. The most commonly used solid matrices in the life science industry are Sepharose and agarose based. Both agarose and Sepharose are polysaccharide polymers, with agarose bearing more charged polysaccharides (Axen et al. 1971).

In the study from Trapiella-Alfonso et al., magnetic beads were utilized to immobilize biotinylated recombinant VEGF95 as a capturing molecule for sFlt-1. A matrix of magnetic beads binds to the ligand via a non-covalent linkage, making it unsuitable for clinical applications in humans. Besides, the biotin-avidin interaction between the biotinylated VEGF95 and the beads can cause serious immunogenicity in human patients (Trapiella-Alfonso et al. 2019).

We took advantage of CNBr-activated Sepharose, aldehyde-activated agarose, and Strep-Tactin solid resin to immobilize recombinant proteins in a small-scale chromatography gravity-flow column. While the interaction between resin and protein in the case of Strep-Tactin beads is based on biotin-avidin, non-covalent interaction, the two chemistry-activated polysaccharide resins (Sepharose and agarose) form strong covalent bonds with the bait protein. When generating custom-designed affinity columns, especially for clinical applications, the covalent bond between the ligand and the resin is of great importance. The solid covalent interaction facilitates a tighter linkage between protein and resin, reducing the risk of leakage, i.e., loss of protein during the course of apheresis.

An aldehyde-activated agarose resin binds to the proteins either by the alpha-amine group on the N-terminus of the protein or the epsilon-amine from the lysin side-chain residue of the proteins (Raj et al. 2015). The CNBr-activated Sepharose matrix also reacts with primary amines creating a covalent bond that results in the formation of non-charged imidocarbonate (Urh et al. 2009). However, the optimal coupling efficiency between CNBr-activated Sepharose, and the protein occurs at higher than physiological pH (between 8-10). In an

environment with lower pH, the coupling efficiency is reduced (Kavran et al. 2014). Moreover, in order to block the uncoupled reactive groups of the matrices, in the case of aldehyde-activated agarose resin, cyanoborohydride solution is used to reduce the aldehyde groups, and for CNBr-activated Sepharose, unspecific primary amines are being added to the matrix.

We achieved the highest specific elimination of sFlt-1 when utilizing agarose resin. At the same time, the least unspecific binding was observed using this matrix. Furthermore, the agarose column showed significant stability, not losing its clearance capacity after 90 days at 4 °C. Overall, these findings make aldehyde-activated agarose resin the best candidate for clinical application.

7.3. Advantages and disadvantages of scVEGF165 competitive apheresis

As previously mentioned, several different apheresis approaches have been suggested to prolong pregnancy in patients with preeclampsia. The initial apheresis system in proof-of-concept trials used unspecific, charge-dependent dextran sulfate columns to remove sFlt-1 from the circulation of patients (Thadhani et al. 2011; Thadhani et al. 2016). Considering that together with sFlt-1, several other positively charged plasma molecules will be captured in this setup, the side effects caused by the application of dextran sulfate can negatively affect patient health. Moreover, applying an unspecific column significantly reduces the efficiency of the treatment. Therefore, in order to gain the desired outcome, apheresis has to be applied more frequently which increases the risk of side effects and the burden on the patients. Moreover, one should consider that the pilot studies of treating preeclampsia, were carried out in patients suffering from severe preeclampsia with high sFlt-1 plasma levels. A highly efficient and specific treatment option, like scVEGF apheresis can be engaged during the early course of the disease even when the sFlt-1 serum levels are not high, thereby potentially the treatment intervals and ultimately the duration of pregnancy will be prolonged.

Another apheresis system for sFlt-1 removal, which is currently tested in phase II trials, is utilizing a specific antibody against Flt-1 or sFlt-1 to increase the specificity of capturing sFlt-1 from patients' plasma. Antibody-based approaches may efficiently and specifically reduce sFlt-1, yet, they eliminate sFlt-1 bound VEGF and PlGF at the same time. The binding motif of sFlt-1 to its antibody differs from the binding motif of sFlt-1 to VEGF or PlGF. In addition, the binding affinity of an antibody to sFlt-1 is weaker than binding affinity to its specific ligands VEGF or PlGF. Overall, an antibody- dependent apheresis adds specificity but does not reach maximal efficacy of the intervention regarding restoration of the angiogenic balance. Moreover, the potential side effects of antibody leakage from the column as well as immunogenicity of sFlt-1 antibodies should not be neglected.

The competitive apheresis suggested by Trapiella-Alfonso et al., using the truncated VEGF95, enables liberation of only PlGF and not VEGF (Trapiella-Alfonso et al. 2019). VEGF95 has a tenfold higher binding affinity to sFlt-1 when compared to PlGF and, therefore can compete with PlGF for binding to sFlt-1 and influence the sFlt-1/PlGF ratio. However, since the binding

affinity of sFlt-1 to VEGF95 is lower than the affinity to VEGF165, the most abundant VEGF isoform in humans, the sFlt-1/VEGF ratio remains unaltered after VEGF95-apheresis treatment (Trapiella-Alfonso et al. 2019).

Engaging natural binding biomolecules of sFlt-1, namely VEGF and PlGF, in our competitive aphesis makes our approach highly specific and modifications of the molecule enhanced binding affinity. However, the primary concern of VEGF apheresis treatment is the potential adverse effects of VEGF release *in vivo*. Studies in animal models suggested that intravenous application of VEGF in doses of 300-400 µg/kg body weight can cause an increase in vascular permeability, tachycardia, or uncontrolled hypotension 10 to 120 minutes after injection. Therefore, we calculated the potential VEGF release of competitive sFlt-1 apheresis based on ELISA data. During a healthy pregnancy, VEGF and PLGF levels reach a maximum of 15ng/mL and 500 pg/mL in the late trimester, respectively (Hunter et al. 2000; Evans et al. 1997; Kasdaglis et al. 2010; Saffer et al. 2013). Depending on the severity of preeclampsia or in other words initial serum sFl-1 levels, the released VEGF or PLGF levels vary. Based on *in vitro* data using 1 ml serum from a patient containing very high sFlt-1 levels of 20000 pg/mL we extrapolate the released VEGF to a treatment volume of 2 liters plasma. The expected VEGF release is about 55µg which is well below the doses causing side effects in animal studies. Yet, physiological side effects by redistribution of large amounts of VEGF into maternal circulation and its effects on placenta and fetus will have to be addressed in large animal models.

It is critical to have the best possible understanding of side effects evoked by novel approaches of sFlt-1 apheresis. Another valid concern is VEGF- and PlGF-induced differentiation or activation of dendritic cells and macrophages while leading blood over a column with recombinant VEGF. It is proposed that the recruitment of macrophages via VEGFA can indirectly cause lymphangiogenesis and hemangiogenesis (Cursiefen et al. 2004). In addition, studies on cancer patients revealed that VEGFA suppresses the differentiation and maturation of dendritic cells and thereby interferes with the functions of the immune system (Bai, Zhang, and Hu 2018; Takahashi et al. 2004). Consequently, to avoid direct exposure of immune cells to the immobilized VEGF, it is essential to consider a plasma separation step instead of whole blood therapy when elaborating the VEGF-based sFlt-1 apheresis approach.

7.4. The role of sFlt-1 isoforms in the pathogenesis of preeclampsia

There are accumulating data pointing to the role of the increased placental expression of sFlt-1 and spilling of sFlt-1 into the maternal circulation as the source of generalized endothelial dysfunction and multisystem injury of maternal organs in preeclampsia (Maynard et al. 2003; Maynard et al. 2008). Several studies have tried to find a link between the predominant sFlt-1 isoform produced by the placenta and the pathogenesis and progression of preeclampsia.

At least seven different splice variants of sFlt-1 have been identified, of which four have been studied in detail. In all isoforms, the extracellular domain is conserved while the sequence of their C-terminus varies (Ahmad et al. 2011; Sawano et al. 1997). Among all splice variants, two are known to be expressed by the placenta: sFlt-1 i13 and sFlt-1-14. sFlt-1 i13 contains a unique 28 amino acid sequence at its C-terminus and is expressed not only in the placenta but also in other tissues such as the kidney, the brain and the heart (Ahmad et al. 2011). In contrast, sFlt-1-14 contains a unique 31 amino acid sequence at its C-terminus and is predominantly expressed in the placenta. This splice variant is also specific for human and higher-order primates (Szalai et al. 2015).

Recently, Sela et al. identified sFlt-1-14 (also known as sFlt-1 e15a) as an isoform accumulating in the circulation of women with preeclampsia (Szalai et al. 2015). They identified placental syncytial knots as the major source of the sFlt-1-14 isoform. Syncytial knots form in response to ischemia caused by a reduction of maternal blood supply in the placenta and their presence increases with gestational age (Bdolah et al. 2008). These findings are in line with the previous observation that women with preeclampsia experience placental ischemia and hypoxia during the course of the disease and that the sFlt-1 levels constantly increase throughout gestation (McKeeman et al. 2004).

In a more recent study, Palmer et al. compared placental mRNA profiles of 18 cases with preterm preeclampsia to normotensive controls. The study confirmed sFlt-1-14 as the predominant isoform in women with preeclampsia. They validated their findings using a homemade ELISA specific for sFlt-1-14 measuring serum levels of splice variant sFlt-1-14 in the patients with preeclampsia versus controls (Palmer et al. 2015).

In the same year, Szalai et al. investigated the contribution of the sFlt-1-14 splice variant in the pathophysiology of preeclampsia by injecting sFlt-1-14 into the tail-vein of mice. They

could show that sFlt-1-14 is biologically active *in vivo* and can induce liver and kidney-associated symptoms similar to preeclampsia (Szalai et al. 2015).

In a different approach, we aimed to identify sFlt-1 splice variants in the serum of preeclamptic patients by proteomic analysis of sFlt-1 captured by the scVEGF165 apheresis column. After digestion of captured sFlt-1 with trypsin, peptides were analyzed by a mass spectrometer to search for unique peptides belonging to specific sFlt-1 isoforms. In serum samples from women with preeclampsia, we were able to identify only one unique peptide which belonged to sFlt-1-14. Although this finding is ideally in line with previously published data, due to the strong homology between sequences of different splice variants of sFlt-1, we could not exclude the existence of other splice variants in the patients' sera. Likewise, assessing the relative abundance ratio of sFlt-1-14 compared to other isoforms was not possible.

7.5. Animal models for studying preeclampsia

A clear understanding of the pathophysiology of preeclampsia and a detailed molecular mechanism involved in abnormal spiral arterial remodeling as well as how increased levels of sFlt-1 cause proteinuria and hypertension, are missing. The complex nature of preeclampsia is an obstacle for generating versatile experimental animal models. An ideal model to study preeclampsia would be a mouse model recapitulating the imbalance of circulating growth factors while exhibiting the systemic effects of endothelial dysfunction of preeclampsia (namely proteinuria, hypertension) that is promoted by impaired placentation and trophoblast invasion. Additionally, after delivery of the placenta, all symptoms of the disease should resolve (McCarthy et al. 2011). However, due to different placentation mechanisms among mammals, fulfilling all these criteria is not possible. The degree of trophoblast invasion into the basal endometrium and its blood vessels differ in different species (Carter et al. 2020). Although compared to humans, higher-rate primates represent more similarity in placentation, in reality, no animal model is fully suited to study the human placentation and its complications (Carter et al. 2020). Generally, in mammals, based on shape and retained maternal layers in the placenta, there are four types of placentas; diffuse-epitheliochorial, cotyledonary-epitheliochorial, zonary-endotheliochorial and discoid-hemochorial (Furukawa, Kuroda, and Sugiyama 2014). Humans, apes, monkeys, and rodents have a discoid-hemochorial placenta, in which, unlike other types of placentas, fetal chorion and maternal blood have direct contact to each other. Currently, the majority of studies on preeclampsia have been performed utilizing rodent models, preferably rats. In rodent models, despite having a similar hemochorial placenta as humans, there are three trophoblast layers, while in humans, there is only one trophoblast layer. The different cellular barrier between maternal blood and fetus affects the ability of the molecules and proteins to diffuse or move via active transport across the placenta (Furukawa, Kuroda, and Sugiyama 2014). In rodent models, unlike humans, invasion of the placenta into the myometrium does not occur or is limited, and preeclampsia does not progress to eclampsia (Burke et al. 2010). The current rodent models of preeclampsia employ replication-deficient sFlt-1 adenovirus or lentivirus. Animals exhibit preeclampsia-like characteristics after injection of virus-encoded sFlt-1. A downside of using these models is that immune response to virus application may influence experimental outcomes.

The mouse model used in this thesis is a doxycycline inducible, transgenic human sFlt-1 mouse model that overexpresses systemic human sFlt-1 stably and reproducibly. The mouse harbors a rtTA or tetracycline-inducible cassette that enables whole-body overexpression of human sFlt-1. This mouse model was initially generated to study the effects of human sFlt-1 in placental differentiation and vascularization by the research group of Prof'. Alexandra Gellhaus, from the Department of Gynecology and Obstetrics of the University Hospital of Essen (Vogtmann et al. 2021).

In preeclampsia, endothelial dysfunction in the kidney causes glomerular injury, which is manifested by glomerular endotheliosis, endothelial swelling, occlusion of capillary lumen, bloodless looking glomeruli and loss of endothelial fenestrate (Kamba et al. 2006). Glomerular injury is clinically evident as proteinuria, characterized by an increased urinary albumin/creatinine ratio. In our model, systemic hsFlt-1 overexpression was capable of mimicking the hallmarks of glomerular endotheliosis, podocyte damage, and proteinuria. Initial immunostaining of kidney tissue from preeclamptic mice revealed podocyte loss and loss of signal from endothelial cells marker PECAM, which might be due to dedifferentiation of cells and needs to be further investigated.

Due to time restrictions, the mouse experiments in this thesis are limited to primary characterization of the model to validate its value in follow up studies on mechanisms involved in proteinuria.

Coming from a nephrology background, it is in our interest to study the molecular mechanism of proteinuria initiated by preeclampsia. Proteinuria in preeclampsia is unique because, unlike other glomerular diseases, it is reversible, and glomerular function recovers rather quickly after delivery of the placenta or removal of serum sFlt-1. Utilizing our inducible mouse model, by controlling the dose of sFlt-1 expression we can study the effect of sFlt-1 on the severity of glomerular injury and recapitulate proteinuria before and after sFlt-1 peak in the plasma.

It is known that glomerular VEGF expression is critical for the integrity of an intact glomerular filtration barrier and kidney function (Sison et al. 2010; Muller-Deile and Schiffer 2011). Podocytes express mediators such as VEGF that translocate to the glomerular endothelium to activate their signaling activity (Sison et al. 2010). Most likely, podocytes are not directly affected by VEGF-signaling, and glomerular endothelial cells participate in a crosstalk by secretion of endothelial-specific mediators. However, convincing experimental proof in *in vivo*

models is missing. This transgenic inducible mouse model expressing hsFlt-1 dependent on doxycycline-administration allows us to study further the effect of VEGF on the crosstalk between the different layers of the filtration barrier.

8. Conclusion

This work introduces the first specific VEGF-based sFlt-1 apheresis system to treat preeclampsia. This highly specific apheresis utilizes a novel VEGF molecule variant that can immobilize sFlt-1 and liberate the bound VEGF and PlGF, thereby restoring the angiogenic balance in pregnant women with preeclampsia. This therapy is optimized for direct in vivo applications.

Several matters were not addressed in this thesis and need further investigation. For instance, the flow rate and duration of aphesis, and its potential influence on the clearance of the competitive apheresis system. Moreover, the safety and potential side effects caused by the release of the column's recombinant VEGF or PLGF into the circulation need to be addressed by testing in animal models. Furthermore, the side effects of sFlt-1 reduction and VEGF release and redistribution in vivo in both mother and fetus should be assessed in animal models.

Furthermore, we introduce a valid mouse model to study the potential side effects of competitive sFlt-1 apheresis as well as eluting the renal pathophysiology of preeclampsia. We have characterized a whole-body inducible mouse model overexpressing human sFlt-1 upon doxycycline treatment in a collaborative effort. This mouse model could reproduce similar systemic clinical manifestations of preeclampsia as seen in humans. The inducible system enables control over sFlt-1 expression levels in these mice. This model is a promising tool to study the concentration-dependent effects of sFlt-1 on the pathophysiology of preeclampsia and compare the systemic effect of sFlt-1 in early and late preeclampsia in future studies.

9. Bibliography

Ahmad, S., P. W. Hewett, B. Al-Ani, S. Sissaoui, T. Fujisawa, M. J. Cudmore, and A. Ahmed. 2011. 'Autocrine activity of soluble Flt-1 controls endothelial cell function and angiogenesis', *Vasc Cell*, 3: 15.

Bai, W. K., W. Zhang, and B. Hu. 2018. 'Vascular endothelial growth factor suppresses dendritic cells function of human prostate cancer', *Onco Targets Ther*, 11: 1267-74.

Baker, P. N., J. Krasnow, J. M. Roberts, and K. T. Yeo. 1995. 'Elevated serum levels of vascular endothelial growth factor in patients with preeclampsia', *Obstet Gynecol*, 86: 815-21.

Bdolah, Y., C. Lam, A. Rajakumar, V. Shivalingappa, W. Mutter, B. P. Sachs, K. H. Lim, T. Bdolah-Abram, F. H. Epstein, and S. A. Karumanchi. 2008. 'Twin pregnancy and the risk of preeclampsia: bigger placenta or relative ischemia?', *Am J Obstet Gynecol*, 198: 428 e1-6.

Bell, M. J. 2010. 'A historical overview of preeclampsia-eclampsia', *J Obstet Gynecol Neonatal Nurs*, 39: 510-8.

Berzan, E., R. Doyle, and C. M. Brown. 2014. 'Treatment of preeclampsia: current approach and future perspectives', *Curr Hypertens Rep*, 16: 473.

Birkenhager, R., B. Schneppe, W. Rockl, J. Wilting, H. A. Weich, and J. E. McCarthy. 1996. 'Synthesis and physiological activity of heterodimers comprising different splice forms of vascular endothelial growth factor and placenta growth factor', *Biochem J*, 316 (Pt 3): 703-7.

Bober, M., C. Enochsson, M. Collin, and M. Morgelin. 2010. 'Collagen VI is a subepithelial adhesive target for human respiratory tract pathogens', *J Innate Immun*, 2: 160-6.

Bolton, G. R., W. M. Deen, and B. S. Daniels. 1998. 'Assessment of the charge selectivity of glomerular basement membrane using Ficoll sulfate', *Am J Physiol*, 274: F889-96.

Boucher, J. M., R. P. Clark, D. C. Chong, K. M. Citrin, L. A. Wylie, and V. L. Bautch. 2017. 'Dynamic alterations in decoy VEGF receptor-1 stability regulate angiogenesis', *Nat Commun*, 8: 15699.

Boute, N., O. Gribouval, S. Roselli, F. Benessy, H. Lee, A. Fuchshuber, K. Dahan, M. C. Gubler, P. Niaudet, and C. Antignac. 2000. 'NPHS2, encoding the glomerular protein podocin, is mutated in autosomal recessive steroid-resistant nephrotic syndrome', *Nat Genet*, 24: 349-54.

Brenner, B. M., T. H. Hostetter, and H. D. Humes. 1978. 'Molecular basis of proteinuria of glomerular origin', *N Engl J Med*, 298: 826-33.

Brosens, I. A., W. B. Robertson, and H. G. Dixon. 1972. 'The role of the spiral arteries in the pathogenesis of preeclampsia', *Obstet Gynecol Annu*, 1: 177-91.

Brosens, I., W. B. Robertson, and H. G. Dixon. 1967. 'The physiological response of the vessels of the placental bed to normal pregnancy', *J Pathol Bacteriol*, 93: 569-79.

Brunger, A. T. 2007. 'Version 1.2 of the Crystallography and NMR system', *Nat Protoc*, 2: 2728-33.

Buchbinder, A., B. M. Sibai, S. Caritis, C. Macpherson, J. Hauth, M. D. Lindheimer, M. Klebanoff, P. Vandorsten, M. Landon, R. Paul, M. Miodovnik, P. Meis, G. Thurnau, Health National Institute of Child, and Units Human Development Network of Maternal-Fetal Medicine. 2002. 'Adverse perinatal outcomes are significantly higher in severe gestational hypertension than in mild preeclampsia', *Am J Obstet Gynecol*, 186: 66-71.

Burke, S. D., V. F. Barrette, J. Bianco, J. G. Thorne, A. T. Yamada, S. C. Pang, M. A. Adams, and B. A. Croy. 2010. 'Spiral arterial remodeling is not essential for normal blood pressure regulation in pregnant mice', *Hypertension*, 55: 729-37.

Butt, L., D. Unnersjo-Jess, M. Hohne, A. Edwards, J. Binz-Lotter, D. Reilly, R. Hahnfeldt, V. Ziegler, K. Fremter, M. M. Rinschen, M. Helmstadter, L. K. Ebert, H. Castrop, M. J. Hackl, G. Walz, P. T. Brinkkoetter, M. C. Liebau, K. Tory, P. F. Hoyer, B. B. Beck, H. Brismar, H. Blom, B. Schermer, and T. Benzing. 2020. 'A molecular mechanism explaining albuminuria in kidney disease', *Nat Metab*, 2: 461-74.

Caniggia, I., H. Mostachfi, J. Winter, M. Gassmann, S. J. Lye, M. Kuliszewski, and M. Post. 2000. 'Hypoxia-inducible factor-1 mediates the biological effects of oxygen on human trophoblast differentiation through TGFbeta(3)', *J Clin Invest*, 105: 577-87.

Carroll, M. F., and J. L. Temte. 2000. 'Proteinuria in adults: a diagnostic approach', *Am Fam Physician*, 62: 1333-40.

Carter, A. M. 2020. 'Animal models of human pregnancy and placentation: alternatives to the mouse', *Reproduction*, 160: R129-R43.

Cerdeira, A. S., N. Kandzija, P. Pargmae, W. Cooke, T. James, C. Redman, and M. Vatish. 2019. 'Circulating soluble fms-like tyrosine kinase-1 is placentally derived in normal pregnancy: First in vivo evidence', *Pregnancy Hypertens*, 16: 145-47.

Chesley, L. C. 1984. 'History and epidemiology of preeclampsia-eclampsia', *Clin Obstet Gynecol*, 27: 801-20.

———. 1985. 'Hypertensive disorders in pregnancy', *J Nurse Midwifery*, 30: 99-104.

Christinger, H. W., G. Fuh, A. M. de Vos, and C. Wiesmann. 2004. 'The crystal structure of placental growth factor in complex with domain 2 of vascular endothelial growth factor receptor-1', *J Biol Chem*, 279: 10382-8.

Chielie KA, Dhingra R, Bhatla N. Estimation of serum levels of VEGF & SVEGFR-1 (sFLT1) in preeclampsia. J. Evolution Med. Dent. Sci. 2020;9(12):913-918, DOI: 10.14260/jemds/2020/197

Cursiefen, C., L. Chen, L. P. Borges, D. Jackson, J. Cao, C. Radziejewski, P. A. D'Amore, M. R. Dana, S. J. Wiegand, and J. W. Streilein. 2004. 'VEGF-A stimulates lymphangiogenesis and hemangiogenesis in inflammatory neovascularization via macrophage recruitment', *J Clin Invest*, 113: 1040-50.

Davidson, A., R. Bethunaickan, C. Berthier, R. Sahu, W. Zhang, and M. Kretzler. 2015. 'Molecular studies of lupus nephritis kidneys', *Immunol Res*, 63: 187-96.

Dawson, M. R., D. G. Duda, D. Fukumura, and R. K. Jain. 2009. 'VEGFR1-activity-independent metastasis formation', *Nature*, 461: E4; discussion E5.

Duley, L. 1992. 'Maternal mortality associated with hypertensive disorders of pregnancy in Africa, Asia, Latin America and the Caribbean', *Br J Obstet Gynaecol*, 99: 547-53.

Duley, L., D. J. Henderson-Smart, S. Meher, and J. F. King. 2007. 'Antiplatelet agents for preventing pre-eclampsia and its complications', *Cochrane Database Syst Rev*: CD004659.

Eremina, V., J. A. Jefferson, J. Kowalewska, H. Hochster, M. Haas, J. Weisstuch, C. Richardson, J. B. Kopp, M. G. Kabir, P. H. Backx, H. P. Gerber, N. Ferrara, L. Barisoni, C. E. Alpers, and S. E. Quaggin. 2008. 'VEGF inhibition and renal thrombotic microangiopathy', *N Engl J Med*, 358: 1129-36.

Evans, P., T. Wheeler, F. Anthony, and C. Osmond. 1997. 'Maternal serum vascular endothelial growth factor during early pregnancy', *Clin Sci (Lond)*, 92: 567-71.

Fisher, K. A., A. Luger, B. H. Spargo, and M. D. Lindheimer. 1981. 'Hypertension in pregnancy: clinical-pathological correlations and remote prognosis', *Medicine (Baltimore)*, 60: 267-76.

Fuh, G., B. Li, C. Crowley, B. Cunningham, and J. A. Wells. 1998. 'Requirements for binding and signaling of the kinase domain receptor for vascular endothelial growth factor', *J Biol Chem*, 273: 11197-204.

Furukawa, S., Y. Kuroda, and A. Sugiyama. 2014. 'A comparison of the histological structure of the placenta in experimental animals', *J Toxicol Pathol*, 27: 11-8.

Gaber, L. W., and B. H. Spargo. 1987. 'Pregnancy-induced nephropathy: the significance of focal segmental glomerulosclerosis', *Am J Kidney Dis*, 9: 317-23.

Gerber, H. P., F. Condorelli, J. Park, and N. Ferrara. 1997. 'Differential transcriptional regulation of the two vascular endothelial growth factor receptor genes. Flt-1, but not Flk-1/KDR, is up-regulated by hypoxia', *J Biol Chem*, 272: 23659-67.

Gerretsen, G., H. J. Huisjes, and J. D. Elema. 1981. 'Morphological changes of the spiral arteries in the placental bed in relation to pre-eclampsia and fetal growth retardation', *Br J Obstet Gynaecol*, 88: 876-81.

'Gestational Hypertension and Preeclampsia: ACOG Practice Bulletin Summary, Number 222'. 2020. *Obstet Gynecol*, 135: 1492-95.

Giles, T. D., B. J. Materson, J. N. Cohn, and J. B. Kostis. 2009. 'Definition and classification of hypertension: an update', *J Clin Hypertens (Greenwich)*, 11: 611-4.

Gu, Y., D. F. Lewis, and Y. Wang. 2008. 'Placental productions and expressions of soluble endoglin, soluble fms-like tyrosine kinase receptor-1, and placental growth factor in normal and preeclamptic pregnancies', *J Clin Endocrinol Metab*, 93: 260-6.

Hagmann, H., R. Thadhani, T. Benzing, S. A. Karumanchi, and H. Stepan. 2012. 'The promise of angiogenic markers for the early diagnosis and prediction of preeclampsia', *Clin Chem*, 58: 837-45.

Haram, K., E. Svendsen, and U. Abildgaard. 2009. 'The HELLP syndrome: clinical issues and management. A Review', *BMC Pregnancy Childbirth*, 9: 8.

Hauser, S., and H. A. Weich. 1993. 'A heparin-binding form of placenta growth factor (PlGF-2) is expressed in human umbilical vein endothelial cells and in placenta', *Growth Factors*, 9: 259-68.

Heaton, J. M., and D. R. Turner. 1985. 'Persistent renal damage following pre-eclampsia: a renal biopsy study of 13 patients', *J Pathol*, 147: 121-6.

Hiratsuka, S., O. Minowa, J. Kuno, T. Noda, and M. Shibuya. 1998. 'Flt-1 lacking the tyrosine kinase domain is sufficient for normal development and angiogenesis in mice', *Proc Natl Acad Sci U S A*, 95: 9349-54.

Holash, J., S. Davis, N. Papadopoulos, S. D. Croll, L. Ho, M. Russell, P. Boland, R. Leidich, D. Hylton, E. Burova, E. Ioffe, T. Huang, C. Radziejewski, K. Bailey, J. P. Fandl, T. Daly, S. J. Wiegand, G. D. Yancopoulos, and J. S. Rudge. 2002. 'VEGF-Trap: a VEGF blocker with potent antitumor effects', *Proc Natl Acad Sci U S A*, 99: 11393-8.

Holmes, D. I., and I. Zachary. 2005. 'The vascular endothelial growth factor (VEGF) family: angiogenic factors in health and disease', *Genome Biol*, 6: 209.

Holmes, K., O. L. Roberts, A. M. Thomas, and M. J. Cross. 2007. 'Vascular endothelial growth factor receptor-2: structure, function, intracellular signalling and therapeutic inhibition', *Cell Signal*, 19: 2003-12.

Houck, K. A., N. Ferrara, J. Winer, G. Cachianes, B. Li, and D. W. Leung. 1991. 'The vascular endothelial growth factor family: identification of a fourth molecular species and characterization of alternative splicing of RNA', *Mol Endocrinol*, 5: 1806-14.

Huber, T. B., M. Kottgen, B. Schilling, G. Walz, and T. Benzing. 2001. 'Interaction with podocin facilitates nephrin signaling', *J Biol Chem*, 276: 41543-6.

Hunter, A., M. Aitkenhead, C. Caldwell, G. McCracken, D. Wilson, and N. McClure. 2000. 'Serum levels of vascular endothelial growth factor in preeclamptic and normotensive pregnancy', *Hypertension*, 36: 965-9.

'Hypertension in pregnancy. Report of the American College of Obstetricians and Gynecologists' Task Force on Hypertension in Pregnancy'. 2013. *Obstet Gynecol*, 122: 1122-31.

Iyer, S., and K. R. Acharya. 2011. 'Tying the knot: the cystine signature and molecular-recognition processes of the vascular endothelial growth factor family of angiogenic cytokines', *FEBS J*, 278: 4304-22.

Kamba, T., B. Y. Tam, H. Hashizume, A. Haskell, B. Sennino, M. R. Mancuso, S. M. Norberg, S. M. O'Brien, R. B. Davis, L. C. Gowen, K. D. Anderson, G. Thurston, S. Joho, M. L. Springer, C. J. Kuo, and D. M. McDonald. 2006. 'VEGF-dependent plasticity of fenestrated capillaries in the normal adult microvasculature', *Am J Physiol Heart Circ Physiol*, 290: H560-76.

Kanwar, Y. S., F. R. Danesh, and S. S. Chugh. 2007. 'Contribution of proteoglycans towards the integrated functions of renal glomerular capillaries: a historical perspective', *Am J Pathol*, 171: 9-13.

Kappas, N. C., G. Zeng, J. C. Chappell, J. B. Kearney, S. Hazarika, K. G. Kallianos, C. Patterson, B. H. Annex, and V. L. Bautch. 2008. 'The VEGF receptor Flt-1 spatially modulates Flk-1 signaling and blood vessel branching', *J Cell Biol*, 181: 847-58.

Karumanchi, S. A., S. E. Maynard, I. E. Stillman, F. H. Epstein, and V. P. Sukhatme. 2005. 'Preeclampsia: a renal perspective', *Kidney Int*, 67: 2101-13.

Kasdaglis, T., G. Aberdeen, O. Turan, J. Kopelman, R. Atlas, C. Jenkins, M. Blitzer, C. Harman, and A. A. Baschat. 2010. 'Placental growth factor in the first trimester: relationship with maternal factors and placental Doppler studies', *Ultrasound Obstet Gynecol*, 35: 280-5.

Katz, V. L., R. Farmer, and J. A. Kuller. 2000. 'Preeclampsia into eclampsia: toward a new paradigm', *Am J Obstet Gynecol*, 182: 1389-96.

Kendall, R. L., and K. A. Thomas. 1993. 'Inhibition of vascular endothelial cell growth factor activity by an endogenously encoded soluble receptor', *Proc Natl Acad Sci U S A*, 90: 10705-9.

Kestila, M., U. Lenkkeri, M. Mannikko, J. Lamerdin, P. McCready, H. Putaala, V. Ruotsalainen, T. Morita, M. Nissinen, R. Herva, C. E. Kashtan, L. Peltonen, C. Holmberg, A. Olsen, and K. Tryggvason. 1998. 'Positionally cloned gene for a novel glomerular protein--nephrin--is mutated in congenital nephrotic syndrome', *Mol Cell*, 1: 575-82.

Keyt, B. A., H. V. Nguyen, L. T. Berleau, C. M. Duarte, J. Park, H. Chen, and N. Ferrara. 1996. 'Identification of vascular endothelial growth factor determinants for binding KDR and FLT-1 receptors. Generation of receptor-selective VEGF variants by site-directed mutagenesis', *J Biol Chem*, 271: 5638-46.

Khong, T. Y., F. De Wolf, W. B. Robertson, and I. Brosens. 1986. 'Inadequate maternal vascular response to placentation in pregnancies complicated by pre-eclampsia and by small-for-gestational age infants', *Br J Obstet Gynaecol*, 93: 1049-59.

Konner, J., and J. Dupont. 2004. 'Use of soluble recombinant decoy receptor vascular endothelial growth factor trap (VEGF Trap) to inhibit vascular endothelial growth factor activity', *Clin Colorectal Cancer*, 4 Suppl 2: S81-5.

Kornacki, J., and J. Skrzypczak. 2008. '[Preeclampsia--two manifestations of the same disease]', *Ginekol Pol*, 79: 432-7.

Kowarz, E., D. Loscher, and R. Marschalek. 2015. 'Optimized Sleeping Beauty transposons rapidly generate stable transgenic cell lines', *Biotechnol J*, 10: 647-53.

Kuriakose, A., N. Chirmule, and P. Nair. 2016. 'Immunogenicity of Biotherapeutics: Causes and Association with Posttranslational Modifications', *J Immunol Res*, 2016: 1298473.

Levine, R. J., C. Lam, C. Qian, K. F. Yu, S. E. Maynard, B. P. Sachs, B. M. Sibai, F. H. Epstein, R. Romero, R. Thadhani, S. A. Karumanchi, and Cpep Study Group. 2006. 'Soluble endoglin and other circulating antiangiogenic factors in preeclampsia', *N Engl J Med*, 355: 992-1005.

Levine, R. J., S. E. Maynard, C. Qian, K. H. Lim, L. J. England, K. F. Yu, E. F. Schisterman, R. Thadhani, B. P. Sachs, F. H. Epstein, B. M. Sibai, V. P. Sukhatme, and S. A. Karumanchi. 2004. 'Circulating angiogenic factors and the risk of preeclampsia', *N Engl J Med*, 350: 672-83.

Li, Z., Y. Zhang, J. Ying Ma, A. M. Kapoun, Q. Shao, I. Kerr, A. Lam, G. O'Young, F. Sannajust, P. Stathis, G. Schreiner, S. A. Karumanchi, A. A. Protter, and N. S. Pollitt. 2007. 'Recombinant vascular endothelial growth factor 121 attenuates hypertension and improves kidney damage in a rat model of preeclampsia', *Hypertension*, 50: 686-92.

Lote, Christopher J. 1986. *Advances in renal physiology* (Liss: New York).

Mac Gabhann, F., and A. S. Popel. 2007. 'Interactions of VEGF isoforms with VEGFR-1, VEGFR-2, and neuropilin in vivo: a computational model of human skeletal muscle', *Am J Physiol Heart Circ Physiol*, 292: H459-74.

MacKay, A. P., C. J. Berg, and H. K. Atrash. 2001. 'Pregnancy-related mortality from preeclampsia and eclampsia', *Obstet Gynecol*, 97: 533-8.

Madazli, R., E. Budak, Z. Calay, and M. F. Aksu. 2000. 'Correlation between placental bed biopsy findings, vascular cell adhesion molecule and fibronectin levels in pre-eclampsia', *BJOG*, 107: 514-8.

Maglione, D., V. Guerriero, G. Viglietto, P. Delli-Bovi, and M. G. Persico. 1991. 'Isolation of a human placenta cDNA coding for a protein related to the vascular permeability factor', *Proc Natl Acad Sci U S A*, 88: 9267-71.

Makris, A., K. R. Yeung, S. M. Lim, N. Sunderland, S. Heffernan, J. F. Thompson, J. Iliopoulos, M. C. Killingsworth, J. Yong, B. Xu, R. F. Ogle, R. Thadhani, S. A. Karumanchi, and A. Hennessy. 2016. 'Placental Growth Factor Reduces Blood Pressure in a Uteroplacental Ischemia Model of Preeclampsia in Nonhuman Primates', *Hypertension*, 67: 1263-72.

Mamer, S. B., A. Wittenkeller, and P. I. Imoukhuede. 2020. 'VEGF-A splice variants bind VEGFRs with differential affinities', *Sci Rep*, 10: 14413.

Markovic-Mueller, S., E. Stuttfeld, M. Asthana, T. Weinert, S. Bliven, K. N. Goldie, K. Kisko, G. Capitani, and K. Ballmer-Hofer. 2017. 'Structure of the Full-length VEGFR-1 Extracellular Domain in Complex with VEGF-A', *Structure*, 25: 341-52.

Matin, M., M. Morgelin, J. Stetefeld, B. Schermer, P. T. Brinkkoetter, T. Benzing, M. Koch, and H. Hagmann. 2020. 'Affinity-Enhanced Multimeric VEGF (Vascular Endothelial Growth Factor) and PlGF (Placental Growth Factor) Variants for Specific Adsorption of sFlt-1 to Restore Angiogenic Balance in Preeclampsia', *Hypertension*, 76: 1176-84.

Mautner, W., J. Churg, E. Grishman, and S. Dachs. 1962. 'Preeclamptic nephropathy. An electron microscopic study', *Lab Invest*, 11: 518-30.

Maynard, S. E., J. Y. Min, J. Merchan, K. H. Lim, J. Li, S. Mondal, T. A. Libermann, J. P. Morgan, F. W. Sellke, I. E. Stillman, F. H. Epstein, V. P. Sukhatme, and S. A. Karumanchi. 2003. 'Excess placental soluble fms-like tyrosine kinase 1 (sFlt1) may contribute to endothelial dysfunction, hypertension, and proteinuria in preeclampsia', *J Clin Invest*, 111: 649-58.

Maynard, S. E., T. A. Moore Simas, M. J. Solitro, A. Rajan, S. Crawford, P. Soderland, and B. A. Meyer. 2008. 'Circulating angiogenic factors in singleton vs multiple-gestation pregnancies', *Am J Obstet Gynecol*, 198: 200 e1-7.

McCarthy, F. P., J. C. Kingdom, L. C. Kenny, and S. K. Walsh. 2011. 'Animal models of preeclampsia; uses and limitations', *Placenta*, 32: 413-9.

McKeeman, G. C., J. E. Ardill, C. M. Caldwell, A. J. Hunter, and N. McClure. 2004. 'Soluble vascular endothelial growth factor receptor-1 (sFlt-1) is increased throughout gestation in patients who have preeclampsia develop', *Am J Obstet Gynecol*, 191: 1240-6.

Moran, P., P. H. Baylis, M. D. Lindheimer, and J. M. Davison. 2003. 'Glomerular ultrafiltration in normal and preeclamptic pregnancy', *J Am Soc Nephrol*, 14: 648-52.

Morris, R. H., P. Vassalli, F. K. Beller, and R. T. McCluskey. 1964. 'Immunofluorescent Studies of Renal Biopsies in the Diagnosis of Toxemia of Pregnancy', *Obstet Gynecol*, 24: 32-46.

Muller-Deile, J., and M. Schiffer. 2011. 'Renal involvement in preeclampsia: similarities to VEGF ablation therapy', *J Pregnancy*, 2011: 176973.

Muller, Y. A., H. W. Christinger, B. A. Keyt, and A. M. de Vos. 1997. 'The crystal structure of vascular endothelial growth factor (VEGF) refined to 1.93 A resolution: multiple copy flexibility and receptor binding', *Structure*, 5: 1325-38.

Munaut, C., S. Lorquet, C. Pequeux, C. Coulon, J. Le Goarant, F. Chantraine, A. Noel, F. Goffin, V. Tsatsaris, D. Subtil, and J. M. Foidart. 2012. 'Differential expression of Vegfr-2 and its soluble form in preeclampsia', *PLoS One*, 7: e33475.

Munjuluri, N., M. Lipman, A. Valentine, P. Hardiman, and A. B. Maclean. 2005. 'Postpartum eclampsia of late onset', *BMJ*, 331: 1070-1.

Narasimhan, P., J. Liu, Y. S. Song, J. L. Massengale, and P. H. Chan. 2009. 'VEGF Stimulates the ERK 1/2 signaling pathway and apoptosis in cerebral endothelial cells after ischemic conditions', *Stroke*, 40: 1467-73.

Ng, Y. S., M. Ramsauer, R. M. Loureiro, and P. A. D'Amore. 2004. 'Identification of genes involved in VEGF-mediated vascular morphogenesis using embryonic stem cell-derived cystic embryoid bodies', *Lab Invest*, 84: 1209-18.

Norwitz, E. R., C. D. Hsu, and J. T. Repke. 2002. 'Acute complications of preeclampsia', *Clin Obstet Gynecol*, 45: 308-29.

Ogawa, S., A. Oku, A. Sawano, S. Yamaguchi, Y. Yazaki, and M. Shibuya. 1998. 'A novel type of vascular endothelial growth factor, VEGF-E (NZ-7 VEGF), preferentially utilizes KDR/Flk-1 receptor and carries a potent mitotic activity without heparin-binding domain', *J Biol Chem*, 273: 31273-82.

Palmer, K. R., T. J. Kaitu'u-Lino, R. Hastie, N. J. Hannan, L. Ye, N. Binder, P. Cannon, L. Tuohey, T. G. Johns, A. Shub, and S. Tong. 2015. 'Placental-Specific sFLT-1 e15a Protein Is Increased in Preeclampsia, Antagonizes Vascular Endothelial Growth Factor Signaling, and Has Antiangiogenic Activity', *Hypertension*, 66: 1251-9.

Park, J. E., G. A. Keller, and N. Ferrara. 1993. 'The vascular endothelial growth factor (VEGF) isoforms: differential deposition into the subepithelial extracellular matrix and bioactivity of extracellular matrix-bound VEGF', *Mol Biol Cell*, 4: 1317-26.

Patel, T. V., J. A. Morgan, G. D. Demetri, S. George, R. G. Maki, M. Quigley, and B. D. Humphreys. 2008. 'A preeclampsia-like syndrome characterized by reversible hypertension and proteinuria induced by the multitargeted kinase inhibitors sunitinib and sorafenib', *J Natl Cancer Inst*, 100: 282-4.

Peach, C. J., V. W. Mignone, M. A. Arruda, D. C. Alcobia, S. J. Hill, L. E. Kilpatrick, and J. Woolard. 2018. 'Molecular Pharmacology of VEGF-A Isoforms: Binding and Signalling at VEGFR2', *Int J Mol Sci*, 19.

Pennington, K. A., J. M. Schlitt, D. L. Jackson, L. C. Schulz, and D. J. Schust. 2012. 'Preeclampsia: multiple approaches for a multifactorial disease', *Dis Model Mech*, 5: 9-18.

Pollak, V. E., and J. B. Nettles. 1960. 'The kidney in toxemia of pregnancy: a clinical and pathologic study based on renal biopsies', *Medicine (Baltimore)*, 39: 469-526.

Poltorak, Z., T. Cohen, and G. Neufeld. 2000. 'The VEGF splice variants: properties, receptors, and usage for the treatment of ischemic diseases', *Herz*, 25: 126-9.

Powers, R. W., J. M. Roberts, K. M. Cooper, M. J. Gallaher, M. P. Frank, G. F. Harger, and R. B. Ness. 2005. 'Maternal serum soluble fms-like tyrosine kinase 1 concentrations are not increased in early pregnancy and decrease more slowly postpartum in women who develop preeclampsia', *Am J Obstet Gynecol*, 193: 185-91.

Presta, L. G., H. Chen, S. J. O'Connor, V. Chisholm, Y. G. Meng, L. Krummen, M. Winkler, and N. Ferrara. 1997. 'Humanization of an anti-vascular endothelial growth factor monoclonal antibody for the therapy of solid tumors and other disorders', *Cancer Res*, 57: 4593-9.

Rajakumar, A., K. Doty, A. Daftary, G. Harger, and K. P. Conrad. 2003. 'Impaired oxygen-dependent reduction of HIF-1alpha and -2alpha proteins in pre-eclamptic placentae', *Placenta*, 24: 199-208.

Rana, S., S. A. Karumanchi, R. J. Levine, S. Venkatesha, J. A. Rauh-Hain, H. Tamez, and R. Thadhani. 2007. 'Sequential changes in antiangiogenic factors in early pregnancy and risk of developing preeclampsia', *Hypertension*, 50: 137-42.

Redman, C. W., and I. L. Sargent. 2005. 'Latest advances in understanding preeclampsia', *Science*, 308: 1592-4.

'Report of the National High Blood Pressure Education Program Working Group on High Blood Pressure in Pregnancy'. 2000. *Am J Obstet Gynecol*, 183: S1-S22.

Roberts, J. M., R. N. Taylor, T. J. Musci, G. M. Rodgers, C. A. Hubel, and M. K. McLaughlin. 1989. 'Preeclampsia: an endothelial cell disorder', *Am J Obstet Gynecol*, 161: 1200-4.

Robinson, C. J., and S. E. Stringer. 2001. 'The splice variants of vascular endothelial growth factor (VEGF) and their receptors', *J Cell Sci*, 114: 853-65.

Sadeh, M. 1989. 'Action of magnesium sulfate in the treatment of preeclampsia-eclampsia', *Stroke*, 20: 1273-5.

Saffer, C., G. Olson, K. A. Boggess, R. Beyerlein, C. Eubank, B. M. Sibai, and Normals Study Group. 2013. 'Determination of placental growth factor (PlGF) levels in healthy pregnant women without signs or symptoms of preeclampsia', *Pregnancy Hypertens*, 3: 124-32.

Sawano, A., T. Takahashi, S. Yamaguchi, and M. Shibuya. 1997. 'The phosphorylated 1169-tyrosine containing region of flt-1 kinase (VEGFR-1) is a major binding site for PLCgamma', *Biochem Biophys Res Commun*, 238: 487-91.

Seligman, S. P., J. P. Buyon, R. M. Clancy, B. K. Young, and S. B. Abramson. 1994. 'The role of nitric oxide in the pathogenesis of preeclampsia', *Am J Obstet Gynecol*, 171: 944-8.

Shalaby, F., J. Rossant, T. P. Yamaguchi, M. Gertsenstein, X. F. Wu, M. L. Breitman, and A. C. Schuh. 1995. 'Failure of blood-island formation and vasculogenesis in Flk-1-deficient mice', *Nature*, 376: 62-6.

Sibai, B. M. 1998. 'Prevention of preeclampsia: a big disappointment', *Am J Obstet Gynecol*, 179: 1275-8.

———. 2005. 'Diagnosis, prevention, and management of eclampsia', *Obstet Gynecol*, 105: 402-10.

Sison, K., V. Eremina, H. Baelde, W. Min, M. Hirashima, I. G. Fantus, and S. E. Quaggin. 2010. 'Glomerular structure and function require paracrine, not autocrine, VEGF-VEGFR-2 signaling', *J Am Soc Nephrol*, 21: 1691-701.

Spargo, B. H., C. Lichtig, A. M. Luger, A. I. Katz, and M. D. Lindheimer. 1976. 'The renal lesion in preeclampsia', *Perspect Nephrol Hypertens*, 5: 129-37.

Sugimoto, H., Y. Hamano, D. Charytan, D. Cosgrove, M. Kieran, A. Sudhakar, and R. Kalluri. 2003. 'Neutralization of circulating vascular endothelial growth factor (VEGF) by anti-VEGF antibodies and soluble VEGF receptor 1 (sFlt-1) induces proteinuria', *J Biol Chem*, 278: 12605-8.

Sun, Y. Y., M. Lu, X. W. Xi, Q. Q. Qiao, L. L. Chen, X. M. Xu, and Y. J. Feng. 2011. 'Regulation of epithelial-mesenchymal transition by homeobox gene DLX4 in JEG-3 trophoblast cells: a role in preeclampsia', *Reprod Sci*, 18: 1138-45.

Szalai, G., R. Romero, T. Chaiworapongsa, Y. Xu, B. Wang, H. Ahn, Z. Xu, P. J. Chiang, B. Sundell, R. Wang, Y. Jiang, O. Plazyo, M. Olive, A. L. Tarca, Z. Dong, F. Qureshi, Z. Papp, S. S. Hassan, E. Hernandez-Andrade, and N. G. Than. 2015. 'Full-length human placental sFlt-1-e15a isoform induces distinct maternal phenotypes of preeclampsia in mice', *PLoS One*, 10: e0119547.

Takahashi, A., K. Kono, F. Ichihara, H. Sugai, H. Fujii, and Y. Matsumoto. 2004. 'Vascular endothelial growth factor inhibits maturation of dendritic cells induced by lipopolysaccharide, but not by proinflammatory cytokines', *Cancer Immunol Immunother*, 53: 543-50.

Teng, L. S., K. T. Jin, K. F. He, J. Zhang, H. H. Wang, and J. Cao. 2010. 'Clinical applications of VEGF-trap (aflibercept) in cancer treatment', *J Chin Med Assoc*, 73: 449-56.

Terman, B. I., M. Dougher-Vermazen, M. E. Carrion, D. Dimitrov, D. C. Armellino, D. Gospodarowicz, and P. Bohlen. 1992. 'Identification of the KDR tyrosine kinase as a receptor for vascular endothelial cell growth factor', *Biochem Biophys Res Commun*, 187: 1579-86.

Thadhani, R., H. Hagmann, W. Schaarschmidt, B. Roth, T. Cingoez, S. A. Karumanchi, J. Wenger, K. J. Lucchesi, H. Tamez, T. Lindner, A. Fridman, U. Thome, A. Kribs, M. Danner, S. Hamacher, P. Mallmann, H. Stepan, and T. Benzing. 2016. 'Removal of Soluble Fms-Like Tyrosine Kinase-1 by Dextran Sulfate Apheresis in Preeclampsia', *J Am Soc Nephrol*, 27: 903-13.

Thadhani, R., T. Kisner, H. Hagmann, V. Bossung, S. Noack, W. Schaarschmidt, A. Jank, A. Kribs, O. A. Cornely, C. Kreyssig, L. Hemphill, A. C. Rigby, S. Khedkar, T. H. Lindner, P. Mallmann, H. Stepan, S. A. Karumanchi, and T. Benzing. 2011. 'Pilot study of extracorporeal removal of soluble fms-like tyrosine kinase 1 in preeclampsia', *Circulation*, 124: 940-50.

Trapiella-Alfonso, L., L. Alexandre, C. Fraichard, K. Pons, S. Dumas, L. Huart, J. F. Gaucher, M. Hebert-Schuster, J. Guibourdenche, T. Fournier, M. Vidal, I. Broutin, L. Lecomte-Raclet, L. Malaquin, S. Descroix, V. Tsatsaris, N. Gagey-Eilstein, and E. Lecarpentier. 2019. 'VEGF (Vascular Endothelial Growth Factor) Functionalized Magnetic Beads in a Microfluidic Device to Improve the Angiogenic Balance in Preeclampsia', *Hypertension*, 74: 145-53.

Turanov, A. A., A. Lo, M. R. Hassler, A. Makris, A. Ashar-Patel, J. F. Alterman, A. H. Coles, R. A. Haraszti, L. Roux, Bmdc Godinho, D. Echeverria, S. Pears, J. Iliopoulos, R. Shanmugalingam, R. Ogle, Z. K. Zsengeller, A. Hennessy, S. A. Karumanchi, M. J. Moore, and A. Khvorova. 2018. 'RNAi modulation of placental sFLT1 for the treatment of preeclampsia', *Nat Biotechnol*.

Venkatesha, S., M. Toporsian, C. Lam, J. Hanai, T. Mammoto, Y. M. Kim, Y. Bdolah, K. H. Lim, H. T. Yuan, T. A. Libermann, I. E. Stillman, D. Roberts, P. A. D'Amore, F. H. Epstein, F. W. Sellke, R. Romero, V. P. Sukhatme, M. Letarte, and S. A. Karumanchi. 2006. 'Soluble endoglin contributes to the pathogenesis of preeclampsia', *Nat Med*, 12: 642-9.

Verlohren, S., I. Herraiz, O. Lapaire, D. Schlembach, M. Moertl, H. Zeisler, P. Calda, W. Holzgreve, A. Galindo, T. Engels, B. Denk, and H. Stepan. 2012. 'The sFlt-1/PlGF ratio in different types of hypertensive pregnancy disorders and its prognostic potential in preeclamptic patients', *Am J Obstet Gynecol*, 206: 58 e1-8.

Vogtmann, R., J. Heupel, F. Herse, M. Matin, H. Hagmann, I. Bendix, K. Kraker, R. Dechend, E. Winterhager, R. Kimmig, A. Koninger, and A. Gellhaus. 2021. 'Circulating Maternal sFLT1 (Soluble fms-Like Tyrosine Kinase-1) Is Sufficient to Impair Spiral Arterial Remodeling in a Preeclampsia Mouse Model', *Hypertension*, 78: 1067-79.

Vuorela, P., S. Helske, C. Hornig, K. Alitalo, H. Weich, and E. Halmesmaki. 2000. 'Amniotic fluid--soluble vascular endothelial growth factor receptor-1 in preeclampsia', *Obstet Gynecol*, 95: 353-7.

Walsh, S. K., F. A. English, I. P. Crocker, E. J. Johns, and L. C. Kenny. 2012. 'Contribution of PARP to endothelial dysfunction and hypertension in a rat model of pre-eclampsia', *Br J Pharmacol*, 166: 2109-16.

Wiesmann, C., G. Fuh, H. W. Christinger, C. Eigenbrot, J. A. Wells, and A. M. de Vos. 1997. 'Crystal structure at 1.7 A resolution of VEGF in complex with domain 2 of the Flt-1 receptor', *Cell*, 91: 695-704.

Wojtowicz, A., M. Zembala-Szczerba, D. Babczyk, M. Kolodziejczyk-Pietruszka, O. Lewaczynska, and H. Huras. 2019. 'Early- and Late-Onset Preeclampsia: A Comprehensive Cohort Study of Laboratory and Clinical Findings according to the New ISHHP Criteria', *Int J Hypertens*, 2019: 4108271.

Woolard, J., W. Y. Wang, H. S. Bevan, Y. Qiu, L. Morbidelli, R. O. Pritchard-Jones, T. G. Cui, M. Sugiono, E. Waine, R. Perrin, R. Foster, J. Digby-Bell, J. D. Shields, C. E. Whittles, R. E. Mushens, D. A. Gillatt, M. Ziche, S. J. Harper, and D. O. Bates. 2004. 'VEGF165b, an inhibitory vascular endothelial growth factor splice variant: mechanism of action, in vivo effect on angiogenesis and endogenous protein expression', *Cancer Res*, 64: 7822-35.

Yamazaki, Y., Y. Matsunaga, Y. Tokunaga, S. Obayashi, M. Saito, and T. Morita. 2009. 'Snake venom Vascular Endothelial Growth Factors (VEGF-Fs) exclusively vary their structures and functions among species', *J Biol Chem*, 284: 9885-91.

Yang, W., H. Ahn, M. Hinrichs, R. J. Torry, and D. S. Torry. 2003. 'Evidence of a novel isoform of placenta growth factor (PlGF-4) expressed in human trophoblast and endothelial cells', *J Reprod Immunol*, 60: 53-60.

Young, B. C., R. J. Levine, and S. A. Karumanchi. 2010. 'Pathogenesis of preeclampsia', *Annu Rev Pathol*, 5: 173-92.

Zhou, Y., M. McMaster, K. Woo, M. Janatpour, J. Perry, T. Karpanen, K. Alitalo, C. Damsky, and S. J. Fisher. 2002. 'Vascular endothelial growth factor ligands and receptors that regulate human cytotrophoblast survival are dysregulated in severe preeclampsia and hemolysis, elevated liver enzymes, and low platelets syndrome', *Am J Pathol*, 160: 1405-23.

10. Publications and awards

10.1. Publication in academic journals

1. Matin M, Mörgelin M, Stetefeld J, Schermer B, Brinkkoetter PT, Benzing T, Koch M, Hagmann H. Affinity-Enhanced Multimeric VEGF (Vascular Endothelial Growth Factor) and PlGF (Placental Growth Factor) Variants for Specific Adsorption of sFlt-1 to Restore Angiogenic Balance in Preeclampsia. Hypertension. 2020 Oct;76(4):1176-1184. doi: 10.1161/HYPERTENSIONAHA.120.14974. Epub 2020 Jul 6. PMID: 32623922.

2. Vogtmann R, Heupel J, Herse F, Matin M, Hagmann H, Bendix I, Kräker K, Dechend R, Winterhager E, Kimmig R, Köninger A, Gellhaus A. Circulating Maternal sFLT1 (Soluble fms-Like Tyrosine Kinase-1) Is Sufficient to Impair Spiral Arterial Remodeling in a Preeclampsia Mouse Model. Hypertension. 2021 Sep;78(4):1067-1079. doi: 10.1161/HYPERTENSIONAHA.121.17567. Epub 2021 Aug 15. PMID: 34397280; PMCID: PMC8415521.

10.2. Publication in international academic conferences

1. Matin M, Kuczkowski A, Mangold N, Dryer S, Fels J, Brodesser S, Reiser J, Benzing T; Brinkkoetter P, Hagmann H. The paraoxonase PON2 regulates TRPC6 channel activity by modulation of the lipid composition of the plasma cell membrane. Podocyte Conference 2018 (poster presentation and blitz talk)

2. Matin M, Mörgelin M, Stetefeld J, Schermer B, Brinkkoetter PT, Benzing T, Koch M, Hagmann H. Affinity-Enhanced Multimeric VEGF (Vascular Endothelial Growth Factor) and PlGF (Placental Growth Factor) Variants for Specific Adsorption of sFlt-1 to Restore Angiogenic Balance in Preeclampsia. American society of nephrology 2019 (poster presentation)

10.3. Awards

1. A patent for scVEGF165- 2016419.7-118
2. EIT health PhD translational fellowship-University of Köln 2019
3. EIT health Best need prize - University of Oxford 2019
4. Apheresis innovation prize- DGFN 2020 (received by Dr. Henning Hagmann)
5. High Impact Paper for Winter 2020 in the category of Basic science in journal of Hypertension

11. Acknowledgment

Firstly, I would like to express my sincere gratitude to Prof. Thomas Benzing, Prof. Paul Brinkötter and Prof. Bernhard Schermer for their countless support and mentorship during my PhD thesis.

The words definitely fail to convey all my heartiest gratitude to my wonderful, amazing, and kind-hearted supervisor Priv.-Doz. Dr. Henning Hagmann for his endless scientific and moral support and constructive feedbacks.

I would like to extend my gratitude to Prof. Manuel Koch and all members of his group in institute of Biochemistry II for their guidance, cooperation and support.

I would like to acknowledge all friends and members of Brinkötter lab in CMMC, Johanna, Angelika, Duc, and Thomas for their constant motivation, ideas and discussions.

A special thanks to my amazing mom and dad, my parent in-laws and my three dear sisters, Mina, Maryam and Yasemin, as well as Yilmaz and Teo for their love and act of encouragements, I feel blessed to have them in my life.

I would Like to thank my best friend, co-worker, husband, and partner in crime, MY Cem for always believing in me and be there for me in every step of my life. I would not be where I am now without his support. Words fail to convey my love for him.

Finally, I would like to thank my sweet and lovely twin baby boys, Liam and Emil, without whom this thesis would have been finished one year earlier! They have turned my life upside down, and I love them for infinity.

12. Erklärung

„Hiermit versichere ich an Eides statt, dass ich die vorliegende Dissertation selbstständig und ohne die Benutzung anderer als der angegebenen Hilfsmittel und Literatur angefertigt habe. Alle Stellen, die wörtlich oder sinngemäß aus veröffentlichten und nicht veröffentlichten Gymnasium Werken dem Wortlaut oder dem Sinn nach entnommen wurden, sind als solche kenntlich gemacht. Ich versichere an Eides statt, dass diese Dissertation noch keiner anderen Fakultät oder Universität zur Prüfung vorgelegen hat; dass sie - abgesehen von unten angegebenen Teilpublikationen und eingebundenen Artikeln und Manuskripten - noch nicht veröffentlicht worden ist sowie, dass ich eine Veröffentlichung der Dissertation vor Abschluss der Promotion nicht ohne Genehmigung des Promotionsausschusses vornehmen werde. Die Bestimmungen dieser Ordnung sind mir bekannt. Darüber hinaus erkläre ich hiermit, dass ich die Ordnung zur Sicherung guter wissenschaftlicher Praxis und zum Umgang mit wissenschaftlichem Fehlverhalten der Universität zu Köln gelesen und sie bei der Durchführung der Dissertation zugrundeliegenden Arbeiten und der schriftlich verfassten Dissertation beachtet habe und verpflichte mich hiermit, die dort genannten Vorgaben bei allen wissenschaftlichen Tätigkeiten zu beachten und umzusetzen. Ich versichere, dass die eingereichte elektronische Fassung der eingereichten Druckfassung vollständig entspricht."

Mahsa Matin

Köln, 25.03.2022

13. Curriculum Vitae

Persönliche Daten

Name	Mahsa Matin
Anschrift	Franzstrasse 40-42, 50935 Köln
Email	mahsa.matin@uk-koeln.de
Geburtsdatum, -ort	22 April 1990 in Bandar Anzali, Iran

Studium und Ausbildung

Seit 2017	**Promotion, Dr. rer. nat. der Biologie** Universität zu Köln, Graduate School for Biological Sciences, Köln, Deutschland
Seit 2020	**Ph.D., Exzellenz in wissenschaftlicher Ausbildung, Innovation und Unternehmertum** Europäisches Institut für Innovation und Technologie (EIT)
2014 - 2016	**M.Sc., Biomedizinische Wissenschaften** Hochschule Bonn-Rhein-Sieg, Rheinbach, Deutschland (Gesamtnote: 2,0)
2008 - 2013	**B.Sc., Zell- und Molekularbiologie** Universität zu Guilan, Guilan, Iran (Gesamtnote: sehr gut)

Schulische Ausbildung

2007-2008	Sharaf Hochschule, Bandar-anzali, Iran
2004-2007	Imam Ali Gymnasium, Bandar-anzali, Iran